



TECHNISCHE  
UNIVERSITÄT  
WIEN  
Vienna University of Technology



# Diplomarbeit

## Simulation of lower limb joint forces and muscle- activation during isokinetic and vibration leg press training

ausgeführt zum Zwecke der Erlangung des akademischen Grades eines

## Diplom-Ingenieurs

unter der Leitung von

**Ao. Univ.-Prof. DI DDr. Winfried MAYR**

(E325 Institute of Mechanics and Mechatronics, Vienna University of Technology)  
(Center for Medical Physics and Biomedical Engineering, Medical University of Vienna)

**DI Matthias KRENN**

(Center for Medical Physics and Biomedical Engineering, Medical University of Vienna)

eingereicht an der Technischen Universität Wien

**Fakultät für Maschinenwesen und Betriebswissenschaften**

von

**Günter SCHNEIDER, BSc**

Matr.Nr.: 0726129  
Kirchensteig 21  
2264 Sierndorf/March, Austria

Sierndorf/March, im März 2015

---

Günter, SCHNEIDER, BSc





TECHNISCHE  
UNIVERSITÄT  
WIEN  
Vienna University of Technology



MEDICAL  
UNIVERSITY  
OF VIENNA

Ich habe zur Kenntnis genommen, dass ich zur Drucklegung meiner Arbeit unter der Bezeichnung

## **Diplomarbeit**

nur mit Bewilligung der Prüfungskommission berechtigt bin.

Ich erkläre weiters Eides statt, dass ich meine Diplomarbeit nach den anerkannten Grundsätzen für wissenschaftliche Abhandlungen selbstständig ausgeführt habe und alle verwendeten Hilfsmittel, insbesondere die zugrunde gelegte Literatur, genannt habe.

Weiters erkläre ich, dass ich dieses Diplomarbeitsthema bisher weder im In- noch Ausland (einer Beurteilerin/einen Beurteiler zur Begutachtung) in irgendeiner Form als Prüfungsarbeit vorgelegt habe und dass diese Arbeit mit der vom Begutachter beurteilten Arbeit übereinstimmt.

Sierndorf/March, im März 2015

---

Günter, SCHNEIDER, BSc

## Acknowledgement

Foremost, I would like to thank Prof. Winfried Mayr giving me the opportunity doing this diploma thesis and Matthias Krenn for mentoring me during all the time of research and writing of this thesis. Further I would sincerely thank Jan Cvecka for introducing me to a fascinating topic of the biomedical research sector, the possibility to work with his leg press machine and his readiness for spontaneous measurements.

I would like to thank Prim. Prof. Helmut Kern and his team, Dr. Christian Hofer, Samantha Burggraf, Hannah Fruhmann and Stefan Löfler for the endorsement to use their establishment and equipment and the assistance during the measurements at Wilhelminenspital.

My sincere thanks also goes to my colleagues and labmates at the institute, it wouldn't have been that good time without you. Finally I would like to say THANK YOU to my family and friends for supporting me over all the time.

## Abstract

The leg press presents an effective exercise device for the lower limb muscles where the individual works against resistance in both, concentric and eccentric way. Training on a legpress is often used in rehabilitation because it has a defined range of movement which reduces the impact on the joints. In recent years, a unique computer-controlled linear motor powered leg press was developed by the Comenius University (Bratislava, Slovakia) and the Ludwig Boltzmann Institute of Electrical Stimulation and Physical Rehabilitation (Vienna, Austria). The new device is able to operate in several working modes in a flexible way which enhances the efficacy of the training procedure. Next to classical isokinetic and isotonic loads, the computer-controlled linear-motor of this leg press can also generate vibrations with customized parameter setting.

Former investigations estimate higher muscle activity during vibration training compared to isokinetic movement. The aim of this thesis is to examine these thoughts with the aid of simulation software. Various vibration and isokinetic training protocols were simulated and verified by EMG measurements. The simulation of the joint forces and muscle activation was conducted with the open-source software OpenSim 3.2 (Simbios, Stanford University, CA USA). In a subject input data to the simulation was acquired consisting of the foot movement and the leg press load. Simulation contained joint moments, muscle forces and muscle activities of lower limbs and was executed for isokinetic and vibration training at muscle force levels of 0%, 50%, and 100% of the maximum voluntary activation.

The simulation results show most activity and force production in the vastus lateralis muscle. Isokinetic simulations featured higher muscle activity than vibration simulations as well as calculated muscle forces which behave the same way.

In addition, EMG measurements were performed to verify the simulation results. Eleven muscles were record on the left lower limbs to monitor the muscle activities during the leg press training.

Simulation results and EMG signals stated higher muscle activity during knee flexion phase. In contrary to simulation results, activation of knee extension antagonist muscles could be observed in EMG signals. In both cases, knee extension agonists became more dominant when voluntary muscle activation was raised. Most activity and force production was simulated for musculus vastus lateralis (VL) followed by other quadriceps heads. Simulation results featured higher muscle activities and forces while isokinetic training, unlike EMG data where that behavior could not be observed.

Vibration training affects muscles on deep structural levels making simulations close to reality very complex. For analyzing e.g. knee force or similar parameters researchers are not able to measure in vivo, simulations are common.

**Keywords:** OpenSim, simulation, muscle simulation, leg press, computer-controlled linear-motor powered leg press, muscle activity, quadriceps muscles, EMG,

# Table of contents

<b>Table of contents</b> .....	<b>4</b>
<b>1 Introduction</b> .....	<b>6</b>
<b>2 Theoretical background</b> .....	<b>7</b>
<b>2.1 Project: “MOBIL” – Mobility of elderly</b> .....	<b>7</b>
<b>2.2 Computer-controlled, linear motor-powered leg press</b> .....	<b>8</b>
2.2.1 Technical specifications of the leg press .....	8
2.2.2 Different training modes on the leg press.....	10
2.2.3 Leg press - software (FITRONIC) .....	11
<b>2.3 Skeletal muscles</b> .....	<b>11</b>
2.3.1 Muscle structure .....	11
2.3.2 Muscle shapes.....	13
2.3.3 Muscle force control.....	14
2.3.3.1 Types of exercise, open and closed kinetic chain exercise .....	16
2.3.3.2 Types of contraction.....	16
2.3.3.3 Vibration stimulation – serial stretch loading, stretch-shortening .....	18
2.3.3.4 Quick-Release behavior.....	19
<b>2.4 Muscle Model: Hill and Huxley type model, Thelen2003, Millard2012</b> .....	<b>20</b>
2.4.1 General Muscle Model: Hill and Huxley type model.....	20
2.4.1.1 Hill Type Model .....	20
2.4.1.2 Huxley Type Model .....	24
2.4.2 OpenSim Muscle Models: Thelen2003, Millard2012 .....	26
2.4.2.1 Thelen 2003 Muscle Model - OpenSim .....	27
2.4.2.2 Millard 2012 Muscle Modell – OpenSim .....	30
<b>2.5 Electromyography and joint angle measurements</b> .....	<b>33</b>
<b>2.6 Simulation Software – OpenSim 3.2</b> .....	<b>34</b>
2.6.1 Modeling of the human musculoskeletal system.....	35
2.6.1.1 Biological vs. engineered joints .....	35
2.6.1.2 Interaction with the environment.....	36
2.6.1.3 Passive structures and physiological actuators .....	36
2.6.1.4 Neuromuscular control.....	37
2.6.2 Scale Tool.....	38
2.6.3 Analyze-Tools .....	39
2.6.3.1 Inverse Kinematics (IK).....	39
2.6.3.2 Inverse Dynamics (ID) .....	41
2.6.3.3 Computed Muscle Control (CMC).....	41
<b>3 Materials and Methods</b> .....	<b>44</b>
<b>3.1 Software: OpenSim 3.2</b> .....	<b>44</b>
3.1.1 Body model.....	44
3.1.2 Body Marker Set.....	45
3.1.3 Muscle model.....	46
3.1.4 Modeling of motion and force data .....	48
3.1.4.1 Motion data .....	49
3.1.4.2 Force data .....	50
3.1.5 OpenSim: Scale Tool – Specifications .....	51

---

3.1.6	OpenSim: Inverse Kinematics (IK) - Specifications .....	52
3.1.7	OpenSim: Inverse Dynamics (ID) - Specifications .....	53
3.1.8	OpenSim: Computed Muscle Control (CMC) - Specifications .....	54
<b>3.2</b>	<b>Muscle activation measured in a human subject .....</b>	<b>56</b>
3.2.1	EMG electrode placement .....	57
3.2.2	Goniometer .....	58
3.2.3	Data acquisition and analysis .....	58
3.2.4	Training protocol .....	59
<b>4</b>	<b>Results: OpenSim – Simulation .....</b>	<b>62</b>
4.1	Results: Inverse Kinematics (IK) .....	62
4.2	Results: Inverse Dynamics (ID) .....	63
4.3	Results: Computer Muscle Control (CMC) .....	68
4.4	Discussion .....	77
<b>5</b>	<b>Results: EMG/goniometer measurement .....</b>	<b>81</b>
5.1	Results EMG .....	81
5.2	Results: GONIOMETER .....	85
5.3	Discussion .....	86
<b>6</b>	<b>Comparison of simulation and EMG results .....</b>	<b>89</b>
<b>7</b>	<b>Bibliography .....</b>	<b>90</b>
<b>8</b>	<b>List of abbreviations .....</b>	<b>96</b>

# 1 Introduction

In recent years many studies used vibration training to enhance the muscle performance of athletes and patients (Cvecka et al. 2009; Bird et al. 2005; Rønnestad 2004; Verschueren 2004; Fleck & Kreamer 1997). It was shown that vibration training enhance the muscle performance by potentiation of the neuromuscular system by activation of muscles spindles reflexes which increased spatial recruitment (Komi 2000; Romaguère et al. 1993). Cvecka et al. (2009) designed a computer-controlled leg press where those principles where used to strengthen muscles of the lower limb to preserve agility, autonomy and the quality of life for elderly (Krenn et al. 2011). Produced external forces during the training and impact of the different training modes (isokinetic and vibration) on subjects performance after a period of time where documented.

Detailed investigation of lower limb muscle excitation and force production on musculoskeletal basis of this particular leg press training is missing. Prior considerations estimate higher muscle activity during vibration training compared to isokinetic movement. The aim of this thesis is to examine these thoughts with the aid of simulation software. The simulation provides an insight on the behavior of lower limb muscles (activation and force). Further, joint moments are simulated and compared between the two different training modes and EMG signals of eleven lower limb muscles are recorded.

The thesis is structured in a theoretical section about of the leg press and the controlling software and the performed OpenSim simulation including verification with EMG measurements. Additionally, in the background the basic physiology and anatomy of the neuromuscular system is presented. Finally, the results of OpenSim simulations and EMG-measurements were discussed in detail in the last chapter.

## 2 Theoretical background

### 2.1 Project: “MOBIL” – Mobility of elderly

In the EU-Project Interreg IVa: “Mobilität im Alter” (mobility for elderly) new methods were studied to strengthen muscles of the lower limb of the elderly. The aim was to preserve agility, autonomy and the quality of life. The project partners were Ludwig Boltzmann Institute of Electrical Stimulation and Physical Rehabilitation (Vienna, Austria), Faculty of Physical Education and Sport at Comenius University (Bratislava, Slovakia), Center for Medical Physics and Biomedical Engineering of the Medical University of Vienna (Vienna, Austria) and the Otto Bock HealthCare Products GmbH (Vienna, Austria).

Here, volunteers were randomly subdivided in three groups, leg press group, electrical stimulation group and the control group. All participants were subjected to a preliminary investigation before they started with their individual training. After completion of the training all members had three more check-ups. First as soon as possible after completion of the training, second and third check-up at intervals of six months after the individual training (Kern 2012).

*Leg press group:* Members of the leg press group are trained by a vibration-proprioceptive stimulation (VIB training) on the computer-controlled, linear motor-powered leg press machine (q.v. 2.2) developed by the Faculty of Physical Education and Sport at Comenius University. VIB training induces a series of eccentric muscle tetanic contractions at high frequency.

*Electrical stimulation group:* Subjects of the second group are trained with a Neuromuscular Electrical Stimulation device developed at the Center for Medical Physics and Biomedical Engineering of the Medical University of Vienna (Krenn et al. 2011). Electro-stimulation training invokes motor nerves of the muscles due to electrical impulse resultant the muscle gets activated.

*Control group:* This group only performs the same measurements and check-ups as the intervention groups and lives their lives as usual in between. After the survey, members of that group can choose one of the two other therapies to train.

The focus of this diploma thesis will be on the first group – the leg press group – of the three listed above and deals with the investigation of the stress applied to the lower extremity and the activation of the respective muscles, as well as the development of a suitable simulation in OpenSim, an open source software to create and analyze dynamic simulations of movements (Delp et al. 2007).

## 2.2 Computer-controlled, linear motor-powered leg press machine

In course of the MOBIL survey (q.v. 2.1) subjects underwent strength training on a novel, computer-controlled, linear motor-powered leg press machine (Figure 2.1) developed by the Faculty of Physical Education and Sport at Comenius University in Bratislava. The present work is concerned with the stress resulting due to the training on this leg press machine to the lower extremity, as well as with the simulation of loads and muscle activities resulting of the leg press-training.

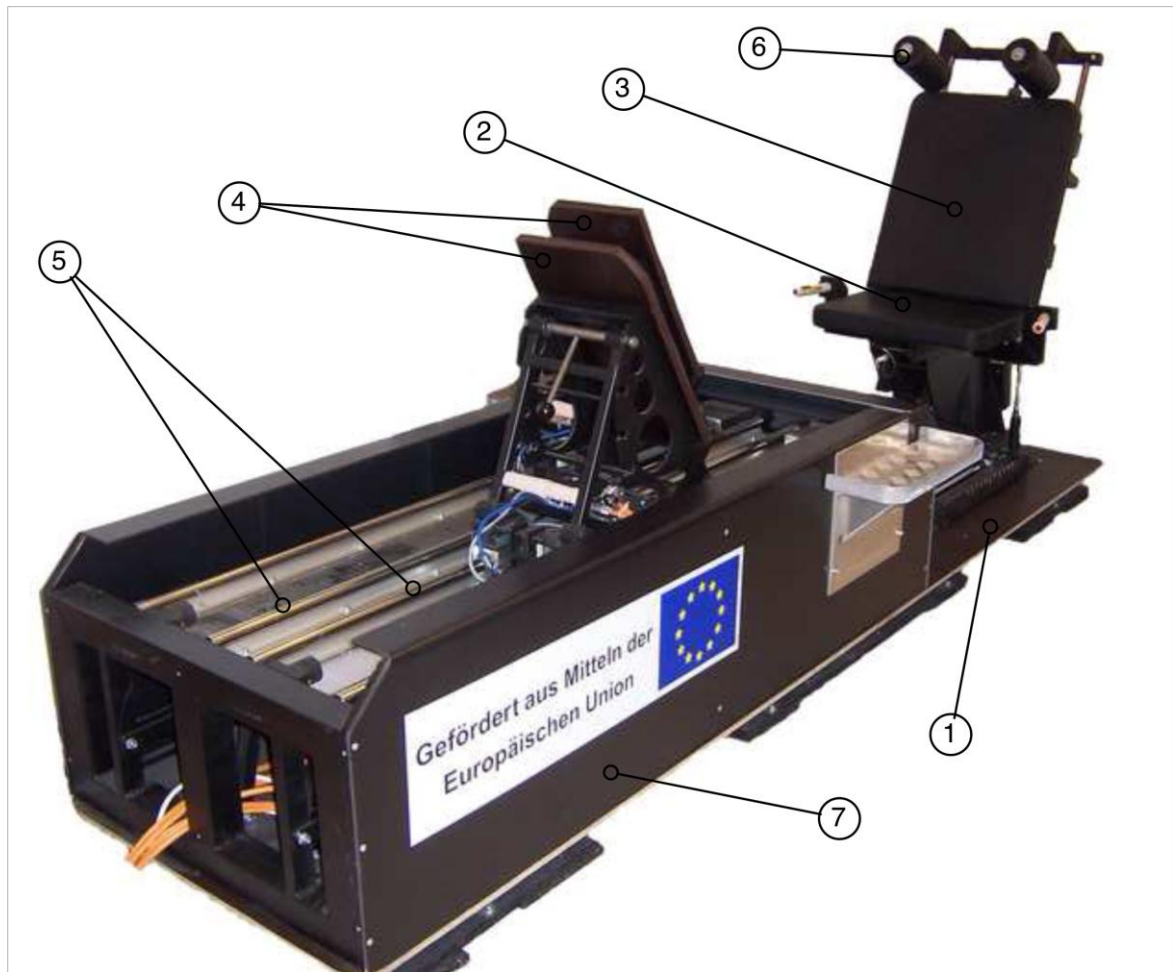


**Figure 2.1: Computer-controlled, linear motor-powered leg press machine**  
*base-framework, (2) bolstered seat-base, (3) bolstered backrest, (4) foot-sledges, (5) linear-bearing, (6) horizontal shoulder-rest, (7) body housing*  
*source: Cvecka et al. 2009; Kern et al. 2011*

### 2.2.1 Technical specifications of the leg press

Instead of classical weights, like in conventional leg press machines, the resistance of leg press pedals is generated by two independent linear electric motors (Kollmorgen IC33-075 A1 TS C1, Radford, USA, Table 2.1). For the movements of the pedals there are three different modes available: coupled, reciprocal and independent. To measure stress, in each of the two pedals there is a strain gauge

(EMS100 5kN, EMSYST, Trencin, Slovakia) that is connected via a 12-bit AD converter to the computer. Sampling frequency is about 1000 Hz. Because of the patented technical design (Kern et al. 2009) the machine can be operated not only in traditional isokinetic and isometric mode (concentric and eccentric), but also in “swinging” vibration-proprioceptive mode, as used in the paper of Kern and colleagues (Kern et al. 2011).

rated performance	symbol	value
peak force	$F_p$	2358 [N]
continuous force @ $T_{max}$	$F_c$	1238 [N]
coil assembly weight $\pm 15\%$	$M_c$	14.4 [kg]
electric time constant	$T_e$	11.2 [ms]
max. theoretical acceleration	$A_{max}$	19.9 [ $g's$ ]
max. allowable coil temperature	$T_{max}$	130 [ $^{\circ}C$ ]

**Table 2.1: Specification linear electric motor**  
*IC33-075 A1 TS C1, Radford, USA*

### **Mechanical implementation**

The whole construction can be split up into three main parts – the base (1), the seat (3) and the biggest part, the body housing (7) of the leg press that includes the two locomotive pedals (4), the box where the linear motors and the control unit are mount and the linear bearing (5) for the guidance of the sledge with the footplates on it.

The base (length: 2900mm, width: 730mm, height: 80mm) a weld steel section covered with a composite panel to avoid slippage acts as groundwork for all the other parts. The seat consisting of a seat-base (2), 400mm in length and 400mm width, the backrest (3) (length: 600mm x width: 400mm) and a horizontal shoulder-rest (6) (length: 60mm x width: 80mm). Two former are constructed in the same way, out of steel framework, bolstered and covered with synthetic leather to provide comfort to the subjects. The backrest is adjustable to the seat-base in steps of  $10^{\circ}$  over a range from 0 to 90 degrees and is secured with a variable pin. Like the backrest the horizontal shoulder-rest is variable too, and can be positioned in steps of 3cm. For adjustment a welding spot is used. Subjects are fixed with a shoulder belt to the backrest and around the pelvis to the seat-base. For the movement of the sledge the linear bearing of each is mount in a robust steel frame work. Thereon the linear motor is moving the whole sledge via magnetic work. Working range of the sledge is 1200mm and contains the pedals where subjects put their feet on it. Pedals are variable from 10 to  $40^{\circ}$  in steps of 10 degrees and in 400mm distance of the base. Fixed via Tensometer to the moveable rotor the force is transferred from the pedal to the linear motor.

### **Electrical control implementation**

All electrical supplies and connections are housed in a separate electrical cabinet. These are the leg press's main power supply (3x400V, 50Hz), the USB connection for data transfer with an external PC, the two data channels from force sensors of the pedals and the power supply and control unit (Servostar 346, 6A/3x400V) for the linear electrical motors. Analog force signals from the Tensometer and the Hall-sensors, used for positioning information of the sledge, are digitized by a 12-bit AD-Converter (ADS 7816) with sampling rate of 1000Hz. The resolution of the positioning system is limited to 0,1mm and used data from these Hall-sensors are also used for online monitoring and emergency shutdown if the sledge's position is out of the defined range.

### **2.2.2 Different training modes on the leg press**

As mentioned above, the new developed computer-controlled, linear motor-powered leg press machine allows subjects to train in four different modes: (a) isotonic, (b) isometric, (c) isokinetic and (d) vibration-proprioceptive (Kern et al. 2009). In order to change major characteristic of the modes, velocity of the movement, range of motion, acceleration ramp and frequency and amplitude of the vibration can be modified. The system allows also to adjust the range of motion individual for every subject.

#### **(a) Isotonic mode**

A predefined resistance of the pedal is adjusted and pedals are positioned at an individual position. During the training, pedals are stagnant at that position, as long as the force produced by the subject does not increase the predefined resistance of the pedal. If so, pedals will move in the direction of the resultant force (away from the body). Isotonic mode can be use for diagnostic of subjects strength capability as well as for training or intervention.

#### **(b) Isometric mode**

The pedals of the leg press are positioned in an individual position and the maximal resistance of the system (1870N per leg) is adjusted. The pedals stay stagnant at the predefined position during the whole time of muscle contraction. Isometric mode is used for diagnostic purpose only.

#### **(c) Isokinetic mode**

Starting at a predefined position the pedals move with constant, predefined velocity till the defined end position (concentric phase) and backward (eccentric phase). Isokinetic mode can be used in diagnostic as well as in training and due to increased safety of the movement it is very popular in rehabilitation of lower limbs.

#### (d) Vibration-proprioceptive mode

In order to produce short force peaks, the constant velocity of pedals is alternated by short periods of movement at different velocities. E.g. velocity during the concentric phase of 0.3 m/s repeatedly replaced after 20mm by short 0.5mm countermovement at 0.2m/s. In the eccentric phase, velocity of 0.2 m/s is alternated after every 15mm by short 5mm segments of higher velocity (0.7m/s). Vibrations-proprioceptive mode is only used for training or therapy purposes.

### 2.2.3 Leg press - software (FiTRONiC)

All software components needed to operate the leg press and for visualization of the recorded data, are realized by *FiTRONiC s. r. o. - Diagnostic and Training Systems* settled in Bratislava (SVK). The software allows the training supervisor to specify all specifications like moving path, moving velocity, acceleration ramp, vibration frequency, vibration amplitude and more for an individual training balanced to the needs and competence of every single subject. Due to safety and adjustment reasons the software offers live monitoring of the produced force and motion to the supervisor. Posterior, the software offers the user a wide selection of options to view the recorded data and provides a considerable tool to take a detailed look at the produced force and movements.

## 2.3 Skeletal muscles

Skeletal muscle connects two bones and is the primary part of the organ muscle. Connective tissues (internal and external to the muscle) as well as nerve tissue play an integral part in the formation and function of muscle whose main function is to produce force and movement. Muscles are only able to create forces or movements when they shorten, though muscle also produces a significant amount of heat upon contraction, as Epstein et al. illustrate (Epstein & Herzog 1998).

Basically there are three major types of muscle in human body: skeletal muscle, cardiac muscle and smooth muscle (Schmiedmayer 2011). Skeletal muscle, in difference to cardiac and smooth muscle, can be controlled voluntarily. Skeletal muscles are extremely powerful during contraction, shorten at great speed and operate over large distances. But they also can be controlled very accurately for precision tasks, like handwriting or moving the eyes. This thesis gives attention to the lower extremities and therefore to the skeletal muscle.

### 2.3.1 Muscle structure

In both directions, cross-sectionally and longitudinally, skeletal muscles are structurally organized in an intricate way. Two layer of connective tissue called fascia

and epimysium surrounds the entire muscle. The next smaller structure is the muscle bundle, or fascicle. The fascicle itself consists of a number of muscle fibers surrounded by a connective tissue cover named the perimysium. The muscle fiber, an individual muscle cell surrounded by a thin cover of connective tissue (endomysium), which connects the individual fibers within a fascicle, is the next smaller unit of a skeletal muscle. Muscle fibers are cells with delicate membrane, called the sarcolemma and are made up of myofibrils. Myofibrils, by itself are discrete bundles of myofilaments. The repeat unit in this pattern is the basic contractile element of skeletal muscle, the sarcomere (Denoth 2005; Epstein & Herzog 1998).

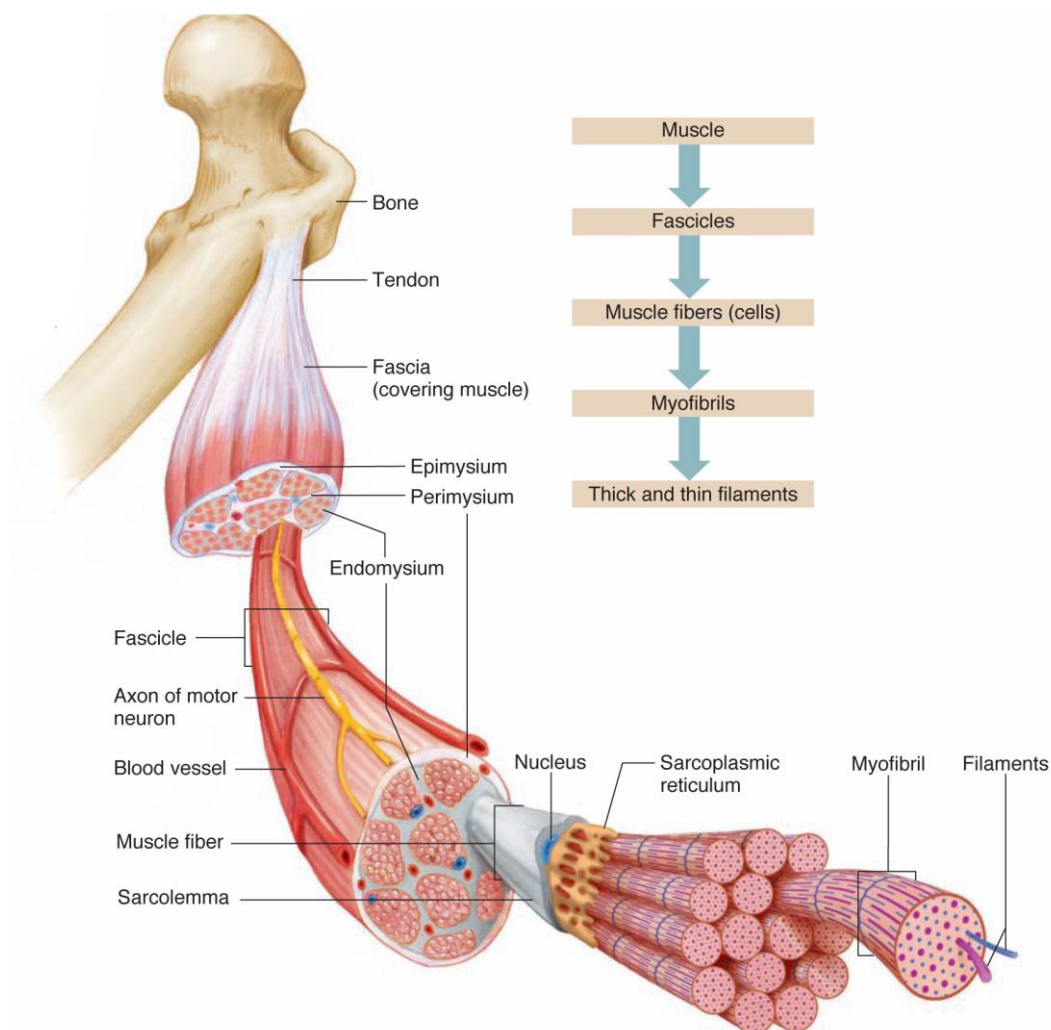


**Figure 2.2: Skeletal muscle, cross section**

*source: Shier, Butler, and Lewis 2003*

Sarcomeres are bordered by Z-lines (Z-discs) that are thin strands of protein extending perpendicular to the long axis of the myofibrils and contain thick and thin filaments (myosin and actin). Z-lines intersect the thin myofilaments at regular intervals.

Thick filaments are typically located in the center of the sarcomere and contain a binding site for actin (thin filament) and an enzymatic site that catalyzes the

hydrolysis of adenosinetriphosphate (ATP), which releases the energy required for muscular contraction. Since the myosin heads have the ability to establish a link between the thick and thin filaments, they have been termed cross-bridges.

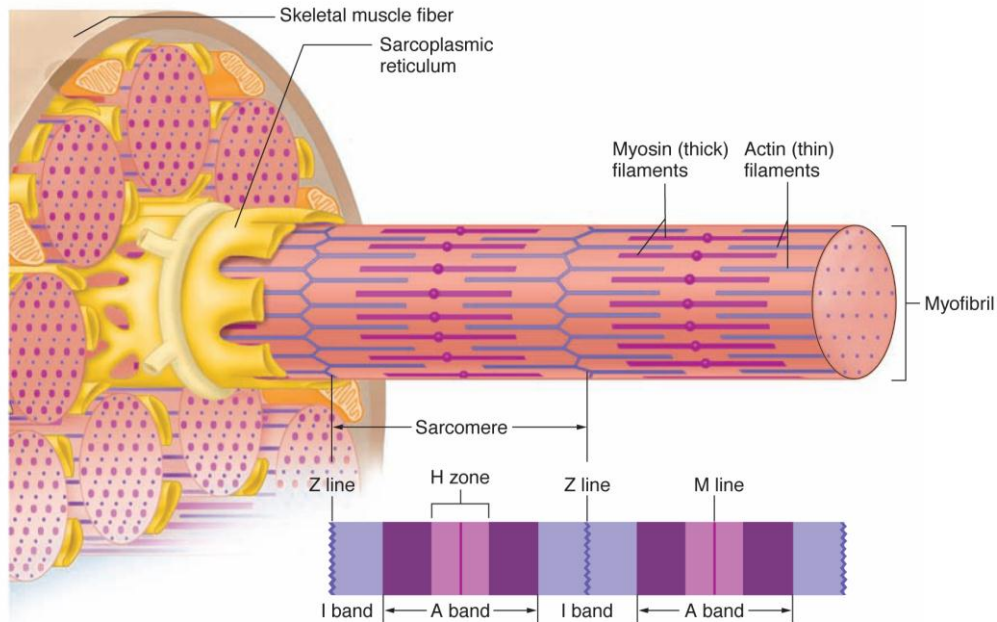


**Figure 2.3: Sarcomere in detail**

*source: Shier, Butler, and Lewis 2003*

Aside from the contractile proteins actin and myosin (thin and thick filaments), sarcomeres of skeletal muscle contain a variety of other proteins. These proteins are associated with structural and passive functional properties, rather than active force production. From a functional point of view, the most important protein is titin. Within the sarcomere, titin spans from the Z-disc to the M-line. The titin protein works as a molecular spring that develops tension when sarcomeres are stretched. The location of the protein prompted the idea that it might stabilize the thick filaments within the center of the sarcomere. Horowitz and colleagues provided evidence for the role of titin in thick filament centring in chemically skinned rabbit psoas fibers (Horowitz et al. 1989; Horowitz & Podolsky 1987; Horowitz & Podolsky 1988).

### 2.3.2 Muscle shapes

The organizational structure of the fibers within a muscle is extraordinary. Skeletal muscles contain fibers from a few millimeters to several centimeters in length which can be arranged either parallel to the longitudinal axis or at a distinct angle to the longitudinal axis of the muscle. The former named parallel or fusiform muscle, the last called pennate muscle. Depending on the number ( $n$ ) of distinct fiber directions, a muscle is called unipennate ( $n = 1$ ), bipennate ( $n = 2$ ), or multipennate ( $n \geq 3$ ). Furthermore the number of heads the muscle is connected to the bone is used for

classification of muscles. For example illustrated by Denoth or Epstein and Herzog, musculus quadriceps femoris, latin for "four-headed muscle of the femur" or the triceps brachii muscle which is latin for "three-headed arm muscle" (Denoth 2005; Epstein & Herzog 1998).

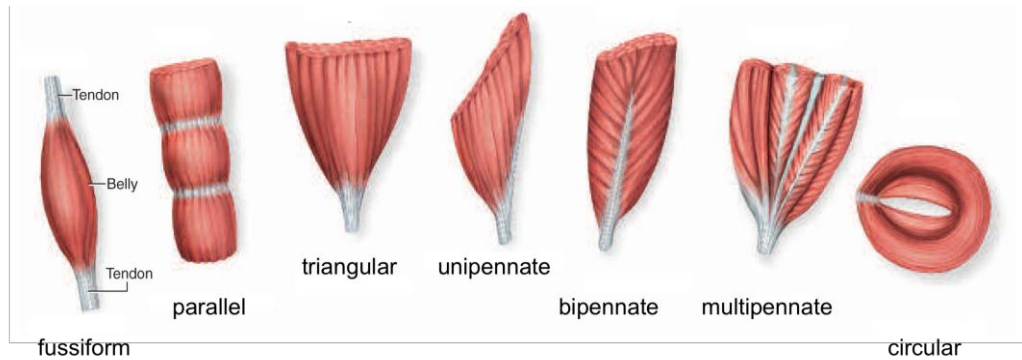


**Figure 2.4: Classification of muscle**  
source: McGraw-Hill 2009

**Fusiform muscles** are thick in the middle (belly) and tapered at each end, descending to the tendon. Example of that type of muscle is the gastrocnemius muscle of the calf.

**Parallel muscles** have a fairly uniform width and parallel fascicles. Some are elongated straps, like the sartorius of the thigh, others are more squarish and called quadrilateral. They can span long distances, e.g. from hip to knee, and shorten more than other muscle types.

**Triangular muscles** are fan-shaped-broad at the origin and converging toward the tendon. Despite their small localized insertation on a bone, triangular muscles are relatively strong because of a large number of fibers in their wider part.

**Pennate muscles** are feather-shaped and their tendon runs the length of the muscle, like the shaft of a feather. As written above, there are three different types of pennate muscles. Depending on the number of sides fascicles approach to the tendon there are: **unipennate**, like the semimembranosus muscle of the thigh, have only one tendon where all fascicles approach from one side; **bipennate** in which fascicles approach the tendon from both sides (e.g. the rectus femoris of the thigh); and **multipennate**, shaped like a bunch of feathers. Pennate muscles generate more force than the other types, because they fit more muscle fibers into a given length of muscle (McGraw-Hill 2009).

### 2.3.3 Muscle force control

Muscles receive the commands for force production from nerves, those who contain afferent and efferent axons. As explained by Epstein and Herzog (Epstein & Herzog 1998) afferent nerves deliver information about the contractile status of the muscle to

the central nervous system (CNS) and efferent nerves, on the other hand deliver action potentials to the muscle for contraction. The primary efferent pathways are called alpha-motorneuron and each alpha motor neuron innervates a group of muscle fibers. One motorneuron and all the muscle fibers it innervates, is called motor unit and is the smallest controlled unit of a muscle. Therefore, all muscle fibers of a motor unit will contract and relax in a synchronized manner.

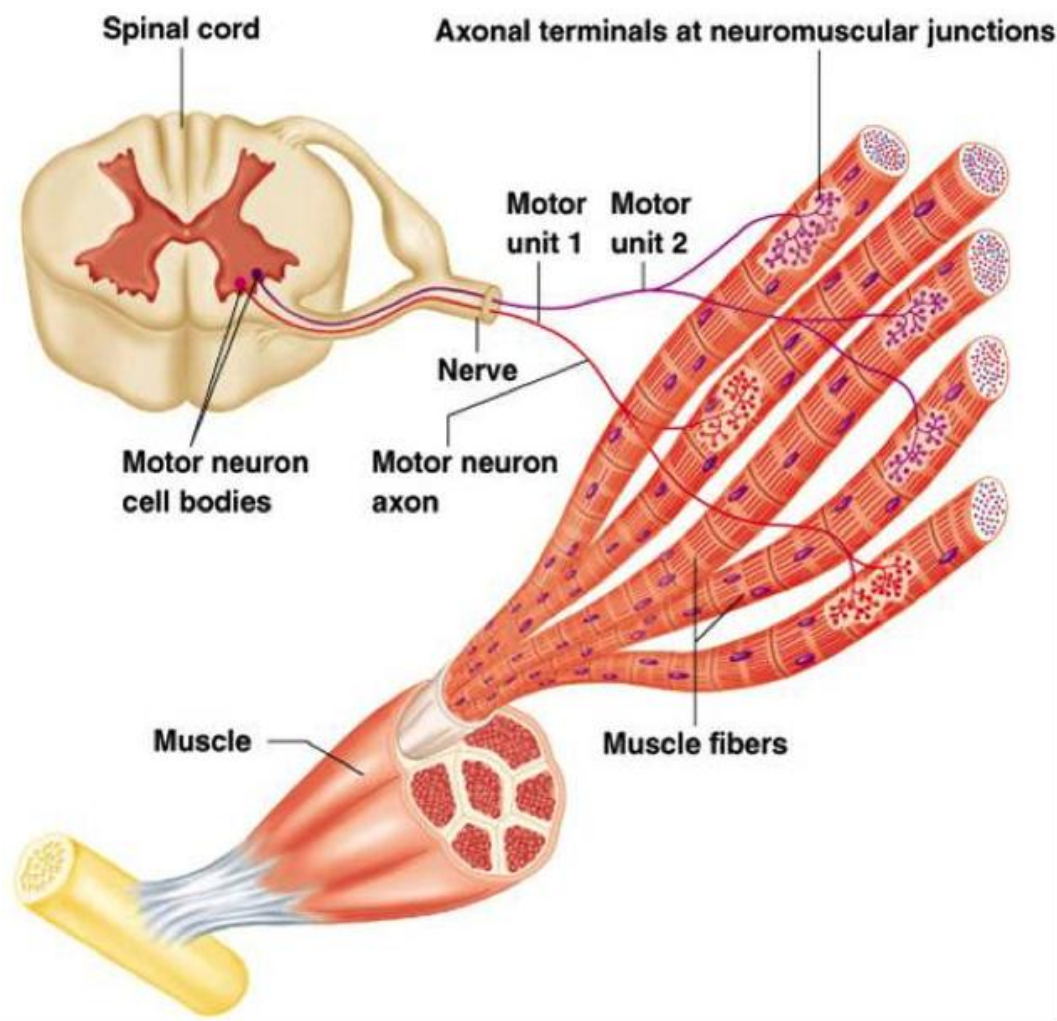


**Figure 2.5: Peripheral nerve / motor unit**

*source: Elaine and Marieb 2001*

There are two different ways to increase the force produced by muscle. First the number of active motor units can be increased and second by increasing the frequency of stimulation to a motor unit.

With external control with electrical stimulation a motor neuron a single action potential is sent to a motor unit, the corresponding force response is a single twitch. If a motor unit will be stimulated with a series of stimulation pulses, it will show a series of individual twitch responses with increasing power output. After stimulation frequency reaches an adequate level, the single twitches will coalesce to a permanent constant contraction also known as tetanus (Figure 2.6).

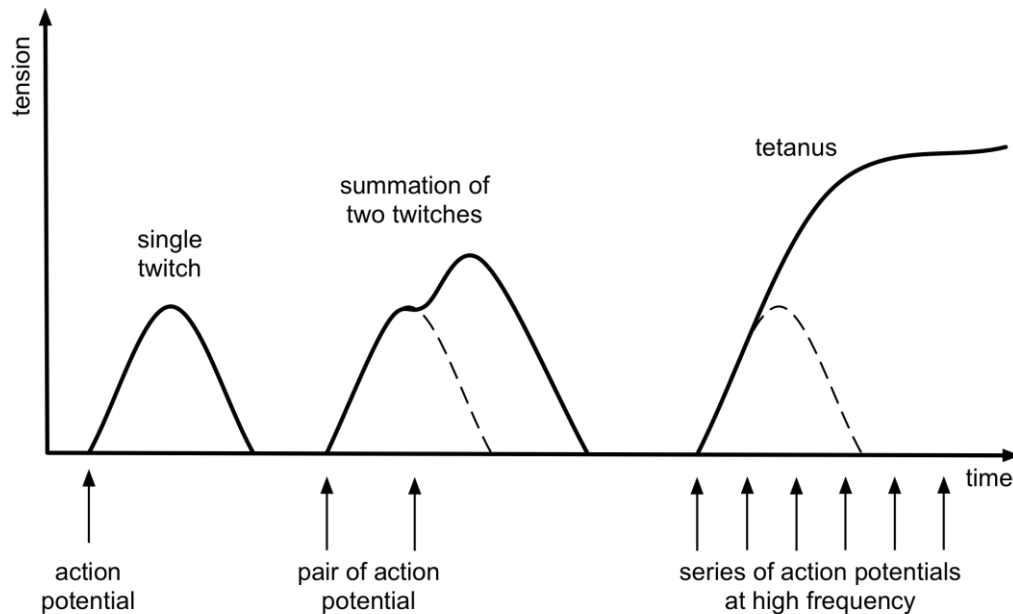


**Figure 2.6: Different force response due to stimulation**  
*adapted by Denoth 2005*

The recruitment order of a muscle, and therefore of motor units, generally follows the “principle of size” (Henneman & Olson 1965; Henneman et al. 1965). Henneman and colleagues showed that during a graded increase of force in a muscle, the small motor neurons innervating the small and slow motor units were recruited first. With increasing force demands, larger motor neurons innervating progressively larger motor units with increasingly fast-type properties were recruited. Therefore, a graded increase in force was accomplished by recruiting the smallest and slowest motor units first and the largest and fastest motor units last.

### 2.3.3.1 Types of exercise, open and closed kinetic chain exercise

Steindler (1955) defined two types of exercise, open kinetic chain exercises (OKCE) and closed kinetic chain exercises (CKCE). He defined a CKCE as an exercise where the distal segment is opposed by considerable resistance. On the contrary, in an OKCE the distal segment is free to move without any external resistance.

Recently CKCE, like leg press exercises are, have been used and recommended on clinical environments e.g. during knee rehabilitations.

### 2.3.3.2 Types of contraction

A muscle produces force and will shorten, when stimulated, provided that shortening isn't prevented by some external constraints.

A shortening contraction is referred to as a *concentric (a)* contraction. If the ends of the muscle are fixed rigidly, there won't be any change of length, the contraction is called *isometric (b)*. When the external force exceeds the isometric force capability of

a contracting muscle, the muscle is forcibly stretched and the resulting contraction is called *eccentric* (c).

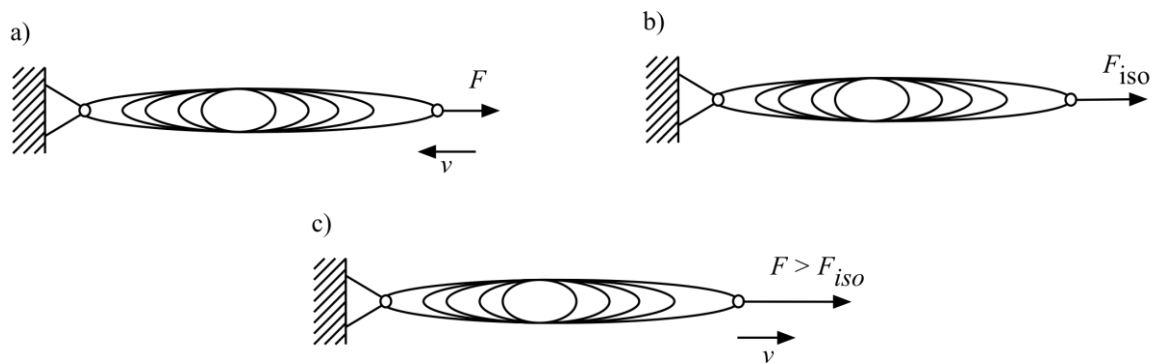


**Figure 2.7: Types of contraction (a) concentric, (b) isometric and (c) eccentric**  
*adapted from Schmiedmayer 2011*

The type of contraction may depend on the level at which it is observed. For example, Gordon and colleagues documented that during an isometric contraction of an isolated fiber, sarcomeres within that fiber may contract concentrically and eccentrically (Gordon et al. 1966). Concentric contraction takes place typically towards the end regions of the fiber, eccentric contractions are noticed in the middle portion of the fiber. For the paper in hand the concentric and eccentric phase is defined by the quadriceps muscle and is shown in Figure 2.8. It is preassigned that the extension of the knee joint is documented as concentric phase and flexion is defined as the eccentric phase of the motion.

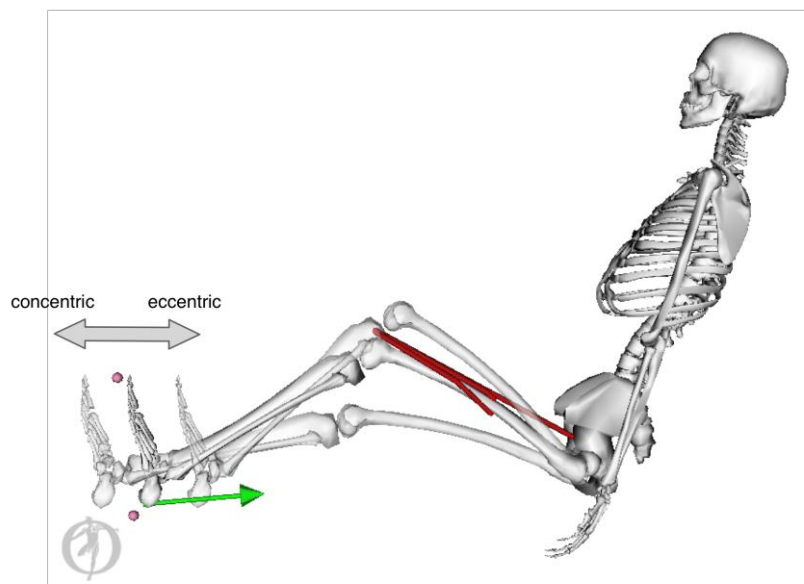


**Figure 2.8: Concentric/Eccentric phase, OpenSim model with quadriceps muscles**  
*source: OpenSim, Model of Simulation*

### Isokinetic - isotonic

During experimental tests it has been found useful to control either the speed or the force of contraction. Movements performed at constant speeds (concentrically or eccentrically) are referred to as *isokinetic*. Contractions performed at a constant resistive force are referred to as *isotonic* (Epstein & Herzog 1998).

#### **2.3.3.3 Vibration stimulation – serial stretch loading, stretch-shortening**

Serial stretch loading applies a series of mechanical stretches to an isotonic contracting muscle or muscle group by moving the joint through a partial or full range of motion (Benn et al. 1998). Other researchers named these observations of body segments periodically subjected to impacts or stretch forces stretch-shortening cycle (SSC). Komi et al. (2000) names walking, running and hopping as typical examples in human locomotion of how external forces (e.g. gravity) lengthen the muscle (Komi 2000). During this lengthening phase the muscle is acting eccentrically, followed by a concentric, shortening action (Komi 2000; Norman & Komi 1979; Komi 1984; Komi & Nicol 2000; Bosco et al. 1998). Also involved in the sequence of muscle function are the important features of preactivation and variable activation. Compared to the isolated concentric action, the purpose of SSC is the enhancement of performance during the final, concentric phase (Komi 2000)

The first part (*forward-backward*) of vibration-proprioceptive stimulation uses this principle in a smaller, modified dimension. So that the length of skeletal muscles changes slightly during vibration and facilitation of excitability of spinal reflex can be elicited (Burke et al. 1996). Rothermuller and Cafarelli suggests that vibration drives alpha-motorneuron via the Ia loop, producing force without descending motor drive (Rothmuller & Cafarelli 1995). Cvecka et al. (2009) reported that tonic vibration reflex includes stimulation of neuromuscular spindles (Cvecka et al. 2009). Resulting in an increase of activated motor units.

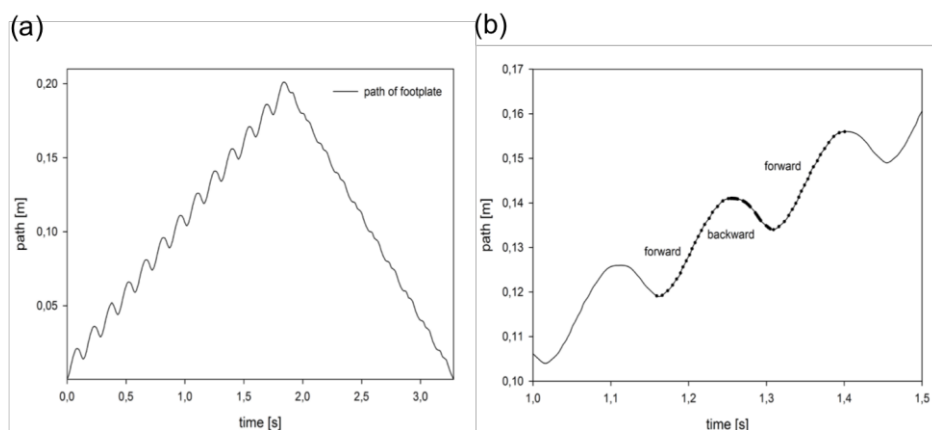


**Figure 2.9: Vibration motion, detail forward-backward-forward**  
*Overview (a) concentric phase in detail (b)*

In the present study, this special stimulation (VIB training) is realized by the computer-controlled, linear motor-powered leg press machine (q.v. 2.2). VIB training induces a series of eccentric muscle tetanic contractions at high frequency.

#### 2.3.3.4 Quick-Release behavior

The second part of the concentric phase (*backward-forward*) may be interpreted as the quick release behavior McMahon explained in his work (McMahon 1984). Before the pedals move away from the body, the muscle is developing a tetanic force ( $T_0$ ) appropriate for its length. After the release, it is no longer held at constant length, but at constant force ( $T$ ).

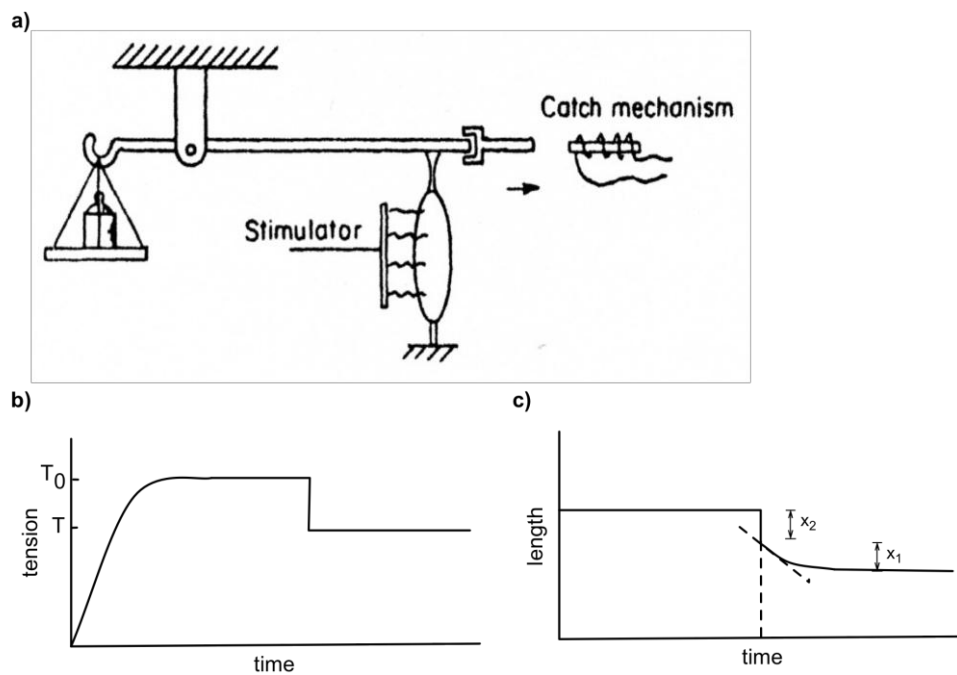


**Figure 2.10: Quick-release, schematic built-up (a), tension (b), length (c)**  
source: McMahon 1984

## 2.4 Muscle Model: Hill and Huxley type model, Thelen2003, Millard2012

The aim of every muscle model is to describe how a muscle behaves under different operating conditions and what this behavior means to the other parts of the system. There are two scientific thoughts within this topic all other models are based on, to describe different and special key aspects in this field.

### 2.4.1 General Muscle Model: Hill and Huxley type model

Compare to the structural classification of Zahalak (Zahalak 1992), muscle models can be categorized as: (i) microscopic models, (ii) fiber models, and (iii) macroscopic models. The boundaries between these groups are not always precise and some models bear characteristics of more than one group. Following Rosen and colleagues the muscle models, which are considered herein, belong to the microscopic (Huxley-Models) and the macroscopic (Hill-Models) category (Rosen et al. 1999). Epstein and Herzog treat those two model types in their book as well, but classify them into phenomenological and structural models (Epstein & Herzog 1998).

Models of Hill, named after Archibald Vivian Hill, are phenomenological in nature. They describe the force behavior of muscles for precisely defined contractile conditions, which are the length and the speed of the muscle during contraction.

Huxley models, named after Andrew Fielding Huxley, and also known as cross-bridge models are structural models, which are based on the assumed interaction of thin (actin) and thick (myosin) myofilaments via cross-bridges and the corresponding ideas of force production in sarcomeres.

Although the fact that cross-bridge models have the advantage of being derived from the fundamental structure of muscle, these models are rarely used in muscle-driven simulations with many muscles because of the many parameters that are difficult to measure (Millard et al. 2013). The main focus will be on Hill's models because they are widely used in muscle-driven simulations (Millard et al. 2013).

#### 2.4.1.1 Hill Type Model

Because mechanical response of skeletal muscles is like the behavior of anelastic materials, rheological models are often used as phenomenological tools to describe them mathematically. These models consist of various arrangements of rheological elements. Rheological elements can be seen as "black box" with a definite deterministic relation between force and elongation history. So e.g., if a force history  $f(t)$  is used as an input, then the displacement  $u(t)$  is obtained uniquely by some mathematical operation characterizing the element, and vice versa. See Epstein and Herzog for more detailed illustration about that (Epstein & Herzog 1998). In many

cases it is convenient to make the force-displacement history relation depend on one or more parameters, e.g. temperature or neural activation.

Most common elements of rheological models are the linear elastic element or spring, Figure 2.11 a) and the linear viscoelastic element or dashpot, Figure 2.11 b).

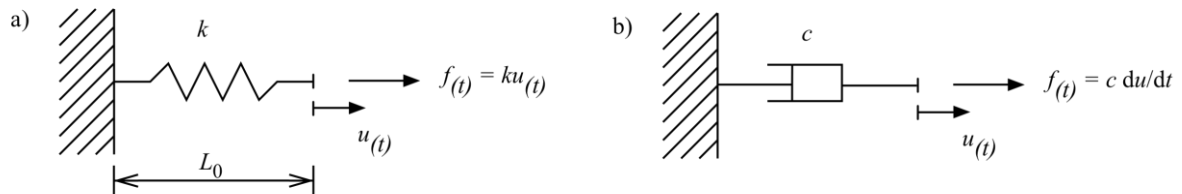


**Figure 2.11: Linear spring (a) and linear dashpot (b)**

*source: Epstein and Herzog 1998*

The spring is characterized by an unstretched length,  $L_0$  and a stiffness constant,  $k$ . At any instant, the force is proportional, with the constant of proportionality being  $k$ , to the displacement measured from the unstretched configuration.

The dashpot is characterized by a viscous constant,  $c$  whereby the force at any instant of time is proportional to the instantaneous value of the velocity  $\dot{u} = \frac{du}{dt}$ .

There are more than these two examples of rheological elements. Others are e.g. nonlinear springs and dashpots, dry-friction elements, thermo elastic elements, and purely contractile elements as you can find in Epstein's and Herzog's publication.

Combination of rheological elements can be in series or in parallel. When combined in series, the force is always the same in both elements, while the elongations of every single item sum to the total elongation of the combined element (see Figure 2.1). In a parallel arrangement, the elongations are the same and the forces are added.

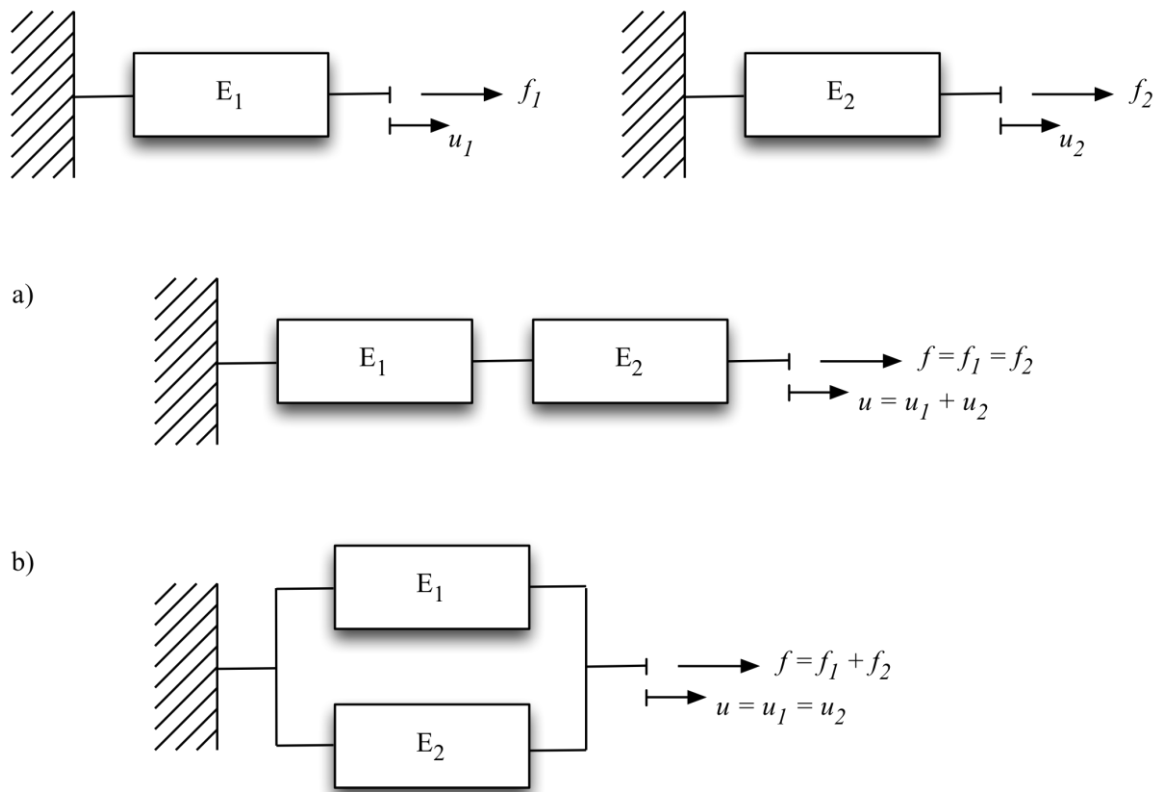


**Figure 2.12: Combination of rheological elements**

*source: Epstein and Herzog 1998*

In 1938, Hill concluded, that skeletal muscle may be seen as a two-component system, consisting of an undamped purely elastic element in series with a contractile element (Hill 1938). The combination of Hill's two-component model with an extra elastic element in parallel shown in Figure 2.13 is known as Hill's three-element model and as it is shown, consisting of a contractile element (CE), a series-elastic ( $k_s$ ) and a parallel-elastic ( $k_p$ ).

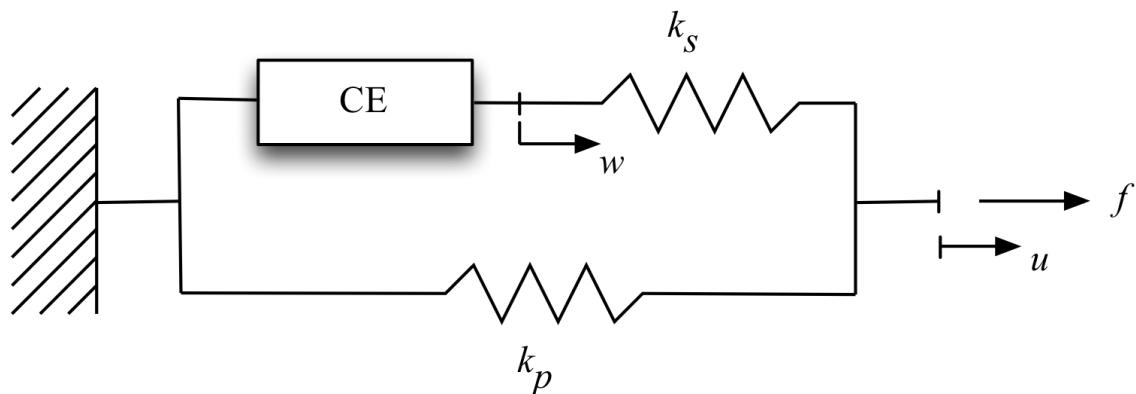


**Figure 2.13: Hill's three-element model, Herzog & Epstein**

*CE represents the contractile element,  $k_p$  the parallel-elastic and  $k_s$  the series-elastic element, source: Epstein and Herzog 1998*

The properties of the contractile element (CE) were governed by the Hill equation (Hill 1938).

$$(F + a)(v + b) = b(F_0 + a) \quad (2.1)$$

Where  $F$  is the instantaneous force,  $F_0$  represents the maximum isometric force generated in the muscle at optimal sarcomere length,  $v$  is the shortening velocity and the two constants  $a$  and  $b$  in the dimensions of force and velocity. Solving for  $F$ , equation (2.1) becomes.

$$F = \frac{F_0 b - av}{b + v} \quad (2.2)$$

For shortening at the maximal velocity,  $v_0$ , the force  $F$  becomes zero, and equation (2.2) may be written for this special case as

$$\frac{a}{F_0} = \frac{b}{v_0} = 0.25 \quad (2.3)$$

$a/F_0$  and  $b/v_0$  are dimensionless quantities approximately equal to 0.25 for many muscles across species and temperatures (Hill 1970). Data concerning force-velocity descriptions of human skeletal muscles are rare. Researchers determined force-velocity properties of isolated fiber bundle segments from human fast and slow-twitch muscles and found values of  $a/F_0$  of 0.25 and 0.15, respectively (Faulkner et al. 1986; Faulkner et al. 1980).

Researchers tried to associate the theoretical elements of the Hill model with a biological structure but had to accept, that this association is not as trivial as it might appear. One assumption is that the series elastic element represents the tendon, the aponeurosis is modeled by the parallel-elastic element and the contractile element stands for the interaction between actin and myosin. However, it has been shown that boundaries between the three elements used in Hill's model are not that sharp. The basic difficulties associated with Hill type models are, the division of the force between the parallel elastic and the contractile element, and the separation of elongations between the series elastic and the contractile element.

Due to the fact that the characteristic equation is only valid for restricted contractile conditions like maximal activation and shortening contraction at or near the optimal length validation of the Hill type model is limited.

Hill models do not provide insight into the mechanisms of force production, they describe the approximate behavior of muscles for certain contractile conditions. Because of mathematical simplicity, the Hill model is used more frequently in biomechanical models of musculoskeletal systems than any other model.

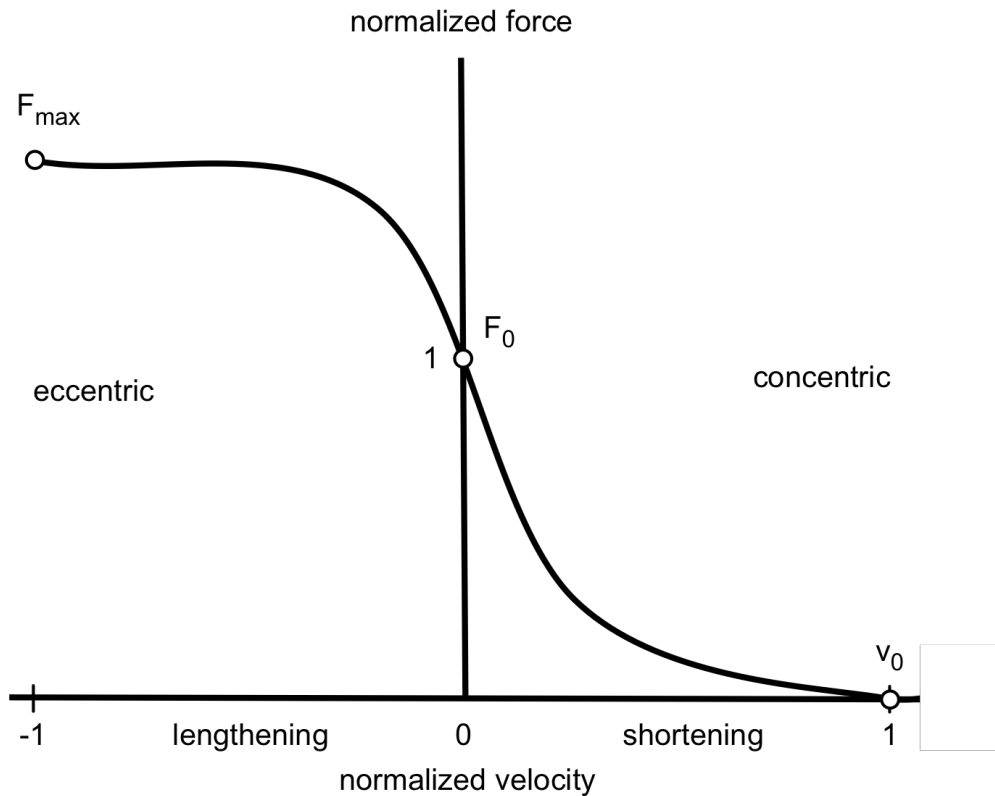


**Figure 2.14: Force-velocity relation of skeletal muscle**

*F<sub>0</sub> represents the maximum isometric force at optimal sarcomere length*  
 adapted from Denoth 2005; Epstein and Herzog 1998; Reeves et al. 2009

#### 2.4.1.2 Huxley Type Model

*“There are side projections (cross-bridges) arising from the thick (myosin) filaments which attach to specialized sites on the thin (actin) filaments, and when attached, the cross-bridges pull the thin past the thick filaments.”* (Epstein & Herzog 1998)  
 That’s the most simplistic form of the cross-bridge model introduced by Andrew Fielding Huxley (Huxley 1957).

As written above, the Huxley type model, or cross-bridge model focus on the contractile element and has been the model of choice when concerned with the biophysical events of muscular force production. They integrate the known structural properties of skeletal muscle with the known mechanical and biochemical aspects of contraction.

In Figure 2.15 the cross-bridge theory by Huxley et al. is graphically presented.

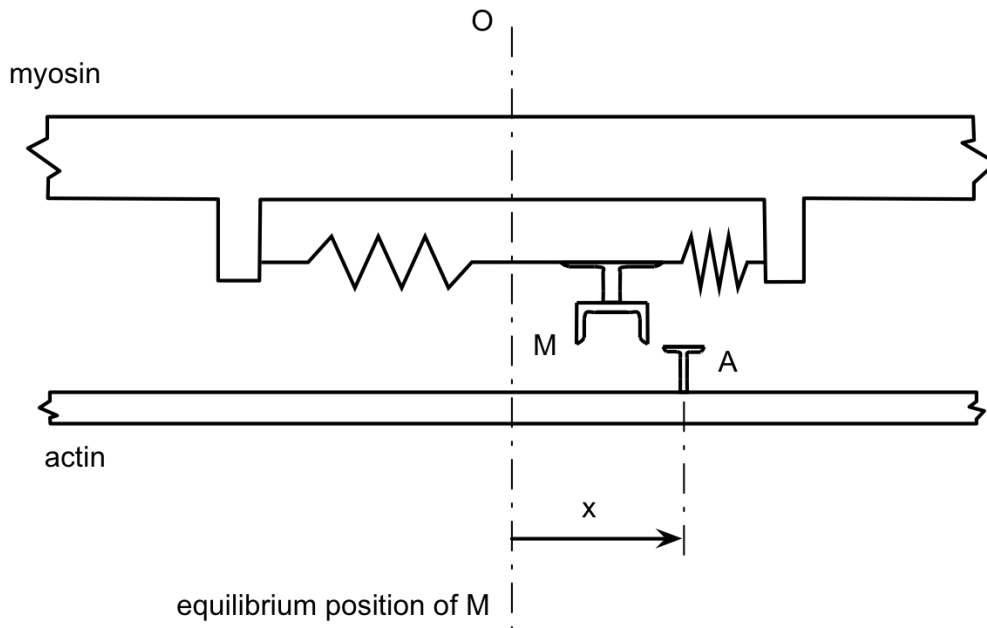


**Figure 2.15: Huxley's cross-bridge model**

*adapted from A. F. Huxley and Niedergerke 1954; H. Huxley and Hanson 1954*

The thick filaments, called myosin and the thin ones, called actin can slide parallel to each other in a one dimensional rectilinear motion. Huxley assumed that the myosin filament is endowed with side-pieces which can slide along the main backbone of the filament, the extent of movement being limited by an elastic connection (Huxley 1957). Following Epstein's and Herzog's population, these movements are denoted by  $M$ , and the total spring constant by  $k$ . The  $M$ -pieces may establish a chemico-mechanical bridge between the filaments by attaching themselves with specific sites,  $A$ , fixed along the adjacent actin filaments. To disconnect these attachments a chemical reaction is needed – hydrolysis of Adenosintriphosphat (ATP) into Adenosindiphosphat (ADP). The unattached sliding element  $M$  oscillates between the equilibrium position  $O$  and the potential attachment site  $A$  and is referred to as distance  $x$ . The probability of attachment is denoted  $f(x)$  and those that the connection will be broken as  $g(x)$ . As Huxley considered a large number of identical  $M - A$  pairs, the proportion  $n_{(t)}$  of attached pairs will be a function of time alone. When Huxley rewrote it in the following way to obtain a formula for the rate of change of  $n_{(t)}$  the Huxley equation is the result.

$$\frac{dn}{dt} = (1 - n)f(x) - ng(x) \quad (2.4)$$

When we look at the special moment of dynamic equilibrium ( $dn/dt = 0$ ) the following value for the proportion of attached pairs will result:

$$n_{eq} = \frac{f(x)}{f(x) + g(x)} \quad (2.5)$$

In order to solve equation (2.4) for  $n_{(t)}$ , it is necessary to specify the global relative motion  $x = x_{(t)}$ , and the initial condition  $x_0 = x_{(0)}$ . Therefore the following integration is needed.

$$x_{(t)} = x_{(0)} + \int_0^t v_{(\tau)} d\tau \quad (2.6)$$

The rate constants of the chemical reactions associated with attachment and detachment of  $M - A$  pairs are represented by the distributions  $f_{(x)}$  and  $g_{(x)}$ , respectively. When  $A$  is to the left of  $M$ ,  $f_{(x)}$  vanishes and  $g_{(x)}$  attains a very large constant value  $g_0$ . Contrary, when  $A$  is to the right of  $M$ , it is assumed that both  $f_{(x)}$  and  $g_{(x)}$  increase linearly,  $f_{(x)}$  being truncated at a value  $x = h$ , representing the range of bonding ability.

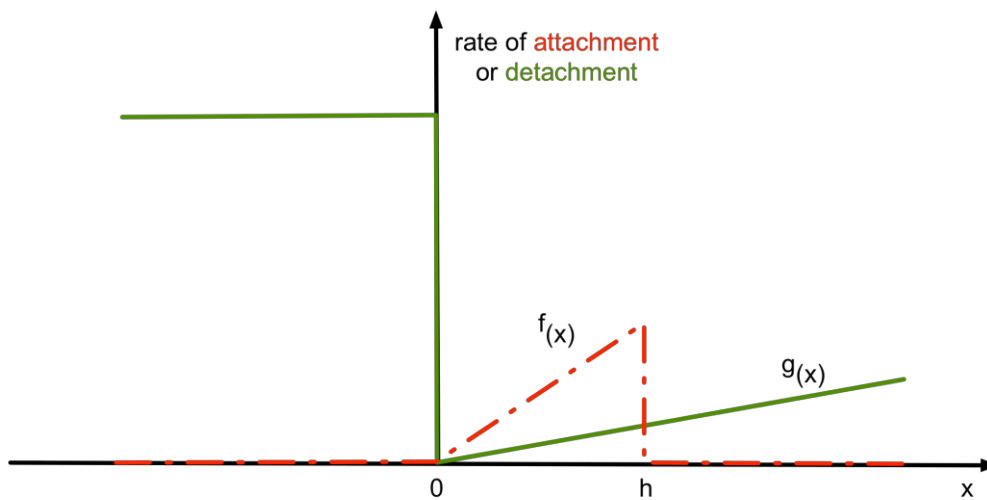


**Figure 2.16: Huxley's probability distributions**

*distribution  $f_{(x)}$  represents the rate of attachment,  $g_{(x)}$  the rate of detachment  
adapted from Epstein and Herzog 1998; A. F. Huxley and Niedergerke 1954*

Because today's general knowledge of the chemical reactions that take place between actin and myosin is greater than in the fifties, researchers know that Huxley's statements aren't made to last. But they are still, from a non-molecular view considered valid (Denoth 2005).

## 2.4.2 OpenSim Muscle Models: Thelen2003, Millard2012

In muscle-driven simulations a model of musculotendon contraction dynamics is used to determine muscle lengths ( $l^M$ ), velocities ( $v^M$ ), and forces ( $f^M$ ) from neural excitations ( $u$ ), generalized coordinates ( $q$ ), and generalized speeds ( $\dot{q}$ ). Muscle activations ( $a$ ) are determined by a model of activation dynamics from neural excitations ( $u$ ), while musculotendon lengths and velocities ( $l^{MT}$  and  $v^{MT}$ ) are determined from the generalized coordinates and speeds ( $q$  and  $\dot{q}$ ) by a musculoskeletal model. The results of the activation dynamics and the

musculoskeletal model are input for the musculotendon contraction dynamics model to produce a forward simulation of muscle length ( $l^M$ ), velocities ( $v^M$ ), and forces ( $f^M$ ) (Millard et al. 2013).

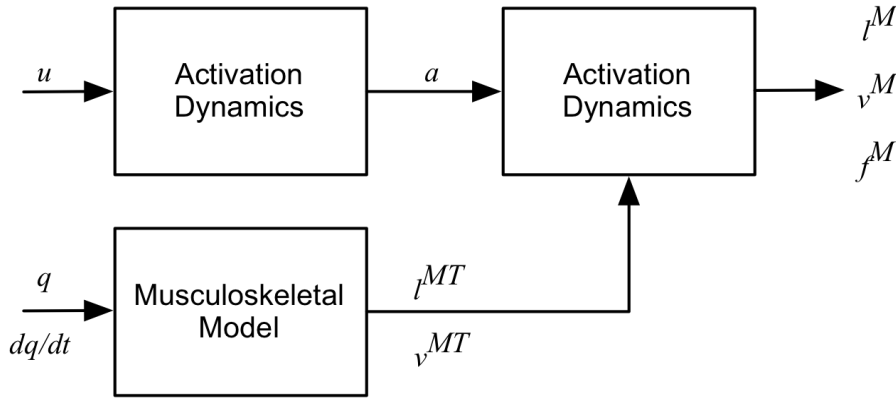


**Figure 2.17: Muscle-driven simulations, workflow**  
adapted from Millard et al. 2013

Muscle models can be seen as an algorithm transforming muscle activation into muscle force. The activation dynamic model used by OpenSim is a first-order dynamic model based on the work of Thelen (Darryl G Thelen 2003) and Winters (Winters 1995) and has been modified to avoid a numerical singularity that occurs when the activation is zero. The differential equation representing the first-order model is shown in (2.7).

$$\frac{da}{dt} = \frac{u - a}{\tau(a, u)} \quad (2.7)$$

An idealized muscle excitation signal ( $u$ ), a dimensionless quantity between 0 (no excitation) and 1 (full excitation), is used as the input to each of the muscle and is related to the muscular activation ( $a$ ) by a non-linear first order differential equation (2.8), where  $\tau(a, u)$  is a time constant that varies with activation level and whether the muscle activation level is increasing or decreasing (Winters 1995).

$$\tau(a, u) = \begin{cases} t_{act}(0.5 + 1.5a) & : u > a \\ t_{deact}/(0.5 + 1.5a) & : u \leq a \end{cases} \quad (2.8)$$

Activation and deactivation time constants can be assumed to be 10 and 40 ms, respectively (Winters & Woo 1990; Zajac 1989).

#### 2.4.2.1 Thelen 2003 Muscle Model - OpenSim

Thelen (D G Thelen 2003) modified the muscle model created by Delp (Delp et al. 1990) in order to follow the documented changes in the mechanical output of skeletal muscle with aging. For this reason, Thelen uses a standard equilibrium muscle model based on Hill's three element model (Figure 2.18) where the generated muscle force is a function of the activation value, the normalized length of the muscle unit, and the

normalized velocity of the muscle unit. To characterize each muscle, parameters like maximum isometric force, optimal muscle fiber length, tendon slack length, maximum contraction velocity, and pennation angle are used (Thelen 2003).

The functions describing the force generated by a muscle as its length varies are called the active length curve for the contractile element and the passive length curve for the parallel element.

Thelen simplified the model into a Gaussian portion representing the active force-length relationship, and an exponential portion for the passive force-length relationship of the muscle. The Gaussian function is expressed mathematically by equation (2.9) where  $f_l$  is the normalized force  $F^M/F_0^M$ ,  $\bar{L}^M$  is the normalized muscle fiber length, and  $\gamma$  is a shape factor. For the shape factor  $\gamma$  a value of 0.45 was selected, which approximates the force-length relationship of individual sarcomeres (Gordon et al. 1966).

$$f_l = e^{-\frac{(\bar{L}^M - 1)^2}{\gamma}} \tag{2.9}$$

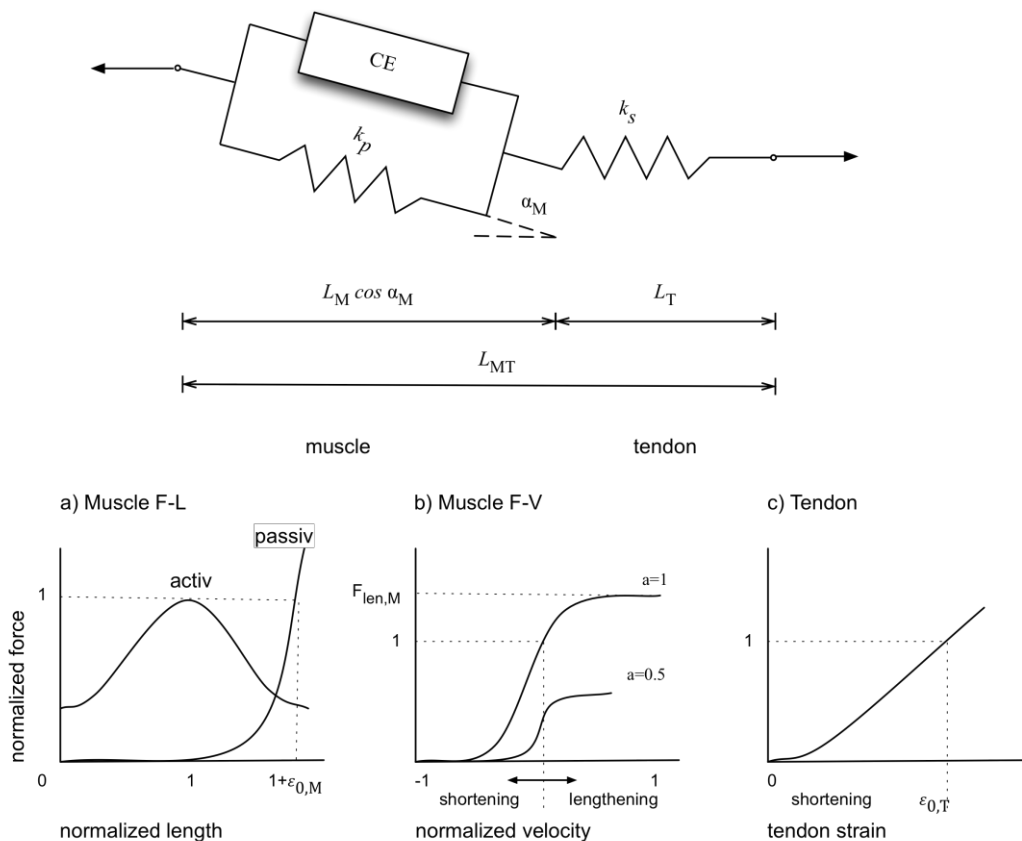


**Figure 2.18: Hill's three element model, Thelen 2003**

(a) muscle force-length behavior, (b) muscle force-velocity behavior, (c) tendon behavior  
source: Thelen 2003

The exponential function, shown in the equation below (2.10), where  $\bar{F}^{PE}$  is the normalized passive muscle force,  $k^{PE}$  is an exponential shape factor, and  $\varepsilon_0^M$  is the passive muscle strain due to maximum isometric force represents the passive length curve. Thelen set the shape factor  $k^{PE}$ , equal for young and old adults to five, while he reduced  $\varepsilon_0^M$  from 0.60 for young adults (Winters 1995) to 0.50 for older adults to account for the relative increase in passive stiffness (Thelen & Anderson 2006).

$$\bar{F}^{PE} = \frac{e^{\frac{k^{PE}(\bar{L}^M - 1)}{\varepsilon_0^M}} - 1}{e^{k^{PE}} - 1} \quad (2.10)$$

Representing the force-strain relationship of tendon an exponential function is used for the initial nonlinear toe region followed by a linear function thereafter.

$$\bar{F}^T = \begin{cases} \frac{\bar{F}_{toe}^T}{e^{k_{toe}} - 1} (e^{k_{toe} \varepsilon^T / \varepsilon_{toe}^T} - 1), & \varepsilon^T \leq \varepsilon_{toe}^T \\ k_{lin}(\varepsilon^T - \varepsilon_{toe}^T) + \bar{F}_{toe}^T, & \varepsilon^T > \varepsilon_{toe}^T \end{cases} \quad (2.11)$$

$\bar{F}^T$  is the tendon force normalized to maximum isometric force,  $\varepsilon^T$  is the tendon strain,  $\varepsilon_{toe}^T$  is the tendon strain above which the tendon exhibits linear behavior,  $k_{lin}$  is a linear scale factor. For  $k_{toe}$  a value of 3 was used and the transition from nonlinear to linear behavior was prescribed to occur for normalized tendon forces greater than  $\bar{F}_{toe}^T = 0.33$  (Proske & Morgan 1987). Thelen also used the following values for  $\varepsilon_{toe}^T = 0.609\varepsilon_0^T$ ,  $k_{lin} = 1.712/\varepsilon_0^T$ .

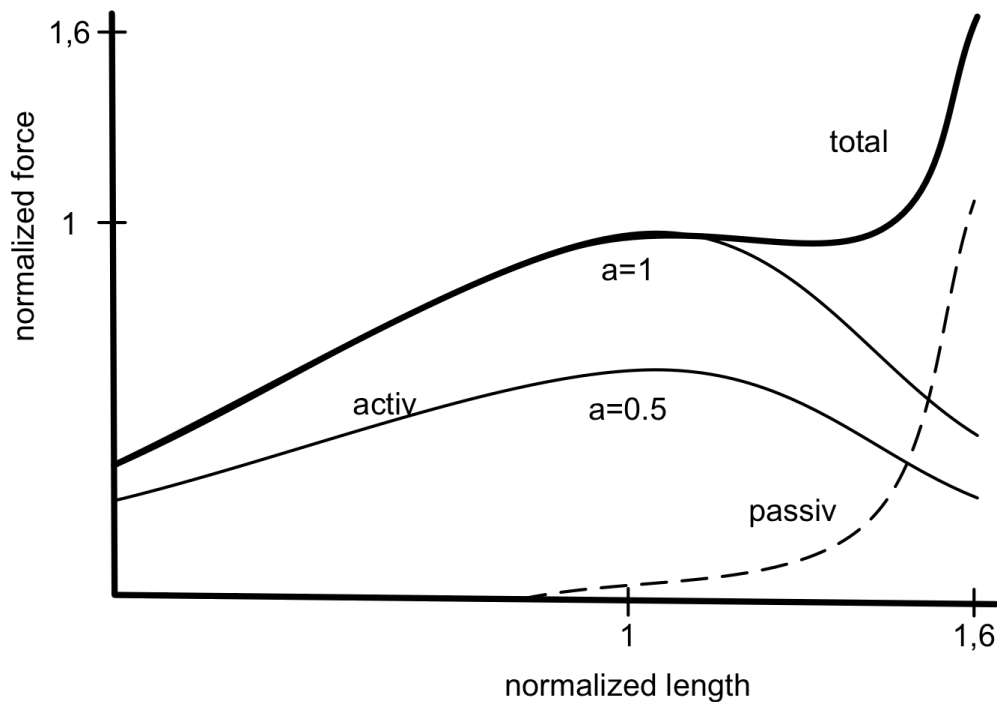


**Figure 2.19: Summation of active and passive muscle force**  
*a* representing the level of activation (0,5 and 1)  
 adapted from Thelen 2003; Wilkie 1968

As written at the beginning the aim of Thelen and colleagues was to develop a muscle model where age-based modifications of the parameters are simple and more transparent. Table 2.2 gives a summary of these parameters.

	$t_{deact}$ [ms]	$V_{max}^M$ [L <sub>0</sub> <sup>M</sup> /s]	$\varepsilon_0^M$	$\bar{F}_{len}^M$
young (30 yrs.)	50	10	0.6	1.4
old (70 yrs.)	60	8	0.5	1.8

**Table 2.2: Thelen2003 muscle-tendon parameters**  
source: Thelen 2003

### 2.4.2.2 Millard 2012 Muscle Modell – OpenSim

Millard’s work based on the muscle model developed by Thelen and colleagues (Darryl G Thelen 2003) described in 2.4.2.1, and results in three musculotendon models, the equilibrium musculotendon model, a damped equilibrium model and a rigid-tendon model. Millard compute, in contrary to Thelen, the activation  $a$  from neural excitation  $u$  in a modified way as shown in the following equations (2.12) and

(2.13):

$$\hat{a} = \frac{a - a_{min}}{1 - a_{min}} \tag{2.12}$$

$$\dot{a} = \frac{u - \hat{a}}{\tau} \tag{2.13}$$

$$\tau(a, u) = \begin{cases} t_{act}(0.5 + 1.5\hat{a}) & : u > \hat{a} \\ t_{deact}/(0.5 + 1.5\hat{a}) & : u \leq \hat{a} \end{cases} \tag{2.14}$$

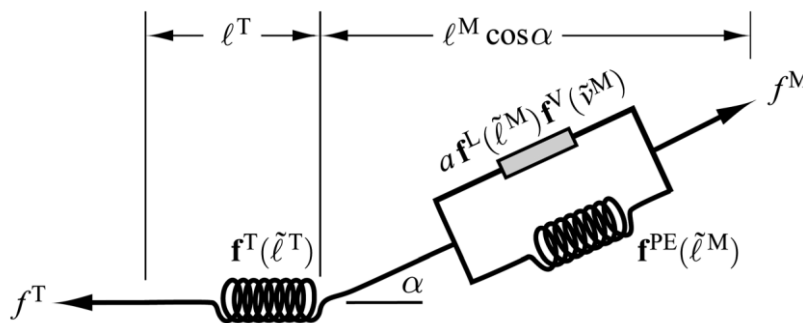


**Figure 2.20: Schematic of the equilibrium musculotendon model of Millard**  
source: Millard et al. 2013

Compared to equation (2.8) the conventional activation  $a$  has been modified, so that activation smoothly approaches an adjustable lower bound ( $a_{min}$ ) and avoid numerical singularity in equilibrium musculotendon model.

### **Millard 2012, equilibrium musculotendon model**

Like Thelen, Millard took Hill's three element model (Figure 2.18) for his equilibrium model illustrated in Figure 2.20, where musculotendon actuators consist of an active contractile element, a passive elastic element, and an elastic tendon. The active force a muscle can develop varies nonlinearly with its length and is represented by the active-force-length curve shown in Figure 2.18 (a), named  $f_{(l^M)}^L$ . In the work of Millard - Millard used the tilde to denote force, velocities, muscle lengths, and tendon lengths that are normalized by  $f_0^M$ ,  $v_{max}^M$ ,  $l_0^M$ , and  $l_s^T$ , respectively (Millard et al. 2013). The force-velocity curve  $f_{(v^M)}^V$  shown in Figure 2.18 (b) represents the force developed by muscle during non-isometric contraction. There is also a force developed when the muscle is stretched beyond a threshold length, regardless there is muscle activation, which Millard named  $f_{(l^M)}^{PE}$  and that is represented by the passive-force-length curve - Figure 2.18 (a). For the equilibrium model, the following equation uses these curves to compute muscle force ( $f^M$ ):

$$f^M = f_0^M \left( a f_{(l^M)}^L f_{(v^M)}^V + f_{(l^M)}^{PE} \right) \quad (2.15)$$

with  $a$  as the muscle activation, which ranges from  $a_{min}$  to 1 and  $f_0^M$  as peak value at a length of  $l_0^M$ .

Because muscle attaches to bone through tendon, force developed by this connector has to be considered. Millard and others modeled the tendon as a non-linear elastic element developing force according to the tendon-force-length curve  $f_{(l^T)}^T$  shown in Figure 2.18 (c) and equation (2.16).

$$f^T = f_0^M f_{(l^T)}^T \quad (2.16)$$

Muscle fibers attach to tendon at a pennation angle ( $\alpha$ ), force transmitted to tendon is scaled. It is assumed, that tendon is elastic and the mass of the muscle is negligible, so muscle and tendon force must be in equilibrium (Millard et al. 2013).

$$f^M \cos \alpha - f^T = 0 \quad (2.17)$$

So equation (2.15) results in

$$f_0^M \left( a f_{(l^M)}^L f_{(v^M)}^V + f_{(l^M)}^{PE} \right) \cos \alpha - f_0^M f_{(l^T)}^T = 0 \quad (2.18)$$

During forward-dynamic simulations, the force generated by a musculotendon actuator must be calculated given the length ( $l^M$ ), velocity ( $v^M$ ), and activation ( $a$ ) of the muscle. Because multiple combinations of muscle length and velocity will satisfy the equation shown in (2.18) it cannot be used to solve the muscle force. Millard and colleagues followed the idea of Zajac and found a unique solution by solving

equation (2.18) for the normalized muscle velocity ( $\tilde{v}^M$ ) to obtain an ordinary differential equation, which can then be integrated to simulate muscle contraction (Millard et al. 2013; Zajac 1989).

$$\tilde{v}^M = f_{inv}^V \left( \frac{f_{(\tilde{l}^M)}^T / \cos \alpha - f_{(\tilde{l}^M)}^{PE}}{a f^L(\tilde{l}^M)} \right) \quad (2.19)$$

Where  $f_{inv}^V$  represents the inverse of the force-velocity curve and to avoid numerical singularities the quantities causing singularities are altered so that singularities are approached but never reached. These quantities are:  $\alpha < 90^\circ$ ,  $a > 0$ ,  $f^L(\tilde{l}^M) > 0$ , and  $\partial f^V(\tilde{v}^M) / \partial \tilde{v}^M > 0$ . Although these modifications, simulation time is slowed down enormous. Because of that researchers defined lower bounds of  $a \geq 0.01$  and  $f^L(\tilde{l}^M) > 0.1$  and they use a unilateral constraint on muscle length to prevent the muscle from becoming unrealistically short (2.20).

$$\tilde{v}^M = \begin{cases} 0 & \text{if } \tilde{l}^M \leq \tilde{l}_{min}^M \text{ and } \tilde{v}^{M*} < 0 \\ \tilde{v}^{M*} & \text{otherwise} \end{cases} \quad (2.20)$$

In equation (2.20)  $\tilde{v}^{M*}$  is a candidate value for  $\tilde{v}^M$  computed using equation (2.19) and  $\tilde{l}_{min}^M$  is the minimum permissible muscle length which is the greater of the minimum active muscle length and the length of the muscle when it is pennated by  $84.26^\circ$ , which Millard and colleagues defined as maximum pennation angle. Higher angles increase simulation time without improving accuracy and equation (2.19) becomes numerically stiff (Millard et al. 2013).

### **Millard 2012, damped musculotendon model**

Another way to avoid singularities of equation (2.18) is realized by introducing a damper element (with damping coefficient  $\beta$ ) in parallel with the contractile element. Like in the equilibrium model the maximum pennation angle is limited. The damped equilibrium musculotendon model, equation (2.21), generates force profiles that are similar to those generated by the equilibrium musculotendon model in equation (2.18) but in a fraction of the simulation time.

$$f_0^M \left( a f_{(\tilde{l}^M)}^L f_{(\tilde{v}^M)}^V + f_{(\tilde{l}^M)}^{PE} + \beta \tilde{v}^M \right) \cos \alpha - f_0^M f_{(\tilde{l}^M)}^T = 0 \quad (2.21)$$

### **Millard 2012, rigid-tendon musculotendon model**

For modeling simplification Millard et al. argued that some tendons are so stiff that they can be treated as inextensible. Because of that, they replaced the tendon spring in Figure 2.20 with an inextensible cable. This modification makes it possible to determine the muscle length ( $l^M$ ) and velocity ( $v^M$ ) from the musculotendon length

( $l^{MT}$ ) and velocity ( $v^{MT}$ ) and compute the force generated by the muscle directly with equation (2.22) with the constraint that the force generated by a muscle can only be positive.

$$f^{M*} = f_0^M \left( a f_{(\tilde{i}^M)}^L f_{(\tilde{v}^M)}^V + f_{(\tilde{i}^M)}^{PE} + \beta \tilde{v}^M \right) \cos \alpha \quad (2.22)$$

## 2.5 Electromyography and joint angle measurements

**Electromyography** (EMG) is an electrical recording and analysis of muscle activity. EMG provides an easy way to access the physiological processes that cause the muscle to generate force or to produce movements; it visualizes the change of electrical potential of the muscle as function of time.

Applying electrodes on the surface of the skin may result in detecting signals of synchronous activation of groups of muscle fibers not only of a specific muscle or fiber. To receive the best quality of EMG signals, researchers should pay attention to the right placement and orientation of the sensors.

From the point of signal quality and signal stability EMG electrodes should be placed on the midline of the belly of the muscle between the nearest innervation zone and the myotendinous junction. DeLuca (1997) states that at this location the EMG signal with the greatest amplitude will be detected.

Referred to DeLuca's publication the best results of EMG recordings will be achieved when electrodes are placed approximately perpendicular to the length of the muscle fibers. A detailed description of the placement of EMG-electrodes during our tests will be given in chapter 3.2.1 below.

A **goniometer** is an instrument that measures an angle between two levers, e.g. the angle of the knee joint during leg press exercises. In general the sensor consists of two small plastic blocks, which are connected by a spring. Within this spring there are two pairs of thin resistor wires that are orthogonally arranged along a flexible steel wire and so constituting two strain gauges for detecting changes in two directions. The principle is based on the deformation of the strain gauges, which affect the electric current passing through the resistor wires. This change of the electric current is proportional to the angle between the two blocks, e.g. the flexion angle of the knee joint. More details about the measurement principle of the goniometer see (Rowe et al. 2001)

## 2.6 Simulation Software – OpenSim 3.2

OpenSim is a freely available open-source software package, developed by the University of Stanford and as a part of and founded by the Simbios National Center for Biomedical Computing through the National Institutes of Health and the NIH Roadmap for Medical Research. Simtk.org serves as a public repository for data, models, and computational tools related to physics-based simulation of biological structures (Anderson et al. 2010).

The software provides a platform on which the biomechanics community can build, exchange, and analyze computer models of the musculoskeletal system and dynamic simulations of movement. Community members set up a library of simulations that can be exchanged, tested, analyzed and improved through multi-institutional collaboration.

The core software is written in C++, and the graphical user interface (GUI) is written in Java. Open-source, third party tools are used for some basic functionality. The graphical user interface (GUI) provides access to key functionality, in more detail see the publication of Delp et al. (2007).

The GUI includes a suite of tools for analyzing musculoskeletal models, generating simulations, and visualizing results (Figure 2.21). Models of many different musculoskeletal structures (e.g., lower extremity, full body model, etc.) can be loaded, viewed and analyzed.

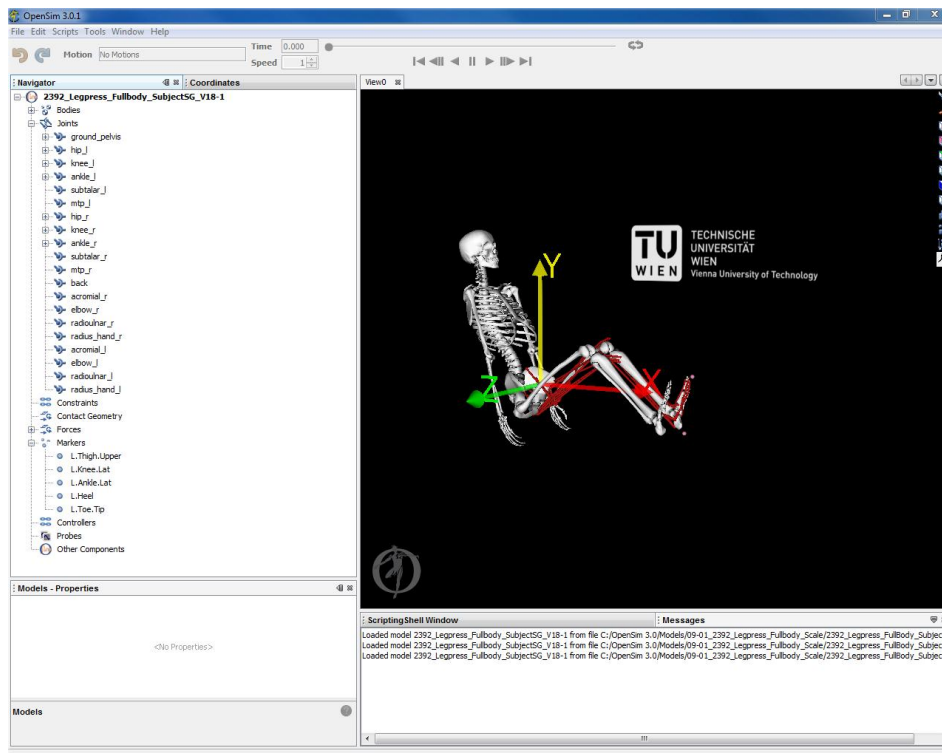


**Figure 2.21: OpenSim – Graphic User Interface (GUI)**  
*source: OpenSim 3.2*

The following chapter will give a brief summary of what the main fields of application of OpenSim are, how the software works and what mathematical sets are met. Full and detailed illustration of the OpenSim-software will give Anderson's paper (Anderson et al. 2010) and Jennifer Hicks's User's Guide (Hicks 2011).

### 2.6.1 Modeling of the human musculoskeletal system

Neurological and muscle physiological processes lead to forces on bones. Those forces generate reaction forces and accelerate joints to result in specific movement. The dominant forces driving the skeletal system are musculotendinous forces, which arise from protein interactions that cause muscle-fibers to contract in response of their state of activation. Multibody dynamics provides the physical basis for transforming physiological forces to movement (Newton's law of motion), the activation of a muscle is modulated by neural inputs from the central nervous system (CNS) and is called muscle excitation. Seth and colleagues (Seth et al. 2011) visualized that context in Figure 2.22, where muscle excitation serve as inputs and the outputs are trajectories for generalized coordinates,  $q$ , and speeds,  $u$ , as well as muscle states,  $z$ , as a function of time,  $t$ .

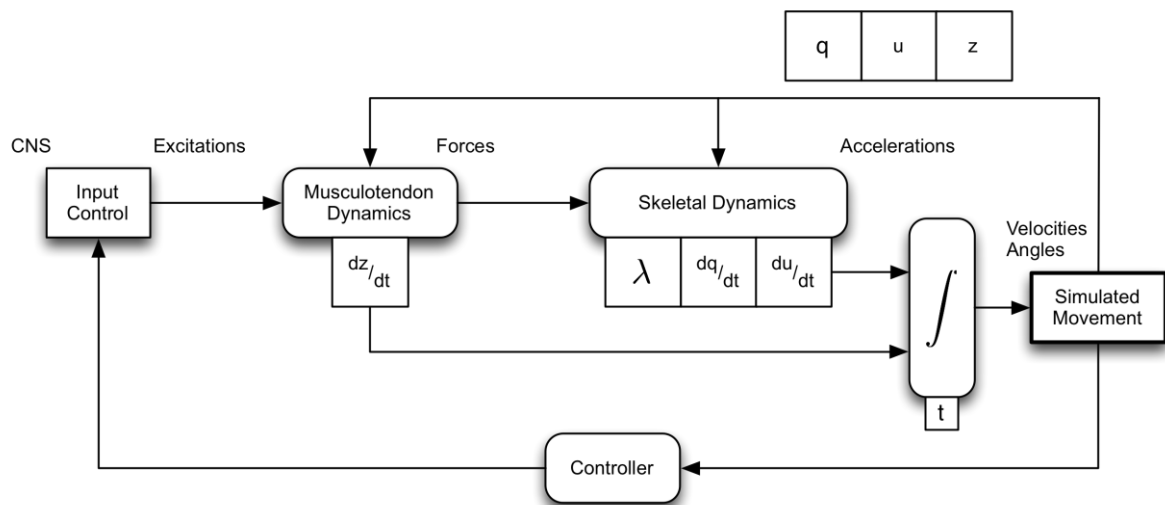


**Figure 2.22: Block-diagram of the dynamic musculoskeletal system**  
adapted from Seth et al. 2011

#### 2.6.1.1 Biological vs. engineered joints

There is a discrepancy between biological joints and joints engineered by human. Slider, universal, planar and ball-and-socket joints insufficient describe the functions of biological joints. So modelers are faced with making unnecessary assumptions and simplifications.

In OpenSim joints and constraints are responsible to fit the needs and functions of biological joints. Joints provide the needed degrees-of-freedom (DOF), whereas constraints are liable for removing them. So, constraints serve two purposes. They

first are necessary for loop closure in the multibody tree and secondly to couple motion between joints. For more details concerning that issue consult Jennifer Hicks's User's Guide (2011) or the publication of Seth et al. (2011).

### 2.6.1.2 Interaction with the environment

OpenSim offers several approaches for modeling external forces. The most used way to apply forces of the environment to the model is to mount measured forces and center-of-pressure data as function of time to a specified body. In absence of experimental data, contact with the environment (e.g. ground) must be modeled.

Therefore developers of OpenSim implemented different options of contact force formulations, the HuntCrossleyForce (Hunt & Crossley 1975), which is based on Hertz contact theory, the elastic-foundation model (Perez-Gonzalez et al. 2008), which calculates deformations and forces using a simplified bed-of-springs elastic model, and last the modeling of interaction with the environment via constraints (Hamner et al. 2010). Sherman and colleagues will give a detailed view of that topic in their paper (Sherman et al. 2011).

### 2.6.1.3 Passive structures and physiological actuators

Forces in OpenSim include springs, dampers, bushings, and ligaments, all of which compute forces as a function of position and velocities from the state. Actuators are forces and can be dependent on the state but must be dependent on a control value. In contrary, passive forces may dependent on the state but not on a control value, as discussed in chapter 2.4.1.1 in detail.

Based on the formulations of muscle dynamics described by Zajac (Zajac 1989), OpenSim offers multiple muscle models. Muscles are musculotendinous actuators with a contractile muscle-fiber and compliant tendon in series. Observations by Hill (Hill 1938) describe the muscle contractile dynamics as relation of the muscle force to activation, muscle-fiber length and contractile velocity.

Seth and colleagues (Seth et al. 2011) formulated the musculotendinous dynamic equations as following:

$$F^{MT} = F^T = F^M \cos(\alpha) \quad (2.23)$$

$$F^T = k^T (L^{MT} - L^M \cos(\alpha)) - L^{ST} \quad (2.24)$$

$$F^M = a \cdot f_l(L^M) f_v(\dot{L}^M) + f_{PE}(L^M) \quad (2.25)$$

∴

$$\dot{L}^M = f_v^{-1} \left( \frac{k^T (L^{MT} - L^M \cos(\alpha)) - L^{ST} / \cos(\alpha) - f_{PE}(L^M)}{a \cdot f_l(L^M)} \right) \quad (2.26)$$

First they assumed that muscle force,  $F^M$ , and tendon force,  $F^T$ , are in equilibrium at all times and that muscle activation,  $a$ , and muscle-fiber length,  $L^M$ , are the two state

variables of the actuator. Furthermore they defined  $k^T$  and  $L^{ST}$  as the tendon stiffness and slack length properties, and  $f_l$  and  $f_v$  as the physiological force-length and force-velocity relationships of the contractile element and  $f_{PE}$  as the passive-element force-length relationship for inputs that are not normalized (Seth et al. 2011).

$$\dot{a} = \begin{cases} (x - a)/\tau_{act} & , \quad x \geq a \\ (x - a)/\tau_{deact} & , \quad x < a \end{cases} \quad (2.27)$$

Related to the electrical activity of a muscle-fiber the produced tension can be described by equation (2.25). Activation dynamics capture the charge and discharge rates of the muscle-fiber membrane and internal structures that can be expressed as a differential equation (2.27) of the muscle excitation,  $x$ , that represent the neural signals from the CNS and can be viewed as the “controls” to the musculoskeletal system (Thelen 2003). Ligaments and muscles share the same path description to apply their computed forces to bones, but unlike a muscle, ligaments generate tension dependent only on path length and velocity, not according to activation. More and more detailed information can be found in the work of Delp (1990) and Seth (2011).

#### 2.6.1.4 Neuromuscular control

To cause muscles to contract and pull on bones in a coordinated way to produce the desired motion, the model must be controlled somehow. There are some specific cases where it is plausible to manually prescribe excitation patterns to muscles, in most cases the transformation from muscle excitation to bone movement is too complex to be adjusted by hand. The fact that solving a nonlinear parameter optimization problem for the control values for every instant is an extremely high-dimensional problem, tracking controllers have recently become successful at reproducing model kinematics. The so called computed muscle control algorithm, CMC (Thelen et al. 2003) is implemented in OpenSim and provides results of model kinematics that are close to experimentally collected kinematics and models muscle activities in good agreement with experimental muscle electromyogram data (Thelen & Anderson 2006; Seth & Pandy 2007).

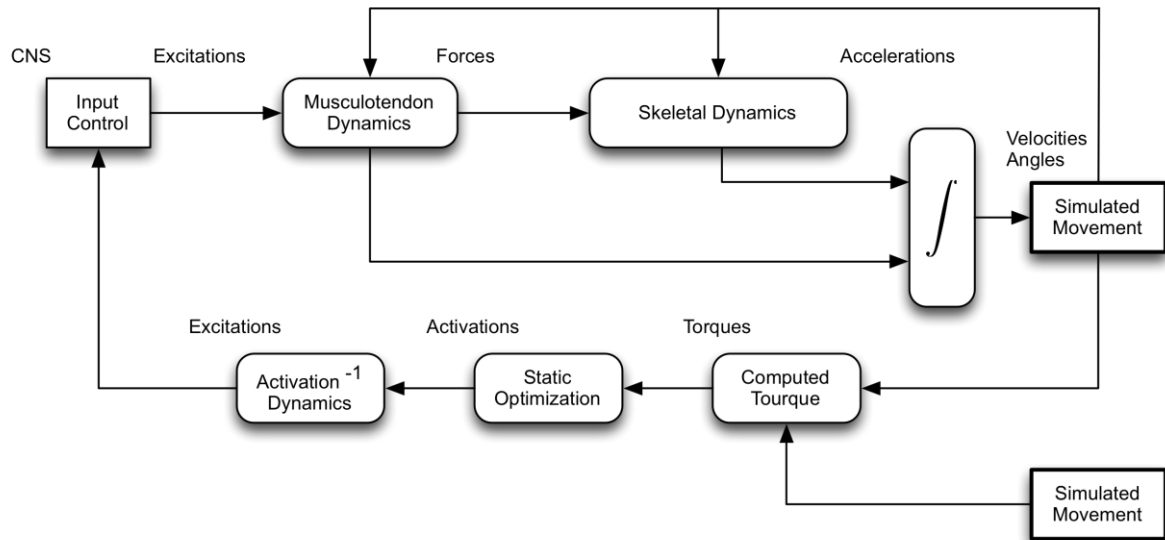


**Figure 2.23: Schematic of the computer muscle control algorithm**  
*adapted from Seth et al. 2011*

### 2.6.2 Scale Tool

The Scaling tool provided by OpenSim is based on a combination of measured distances between x-y-z marker locations and manually-specified scale factors. The unscaled model includes a set of virtual markers that are placed in same anatomical locations as the experimental markers that are obtained using motion capture systems.

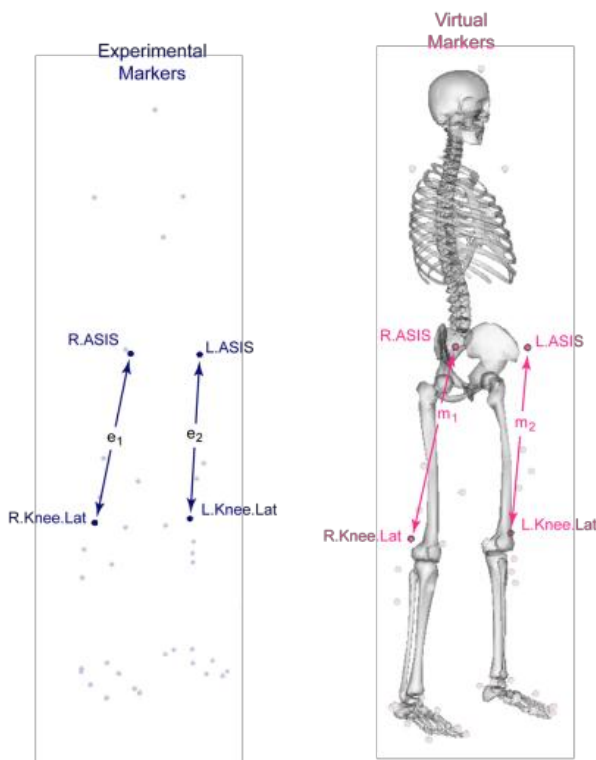


**Figure 2.24: Experimental and virtual markers - Scale Tool**  
*experimental marker set left (purple), virtual marker set on the right (pink)*  
*source: Hicks 2011*

To match the distance between the experimental and the virtual markers OpenSim scales the dimensions of each segment in the model. Thereafter, the Scale Tool moves the virtual markers on the model so that they coincide with the experimental marker locations. As an alternative to the measurement-based scaling, manual scale factors, which may come from other anthropometric analyses can be used.

In measurement-based scaling, scale factors are determined by comparing distances between markers on the model and experimental marker positions provided in the .trc file.

Alternatively to computing scale factors, OpenSim provides the manual scaling option. Thereby it is possible to specify the x-y-z scale factors for every segment manually.

The scaling step not only scales the dimensions of the body segments, it scales the mass properties (mass and inertia tensor) too. Therefore the masses of the segments are adjusted so that the total mass of the body equals the specified subject mass.

### 2.6.3 Analyze-Tools

There are a number of tools provided in OpenSim to analyze and simulate models of the musculoskeletal system. The following chapter will only describe a few of them, especially these that are relevant for this study. More detailed information about both, the tools written above and the these which are not mentioned here can be found in the official OpenSim User's Guide (Hicks 2011).

#### 2.6.3.1 Inverse Kinematics (IK)

Task of the Inverse Kinematics (IK) Tool is to step through each time frame of experimental data to position the model in a pose that "best matches" experimental marker and coordinate data for that time step. As explained in Hicks's User's Guide (Hicks 2011), mathematically the "best match" is expressed as a weighted least squares problem, whose solution aims to minimize both marker and coordinates errors. In short, experimental markers are matched by model markers throughout the motion by varying the joint angles (generalized coordinates) through time (Figure 2.25).

*Marker Errors:* The distance between an experimental marker and the corresponding marker on the model is called marker error. It occurs when the model marker is positioned using the generalized coordinates computed by the IK solver. Specifying how strongly that marker's error term should be minimized, each marker has a weight associated with it.



**Figure 2.25: Inverse Kinematics (IK) Tool Overview**

source: Hicks 2011

*Coordinate Errors:* The difference between an experimental coordinate value and the coordinate value computed by IK is called coordinate error. The IK Tool is able to solve motion trajectories using marker matching alone, so the inclusion of experimental coordinate values is optional. In passing be mentioned, a distinction should be made between prescribed and unprescribed coordinates. Former (also locked coordinate) is a generalized coordinate whose trajectory is known and which will not be computed using IK. It will get set to its exact trajectory value instead. An unprescribed coordinate is a coordinate which is not prescribed, and whose value is computed using IK. So only unprescribed coordinates can vary and appear in the least square equation solved by IK. Like with the marker errors, each unprescribed coordinate being compared to an experimental coordinate must have a weight associated with it, specifying how strongly that coordinate's error should be minimized.

*Weighted Least Squares Equation:* To find the "best match", IK Tool solves the weighted least squares problem, mathematically expressed as the equation (2.28) where  $q$  is the vector of generalized coordinates being solved for,  $x_i^{exp}$  is the experimental position of marker,  $x_i(q)$  is the position of the corresponding marker on the model (which depends on the coordinate values),  $q_j^{exp}$  is the experimental value for coordinate  $j$  and for all of them  $q_j = q_j^{exp}$ .

$$\min_q \left[ \sum_{i \in \text{markers}} w_i \|x_i^{exp} - x_i(q)\|^2 + \sum_{j \in \text{unprescribed coords}} \omega_j (q_j^{exp} - q_j)^2 \right] \quad (2.28)$$

OpenSim allows to specify marker weights ( $w_i$ ) and coordinate weights ( $\omega_j$ ) individually to achieve the specifications of the individual model and/or motion.

The least squares problem is solved using a general quadratic programming solver, with convergence criterion of 0.0001 and a limit of 1000 iterations, that can't be changed. Units of parameters in the equation used by IK are model's unites, which are meters [m] for length and radians [rad] for angles.

### 2.6.3.2 Inverse Dynamics (ID)

The Inverse Dynamics (ID) tool determines the generalized forces (e.g., net forces and torques) at each joint responsible for a given movement. With given kinematics (e.g., states or motion) which describes the movement of a model and perhaps a portion of the kinetics (e.g., external loads) applied to the model, the ID Tool uses these data to perform an inverse dynamic analysis. Classical mechanics mathematically expresses the mass-dependent relationship between force and acceleration,  $F = m \times a$ , with equations of motion. The ID Tool solves these equations, in the inverse dynamics sense, to yield the net forces and torques at each joint, which produce the movement.

The classical equations of motion may be written in the form below. Generalized positions, velocities, and accelerations define the motion of the model completely. The inverse dynamics tool uses the known terms on the left-hand side of the equation (the known motion of the model) to solve the equations of motion for the unknown right-hand side, the generalized forces (Hicks 2011).

$$\underbrace{M(q)\ddot{q} + C(q, \dot{q}) + G(q)}_{\text{knowns}} = \underbrace{\tau}_{\text{unknowns}} \quad (2.29)$$

With  $N$  as the number of degrees of freedom the used terms above are explained in detail now:

- $q, \dot{q}, \ddot{q} \in R^N$  are the vectors of generalized positions, velocities, and accelerations
- $M(q) \in R^{N \times N}$  is the system mass matrix
- $C(q, \dot{q}) \in R^N$  is the vector of Coriolis and centrifugal forces
- $G(q) \in R^N$  is the vector of gravitational forces
- $\tau \in R^N$  is the vector of generalized forces

### 2.6.3.3 Computed Muscle Control (CMC)

The Computed Muscle Control (CMC) Tool's purpose is to compute a set of actuator controls (e.g. muscles) that will drive a dynamic musculoskeletal model to track a set of desired kinematics in the presence of applied external forces.

The CMC tool computes, at user specified time intervals during simulation, muscle excitation levels that will drive the generalized coordinates (e.g., joint angles) of a dynamic musculoskeletal model towards a desired kinematic trajectory. This is

realized by using a combination of proportional-derivative (PD) control and static optimization (Figure 2.26).

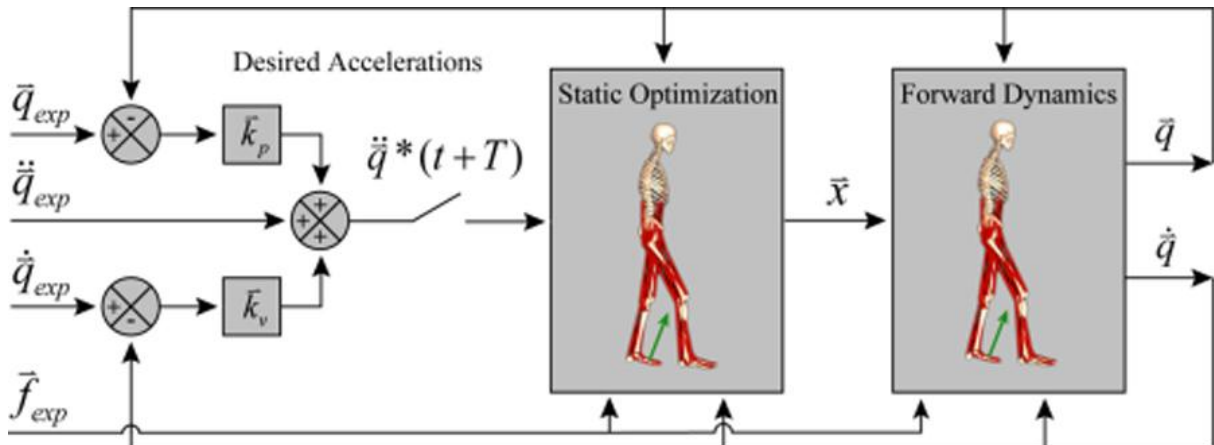


Figure 2.26: Schematic of the CMC Algorithm applied to gait

source: Hicks 2011

Before starting the CMC algorithm, initial states for the model are computed. That states comprise the generalized coordinates (joint angles), generalized speeds (joint angular velocities), plus any muscle states (e.g., muscle activation levels and fiber lengths). While the initial values of the generalized coordinates and speeds can be taken from the desired kinematics that is specified in the motion file, the initial values of the muscle states are generally unknown. To compute viable starting muscle states, CMC is applied to the first 0.03 seconds of the desired movement. Because the muscle states are generally out of equilibrium and muscle forces can change dramatically during this initial time interval, the simulation results during this interval are generally not valid.

CMC's first step is to compute a set of desired accelerations ( $\ddot{\vec{q}}^*$ ), which when achieved, will drive the model coordinates,  $\vec{q}$ , toward the experimentally-derived coordinates,  $\vec{q}_{exp}$ . The desired accelerations are computed using the PD control law shown in the equation below (2.30).

$$\ddot{\vec{q}}^*(t+T) = \ddot{\vec{q}}_{exp}(t+T) + \vec{k}_v [\dot{\vec{q}}_{exp}(t) - \dot{\vec{q}}(t)] + \vec{k}_p [\vec{p}_{exp}(t) - \vec{q}(t)] \quad (2.30)$$

$\vec{k}_v$  and  $\vec{k}_p$  are the feedback gains on the velocity and position errors. Because the forces that muscles apply to the body cannot change instantaneously, the desired accelerations are computed for some small time  $T$  in the future. For musculoskeletal models,  $T$  is typically chosen to be about 0.01 seconds, that's short enough to allow adequate control, and long enough to allow muscle forces to change.

After achieving these desired accelerations, errors between the model coordinates and experimentally-derived coordinates will be driven to zero. To realize a critically damped fashion (i.e., without over-shooting or over-damping), the velocity gains can

be chosen using the following relation (2.31). For musculoskeletal models, it works well if the error gains are chosen to drive any errors to zero slowly. The error gains  $\vec{k}_v = 20$  and  $\vec{k}_p = 100$  will cut down tracking errors.

$$\vec{k}_v = 2\sqrt{\vec{k}_p} \quad (2.31)$$

The next step of CMC Tool is to compute the actuator controls  $\vec{x}$ , that will achieve the desired accelerations,  $\ddot{q}^*(t + T)$ . Most of the time the controls are predominantly comprised of muscle excitations, but this is not required. Static optimization is used to distribute the load across synergistic actuators. The bounds on the controls  $\vec{x}$  can be specified. For muscles excitations, the default upper bound is typically 1.0 (full excitation), and the default lower bound is typically a small number just above 0.0 but (no excitation), such as 0.01 or 0.02. The Lower bound is not set precisely to 0.0 because mathematical models of muscle are not as well-behaved when excitation goes all the way to 0.0.

Currently there are two formulations of the static optimization problem. First, called the slow target, consists of a performance criterion ( $J$ ) that is weighted sum of squared actuator controls plus the sum of desired accelerations errors (2.32). The first summation minimizes and distributes loads across actuators and the second drives the model accelerations ( $\ddot{q}_j$ ) toward the desired accelerations ( $\ddot{q}_j^*$ ).

$$J = \sum_{i=1}^{nx} x_i^2 + \sum_{j=1}^{nq} w_j (q_j^* - \ddot{q}_j)^2 \quad (2.32)$$

The second formulation, called the fast target, is the sum of squared controls augmented by a set of equality constraints ( $C_j = 0$ ) that requires the desired accelerations to be achieved within the tolerance set for the optimizer..

$$J = \sum_{i=1}^{nx} x_i^2 \quad ; \quad C_j = \ddot{q}_j^* - \ddot{q}_j, \text{ for all } j \quad (2.33)$$

The final step in the CMC algorithm is to use the computed controls to conduct a standard forward dynamic simulation, advancing forward in time by  $T$ . These steps – computing the desired accelerations, static optimization, and forward dynamic simulation – are repeated until time is advanced to the end of the desired movement interval.

## 3 Materials and Methods

The following section will be used for a detailed view and the necessary explanations of the used materials and methods for the study in hand. Detailed descriptions of what settings we used for simulation and the needed input-data will be given. Theoretical details about the simulation software, the used tools and mathematical algorithm behind can be read in the previous chapters.

### 3.1 Software: OpenSim 3.2

In the course of the present study, simulations were executed with OpenSim 3.2 the latest version (released in 07<sup>th</sup> March 2014) of a free available software platform developed by Simbios, a NIH Center for Biomedical Computation at Stanford University. Theoretical and mathematical background of OpenSim is written in chapter 2.6.

Alternatively to the GUI, OpenSim allows to interact and conduct simulations via MATLAB. Because of the two different movements we wanted to investigate, and the variety of different parameters, we wrote a batch in MATLAB to execute the simulation sequentially and with a minimum of human effort. Furthermore, CMC simulations were computed on the LINUX server of the Center for Medical Physics and Biomedical Engineering of the Medical University of Vienna.

#### 3.1.1 Body model

As basic body model for all following simulations we took the Gait2392 model created by Darryl Thelen, Ajay Seth, Frank C. Anderson and Scott L. Delp (Millard et al. 2013). This primarily lower extremity, three-dimensional, 23-degree-of-freedom model features lower extremity joint definitions adopted from the work of Delp et al. (Delp et al. 1990), planar knee model adopted from Yamaguchi and Zajac (Yamaguchi & Zajac 1989), and a low back joint and anthropometry adopted from Anderson and Pandy (Anderson & Pandy 1999). It consists of two legs and a lumped torso segment with 92 musculotendon actuators to represent 76 muscles of the lower extremities and torso. To avoid kinematic constraints, authors removed the patella and created moving points in the tibia frame to get insertions of the quadriceps handled. The unscaled, default model represents a subject with 1.8m height and a mass of 75.16 kg. In case of our work we scaled the body model with experimental data. A detailed view about the scaling step will be given in chapter 3.1.4.

The OpenSim specific definitions of the joint angles are shown in the following picture.

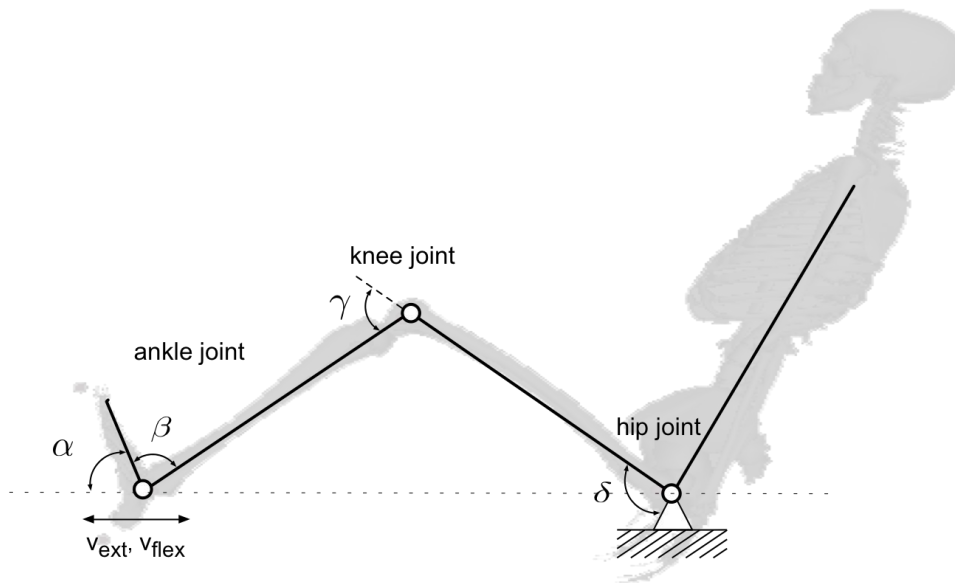


**Figure 3.1: OpenSim Body Model, joints and angles**

For simplification reasons, we defined the ankle angle ( $\beta$ ), as the angle between tibia and pes (foot). Therefore the values provided by OpenSim ( $\beta_{OpenSim}$ ) need to be converted the following way:

$$\beta = 90 - \beta_{OpenSim} \quad (3.1)$$

### 3.1.2 Body Marker Set

OpenSim allows the user to place individual marker anywhere and fix them to any body segment of the model or the environment. We adapted the standard OpenSim marker set and used five of these markers for our investigations, placed on prominent points of the lower extremity. In detail we chose, trochanter major for the hip, epicondylus lateralis femoris for the knee joint, lateral malleolus as the prominent mark for the ankle joint and one on calcaneus and one on the tip of the hallux. The values listed in table 3.1 are absolute coordinates; therefore they are expressed in the coordinate system of the ground, X (red), Y (yellow) and Z (green) in Figure 3.2. As written in table 3.1, they are fixed to an individual body segment, to make sure body and marker operate simultaneous.

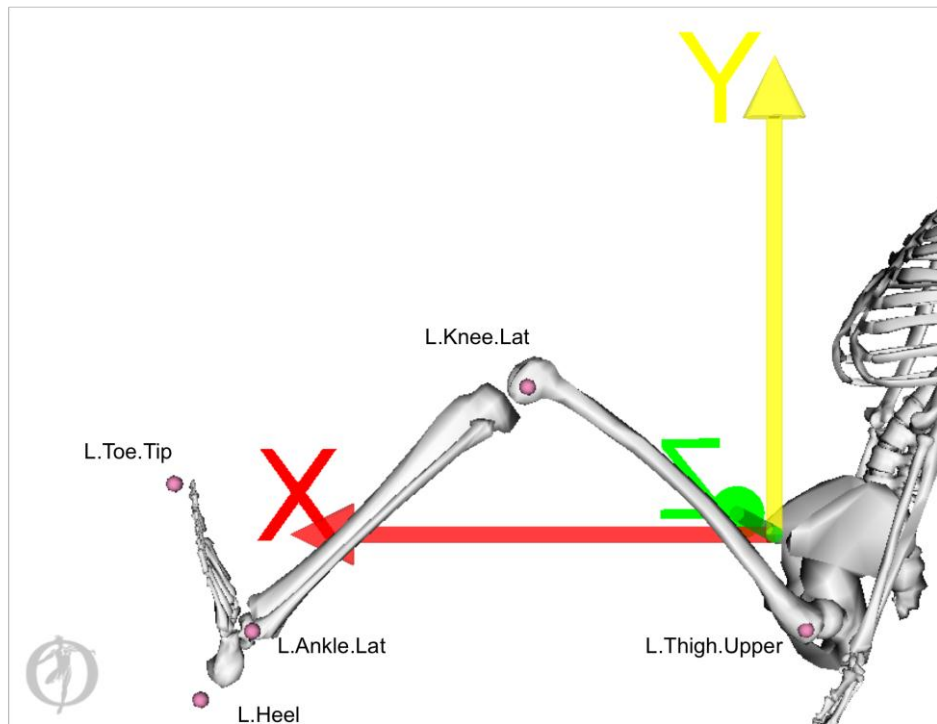


**Figure 3.2: OpenSim MarkerSet, 5 marker, left leg**  
*source: OpenSim, Model of Simulation*

Combination of two markers and calculating the distance in between is used to compute individual scale factors. Applied to the particular segments of the generic musculoskeletal model, we realized an individual model of the subject. More details about the specific used data will give chapter 3.1.4, the theoretical background is discussed in chapter 2.6.2.

#	marker name	position (anatomic)	body	absolute coordinates (X/Y/Z)
1	L.Thigh.Upper	trochanter major	femur_l	-0.0204256/-0.100682/-0.15
2	L.Knee.Lat	epicondylus lateralis femoris	femur_l	0.295453/0.177631/-0.1335
3	L.Ankle.Lat	lateral malleous	tibia_l	0.609449/-0.103405/-0.136501
4	L.Heel	calcaneus	calcn_l	0.672595/-0.187505/-0.0928965
5	L.Toe.Tip	hallux	calcn_l	0.700685/0.0650998/-0.113554

**table 3.1: OpenSim Marker Set, body, coordinates**  
*source: OpenSim, Model of Simulation (Schneider G.)*

### 3.1.3 Muscle model

As mentioned in chapter 2.4.2 there is a variety of muscle models that can be used for simulations in OpenSim. For the study in hand we used Matthew Millard's equilibrium musculotendon model (Millard et al. 2013) which is implemented in OpenSim and is current state of musculotendon models for OpenSim. To reduce calculation time, we disabled all other muscles, beside of the muscles from the left leg operating in the hip, the knee and the ankle joint.

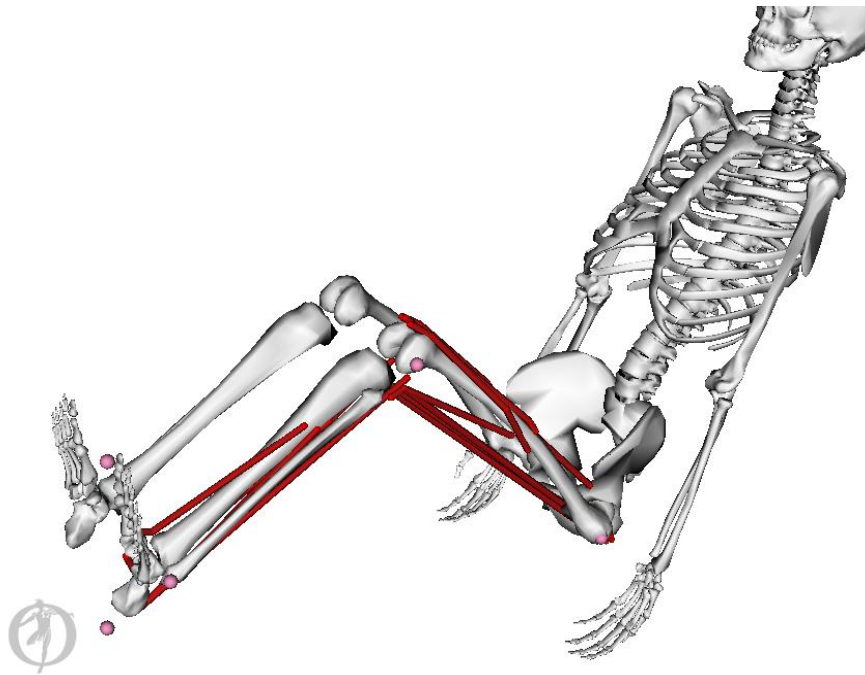


**Figure 3.3: OpenSim model with muscles of interest**  
*source: OpenSim, Model of Simulation*

The following figure and the table below will show what muscles we decided to use for simulation and what Millard et al. defined as maximal isometric force for each of these muscles developers tried to reproduce human anatomy as realistic they can. Therefore some muscles, like musculus gluteus maximus, musculus gluteus medius and other large-area muscles needed to be embedded as two or three co-operating muscles in the model.

	<b>muscle</b> <i>(OpenSim)</i>	<b>muscle</b> <i>(anatomic)</i>	<b>max.</b> <b>isometric force</b>
g1	glut_med1_l	musculus gluteus medius	819 N
g1	glut_med2_l	musculus gluteus medius	573 N
g1	glut_med3_l	musculus gluteus medius	653 N
g2	glut_min1_l	musculus gluteus minimus	270 N
g2	glut_min2_l	musculus gluteus minimus	285 N
g2	glut_min3_l	musculus gluteus minimus	323 N
g3	tfl_l	musculus tensor fasciae latae	233 N
g4	glut_max1_l	musculus gluteus maximus	573 N
g4	glut_max2_l	musculus gluteus maximus	819 N
g4	glut_max3_l	musculus gluteus maximus	552 N
g5	quad_fem_l	musculus quadratus femoris	381 N
g6	gem_l	musculus gemellus	164 N
g7	peri_l	musculus piriformis	444 N
t1	semimem_l	musculus semimembranosus	1.288 N
t2	semiten_l	musculus semitendinosus	410 N
t3	bifemlh_l	musculus biceps femoris long head	896 N
t4	bifemsh_l	musculus biceps femoris short head	804 N
t5	sar_l	musculus sartorius	156 N
t6	add_long_l	musculus adductor longus	627 N
t7	add_brev_l	musculus adductor brevis	429 N
t8	add_mag1_l	musculus adductor magnus	381 N

t8	add_mag2_l	musculus adductor magnus	343 N
t8	add_mag3_l	musculus adductor magnus	488 N
t9	pect_l	musculus pectineus	266 N
t10	grac_l	musculus gracilis	162 N
t11	iliacus_l	musculus iliacus	1.073 N
t12	psoas_l	musculus psoas major	1.113 N
t13	rect_fem_l	musculus rectus femoris	1.169 N
t14	vas_med_l	musculus vastus medialis	1.294 N
t15	vas_int_l	musculus vastus intermedius	1.365 N
t16	vas_lat_l	musculus vastus lateralis	1.871 N
s1	med_gas_l	musculus gastrocnemius media	1.558 N
s2	lat_gas_l	musculus gastrocnemius laterale	683 N
s3	soleus_l	musculus soleus	3.549 N
s4	tip_post_l	musculus tibialis posterior	1.588 N
s5	tib_ant_l	musculus tibialis anterior	905 N
s6	per_brev_l	musculus fibularis brevis (peronaeus brevis)	435 N
s7	per_long_l	musculus fibularis longus (peronaeus longus)	943 N
s8	per_tert_l	musculus fibularis tertius (peronaeus tertius)	180 N
s9	ext_dig_l	musculus extensor digitorum longus	512 N
s10	ext_hal_l	musculus extensor hallucis longus	162 N
f1	flex_dig_l	musculus flexor digitorum brevis	310 N
f2	flex_hal_l	musculus flexor hallucis brevis	322 N

**Table 3.2: list of muscles used in OpenSim**

*g* gluteal muscles, *t* thigh muscles, *s* shank muscles and *f* are muscles of the foot

After few simulations, and concerning to other publications (Cho et al. 2008; Da Silva et al. 2008) investigating in leg press training, we downsized the number of muscles we were interested in. For further research we chose the following muscles of the lower limb:

rect_fem_l	musculus rectus femoris	
vas_med_l	musculus vastus medialis	<b>musculus quadriceps femoris</b>
vas_int_l	musculus vastus intermedius	
vas_lat_l	musculus vastus lateralis	
semimem_l	musculus semimembranosus	
semiten_l	musculus semitendinosus	<b>hamstrings muscles</b>
bifemlh_l	musculus biceps femoris long head	
bifemsh_l	musculus biceps femoris short head	
med_gas_l	musculus gastrocnemius media	<b>musculus triceps surae</b>
lat_gas_l	musculus gastrocnemius laterale	
soleus_l	musculus soleus	
tib_ant_l	musculus tibialis anterior	<b>musculus tibialis anterior</b>

**Table 3.3: 12 muscles of interest**

### 3.1.4 Modeling of motion and force data

To realize the specific motion of the leg press training via simulation software we used the recorded path data from the leg press-software. Equally to motion data we took the stored force values the software recorded. The detailed workflow will be accurately described in the following chapters.

### 3.1.4.1 Motion data

The operating-software provides data about force, velocity and the path of the foot pedals in real time. We used that data to define the motion in our simulation.

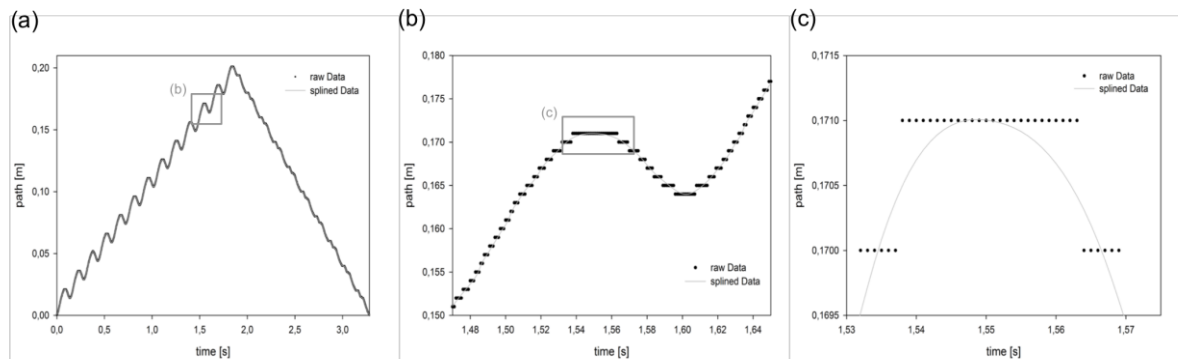


**Figure 3.4: Measured and calculated splined pathway of the foot paddle**  
 (a) measured pathway for the vibration movement, (b) and (c) same but in more detail  
 dotted: data out of LP-software, dashed: calculated data via MATLAB

Therefore we imported path values via MATLAB. Because resolution was about 0.1 mm and to avoid numerical singularities, we had to adapt this data. Thus we looked for the central/mean values of each path step and defined these as sampling points for the spline function. As result of that calculation we got a smooth and well representing motion for our simulation that could be used in OpenSim.

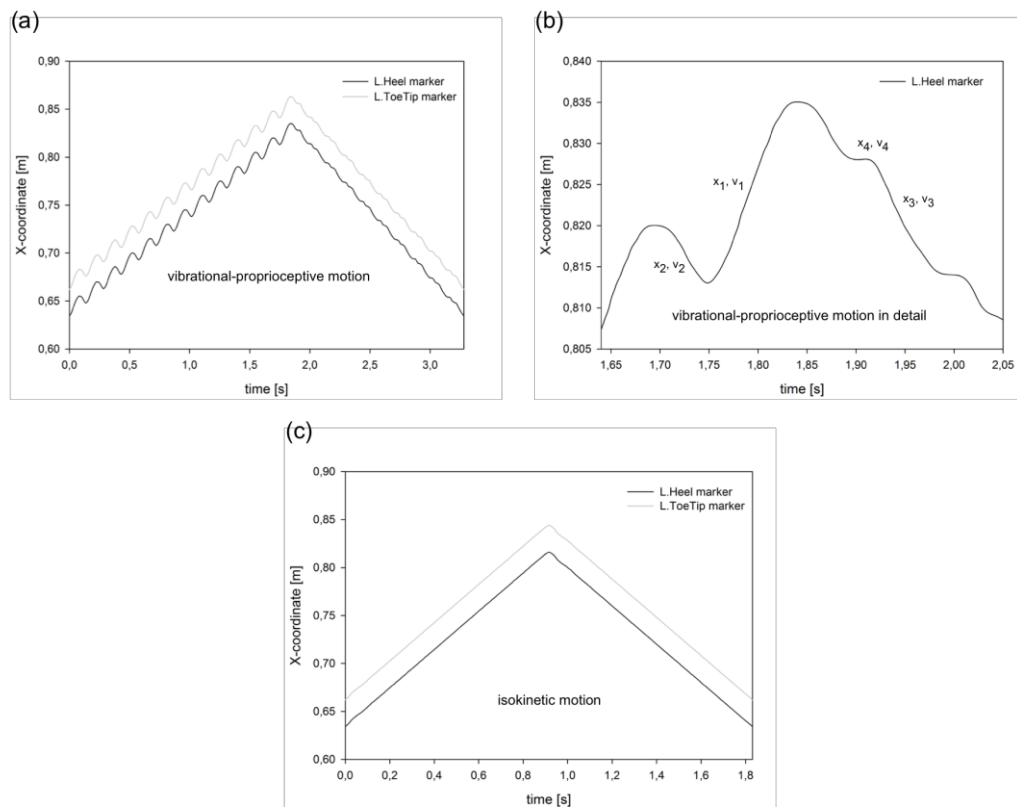


**Figure 3.5: Pathway of left heel marker during different setups.**  
 (a) X-coordinate of left heel (L.Heel) marker, (a) vibration, (b) vibration in detail,  
 (c) isokinetic motion

In Figure 3.4, values of the data output from the software (dotted line) and the calculated, splined data is shown (dashed line). The resulting graph is shown over the whole range in Figure 3.5 (a) and a detailed illustration of the vibration is given in Figure 3.5 (b).

### 3.1.4.2 Force data

As we did in chapter 3.1.4.1 with motion data, we had to adapt the raw force data provided by the software for the usage in our simulation. Therefore, force data was low pass filtered using MATLAB (Table 3.4).

	<b>N</b>	<b><math>F_{3dB}</math></b>
isokinetic data	12	0,007
vibration data	12	0,005

**Table 3.4: Low pass filter settings (isokinetic, vibration)**

*N* filter order,  $F_{3dB}$  cut-off frequency

Likely the synthetic data, the filtered raw force data was stored in a unique named force-file, ready to be used in further simulations. The aim of filtering the raw force data was, to eliminate the sharp peaks which result in big errors and/or the termination of the simulation. As written in earlier we had to avoid numerical singularities due to abrupt changing of the force values.

In Figure 3.6 we illustrate all attempts with different filter parameters. Downsizing of the cut-off frequency ( $F_{3dB}$ ) eliminated the disruptive peaks of force data OpenSim couldn't deal with.

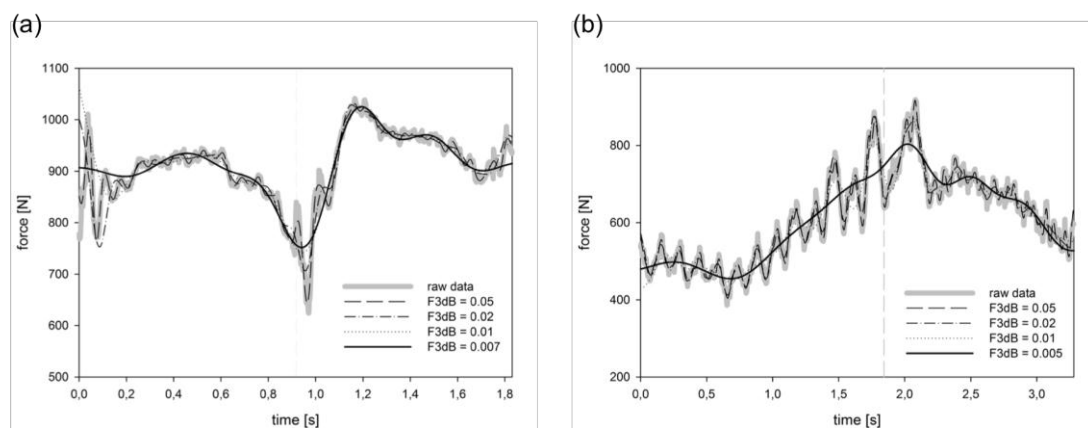


**Figure 3.6: Force data, low pass filtered (a) isokinetic (b) vibration motion**

To eliminate mass inertia, especially of the heavy foot pedals, we considered to subtract values of 50% activation from data recorded with 100% voluntary activation and use these data as our net 50% force data. To get 100% values, we doubled 50% values. For both motions (isokinetic and vibration) 50% and 100% external force data is shown in Figure 3.7 as a training of three cycles.

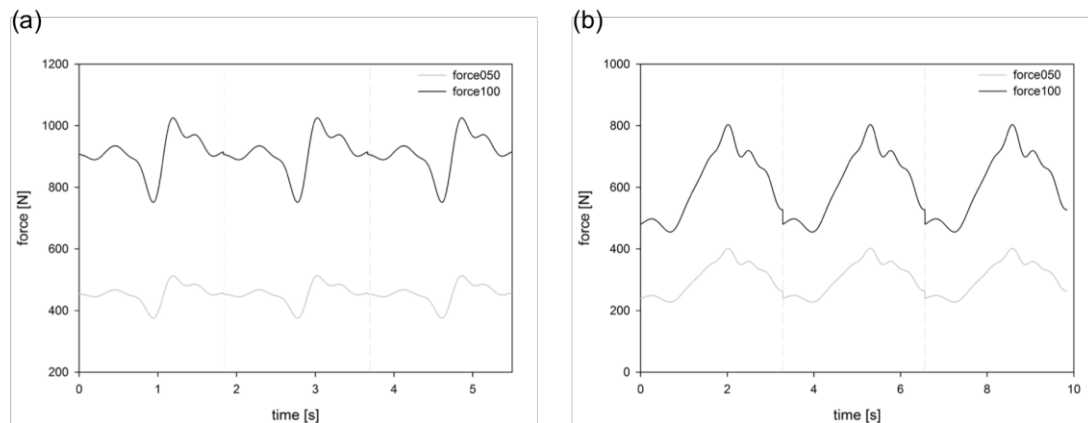


**Figure 3.7: Input data, net force 50% and 100%**  
 (a) isokinetic (b) vibration

### 3.1.5 OpenSim: Scale Tool – Specifications

To alter the anthropometry of our model so that it matches our particular subject we needed specific input data for the Scale Tool.

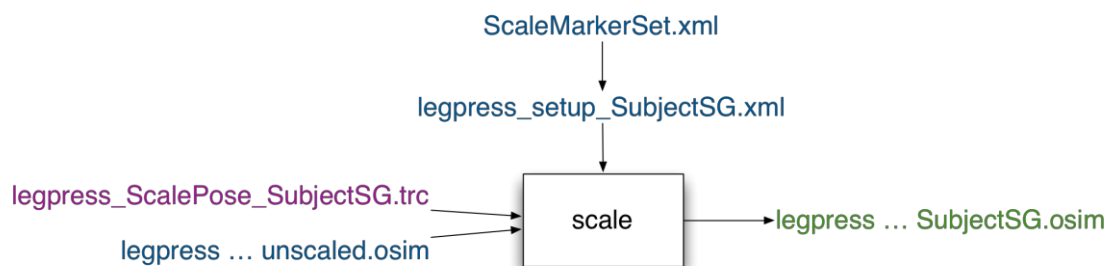


**Figure 3.8: Inputs and Outputs of Scale Tool**  
 source: Hicks 2011

*Note: OpenSim and settings files are shown in blue, experimental data are shown in purple, files generated by the workflow are shown in green.*

**leg press ... unscaled.osim** Generic OpenSim musculoskeletal model that will be scaled to match the anthropometry of the subject.

**leg press\_ScalePose\_SubjectSG.trc** Experimental marker trajectories for a trail recorded the particular subject wearing the full marker set. Data can be obtained from a motion capture system or created in MATLAB. In course of this study a MATLAB script calculated the scaled marker set according to the measured length of shank, thigh and foot (see Table 3.5).

**leg press ... SubjectSG.osim** Scaled OpenSim musculoskeletal model.

For the experimental data, shown above and colored in purple, we took empiric data from one subject (male, 1.72m height, 76kg of mass). Furthermore, out of these values the software calculated specific factors for each body segment and scaled the raw-model to the size/weight/dimension of the real subject.

	Gait2392 (unscaled)	Gait2392 (scaled) SG
body mass	75.16 kg	76 kg
body height	1.8 m	1.72 m
length thigh		0.42 m
length shank		0.415 m
length foot		0.255 m
<b>scale factors</b>		
factor femur	1	1.073756
factor tibia	1	1.032779
factor foot	1	0.910641
factor torso	1	1.073756 (=factor femur)

**Table 3.5: Anthropometry, scale factors, subject SG**

### 3.1.6 OpenSim: Inverse Kinematics (IK) - Specifications

To tell our model how to practice/train on the leg-press we had to generate a motion-file. Therefore OpenSim provides the so-called IK Tool. This tool needed a few files with experimental data and parameters defined to compute generalized coordinate trajectories. Filenames and other specific data, like starting and ending time, were specified in a XML-File (e.g., leg\_press\_setup\_IK.xml). Figure 3.9 will give a schematic overview what is needed and what specific data we used.

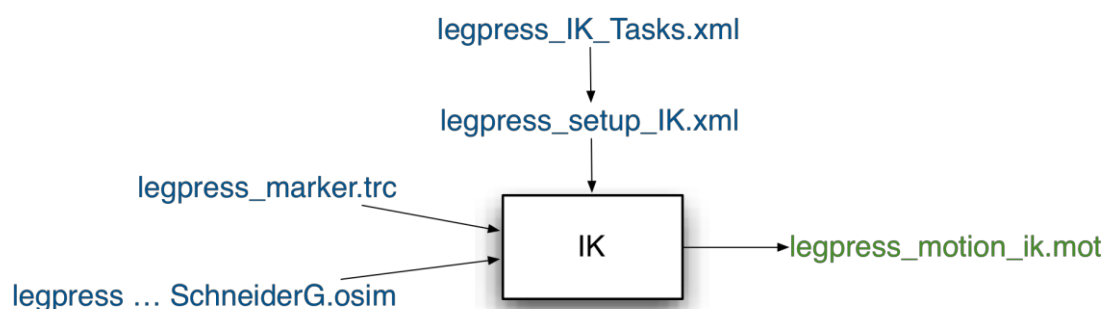


**Figure 3.9: Inputs and Outputs of IK Tool**

source: Hicks 2011

*Note: OpenSim and settings files are shown in blue, experimental data are shown in purple, files generated by the workflow are shown in green.*

**leg press ... SchneiderG.osim** OpenSim musculoskeletal model. This model can be scaled, if needed or wanted, to match the anthropometry of the subject, in the present study

we scaled the generic model like written above. (q.v. Scale Tool, in chapter 2.6.2).

<b><i>leg_press_marker.trc</i></b>	Experimental marker trajectories for a trail (can be obtained from a motion capture system or created in MATLAB)
<b><i>leg_press_IK_Tasks.xml</i></b>	File containing marker weightings.
<b><i>leg_press_motion_ik.mot</i></b>	Motion file containing the generalized coordinates trajectories (joint angles and/or translations) computed by IK.

Because we were interested in two different motions (isokinetic and vibration-proprioceptive mode) we needed different experimental marker trajectory data.

The common way to get these data is to use a motion capture system (e.g. VICON motion capturing system). Because such a system wasn't available for our study, we had to generate our experimental motion data via MATLAB. Like commercial vision capture software does, we calculated individual, chronological coordinate data for each of the two marker of the foot (L.Heel and L.Toe.Tip, pink dots in Figure 3.1: OpenSim Body Model, joints and angles) to simulate the motion of the leg press pedal. Marker coordinates were stored in the .trc file.

Representing the angle of the foot pedals,  $\alpha = 70^\circ$  and is fixed during the whole movement. All others like the ankle angle ( $\beta$ ), knee angle ( $\gamma$ ) and the hip angle ( $\delta$ ) are changing over time due to the defined path of the marker set moving horizontal forwards and backwards. Graphic illustration can be found in chapter 3.1.1.

### 3.1.7 OpenSim: Inverse Dynamics (ID) - Specifications

To determine forces and moments at each joint of our model we had to feed the ID-Tool with the necessary data of our investigations and previous simulations. Figure 3.10, shows output and the required input data with detailed descriptions of each above.

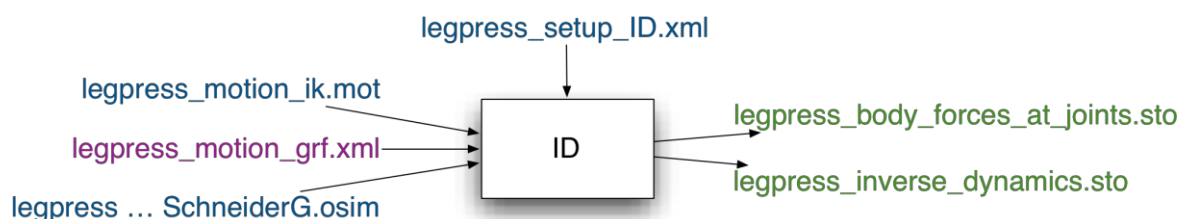


**Figure 3.10: Inputs and Outputs of the ID Tool**

source: Hicks 2011

*Note: OpenSim and settings files are shown in blue, experimental data are shown in purple, files generated by the workflow are shown in green.*

**leg press ... SchneiderG.osim** scaled OpenSim musculoskeletal model (q.v. Scale Tool, in chapter 2.6.2)

**leg\_press\_motion\_ik.mot** Motion file that describe the movement of the model, containing the time of generalized coordinates. Results from the IK-Tool were used here. (q. v. chapter 3.1.6)

**leg\_press\_motion\_grf.xml** External load data (i.e., ground reaction forces, moments, and center of pressure location). This file includes the name of the ground reaction force data file (e.g., leg\_press\_motion\_grf.mot) as well as the names of the bodies to which they are applied.

**leg\_press\_body\_forces\_at\_joints.sto** File where the body forces at specified joints are written (optional data, can be disabled in setup-file).

**leg\_press\_inverse\_dynamics.sto** Storage file containing the time histories of the net joint torques and forces acting along the coordinate axes that produce the accelerations estimated from the measured experimental motion and the external forces applied.

As required, we defined input data for the ID-Tool in a setup file. Out of the previous step a motion-file for individual description of the movement was used.

Within the xml-file (*see table below*) the body which the force data is applied to and their orientation has been defined.

Named like the files in the previous simulation steps, we tied specifications of motion and force data into the filename, like the example below will show.

### 3.1.8 OpenSim: Computed Muscle Control (CMC) - Specifications

This study aimed to simulate activation and resulting forces of muscles of the lower limb. Therefore OpenSim offers the CMC-Tool, which requires special inputs and delivers a wide range of output-data. These data are listed in the figure below (Figure 3.11), followed by a detailed description of each.

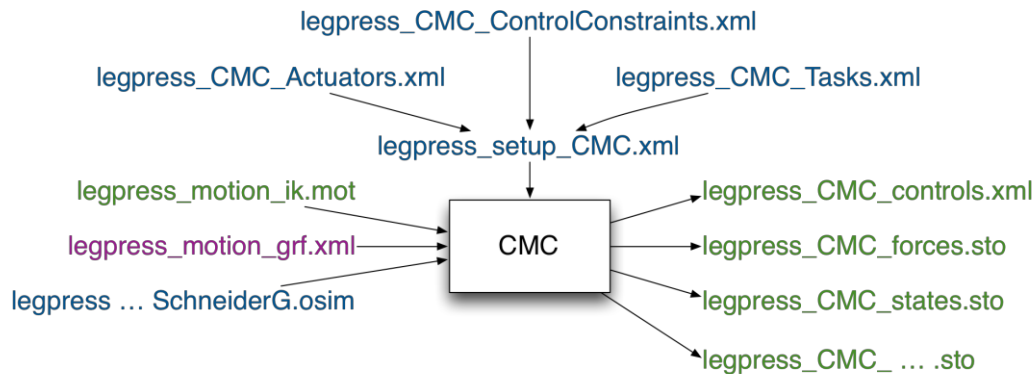


**Figure 3.11: Inputs and Outputs of the CMC Tool**

source: Hicks 2011

Note: OpenSim and settings files are shown in blue, experimental data are shown in purple, files generated by the workflow are shown in green.

**leg press ... SchneiderG.osim** scaled OpenSim musculoskeletal model (q.v. Scale Tool, in chapter 2.6.2)

**leg press\_motion\_ik.mot** Motion file that describe the movement of the model, containing the time of generalized coordinates. Results from the IK-Tool were used here. (q. v. chapter 3.1.6)

**leg press\_motion\_grf.xml** External load data (i.e., ground reaction forces, moments, and center of pressure location). This file includes the name of the ground reaction force data file (e.g., leg\_press\_motion\_grf.mot) as well as the names of the bodies to which they are applied. Same data like used in ID-Tool (q. v. 3.1.7).

**leg press\_setup\_CMC.xml** This file is a setup file for the CMC Tool, which specifies settings, inputs, and outputs that affect the behavior of the tracking controller to determine actuator (including muscles) controls.

**leg press\_CMC\_Tasks.xml** The tracking tasks file specifying which coordinates to track and the corresponding tracking weight (weights are relative and determine how “well” a joint angle will track the specified joint angle.). We used OpenSim default settings for that (*2392\_CMC\_Tasks.xml*).

**leg press\_CMC\_Actuators.xml** This file contains the residual and reserve actuators. We used OpenSim default settings here.

---

<b><i>leg_press_CMC_ControlConstraints.xml</i></b>	Contains limits on the model actuators, which include muscles, reserve and residual actuators. The control constraints file specifies the maximum and minimum “excitation” (i.e., control signal) for each actuator. Control constraints can also be used to enforce when certain actuators are “on” or “off” and the range in which they can operate. We used OpenSim default settings here.
<b><i>leg_press_CMC_controls.xml</i></b>	Contains the excitations to individual muscles as well as controls for any residual and/or reserve actuators.
<b><i>leg_press_CMC_forces.sto</i></b>	File where data about muscle forces and reserve/residual forces and torques is stored.
<b><i>leg_press_CMC_states.sto</i></b>	Model states and muscle states of the simulated motion. For example both, joint angles and velocities, or muscle fiber length and activations.
<b><i>leg_press_CMC_ ... .sto</i></b>	CMC creates some more files, where e.g. power or speed data are stored explicit. Or where position errors are recorded.

---

As we did for IK and ID simulations, we wrote a batch for CMC too. So that simulations were executed sequentially and with a minimum of human effort. Because CMC-simulations need a lot of resources and time, we executed all of our CMC-simulations on the LINUX-Server (*Linux 3.2.0-32.generic x86\_64, Ubuntu 12.04.3*) of the Center for medical physics and biomedical engineering.

OpenSim creates a big amount of results, like shown above. For our research we took a detailed look into two of them. First the file ending with *\_Actuation\_force.sto* where the calculated force data of each enabled muscle is stored, and second the *\_controls.sto* file that contain excitation/activation data of these muscle.

### **3.2 Muscle activation measured in a human subject**

We detected the muscle activity using electromyographic measurements and the joint angles kinematics was monitored with goniometers on ankle, knee and hip. The subject performed all training set-ups (isokinetic and vibration-proprioceptive), in all variations of voluntarily muscle activations (0%, 50%, and 100%), so that we get reference values of muscle activity which we could compare to the results of our simulation.

### 3.2.1 EMG electrode placement

We placed EMG-sensors on dedicated positions of the lower limb to detect muscle activity of the main actuators of leg press training. Placement of these sensors was according to the work of Merletti and colleagues (Merletti et al. 2005) and used for the following muscles.

	position of EMG-sensor	knee	hip	ankle
#0	tensor fascia latae	flexion	flexion	
#1	m. adductor magnus		extension, adduction	
#2	m. rectus femoris	extension	flexion	
#3	m. vastus lateralis	extension		
#4	m. vastus medialis	extension		
#5	m. tibialis anterior			dorsiflexion
#6	m. gluteus maximus		extension	
#7	m. biceps femoris	flexion	extension	
#8	m. semitendinosus	flexion	extension	
#9	m. gastrocnemius laterale	flexion		plantar flexion
#10	m. gastrocnemius media	flexion		plantar flexion

**Table 3.6: EMG placement for specific muscles and their functions**

Finally, to secure positions during training we covered all sensors with gauze bandage wrapped around the limb. Sensor-arrangement, before fixing with the bandage, is shown in Figure 3.12.

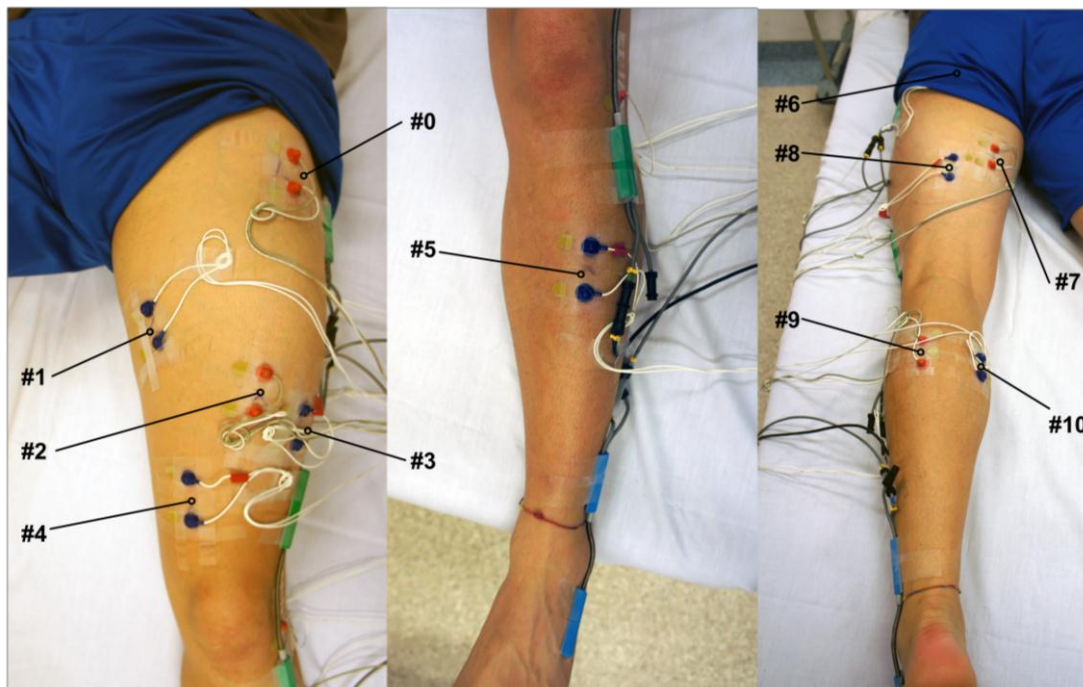


**Figure 3.12: EMG-sensor placement on the left leg (subject SG)**  
*details see Table 3.6*

### 3.2.2 Goniometer

To record kinematics of the lower limb during training we used three twin axis goniometers (SG150, Biometrics Ltd., UK). One for every joint, needed for the movement. First was placed on the ankle joint (*C*), second on the knee (*B*) and the third was used to record the movement of the hip joint (*A*). First and second goniometers were recording ankle and knee flexion, respectively. The third attached to the hip joint recorded separately abduction and flexion data.

placement of goniometer	
A	hip joint <i>Z-axis: hip angle – frontal = abduction</i> <i>Y-axis: hip angle – sagittal = flexion</i>
B	knee joint - <i>knee flexion</i>
C	ankle joint - <i>ankle flexion</i>

**Table 3.7: Goniometer placement and detection**

As we did with the EMG-sensors, we secured placement of goniometers with gauze bandage after the placement.

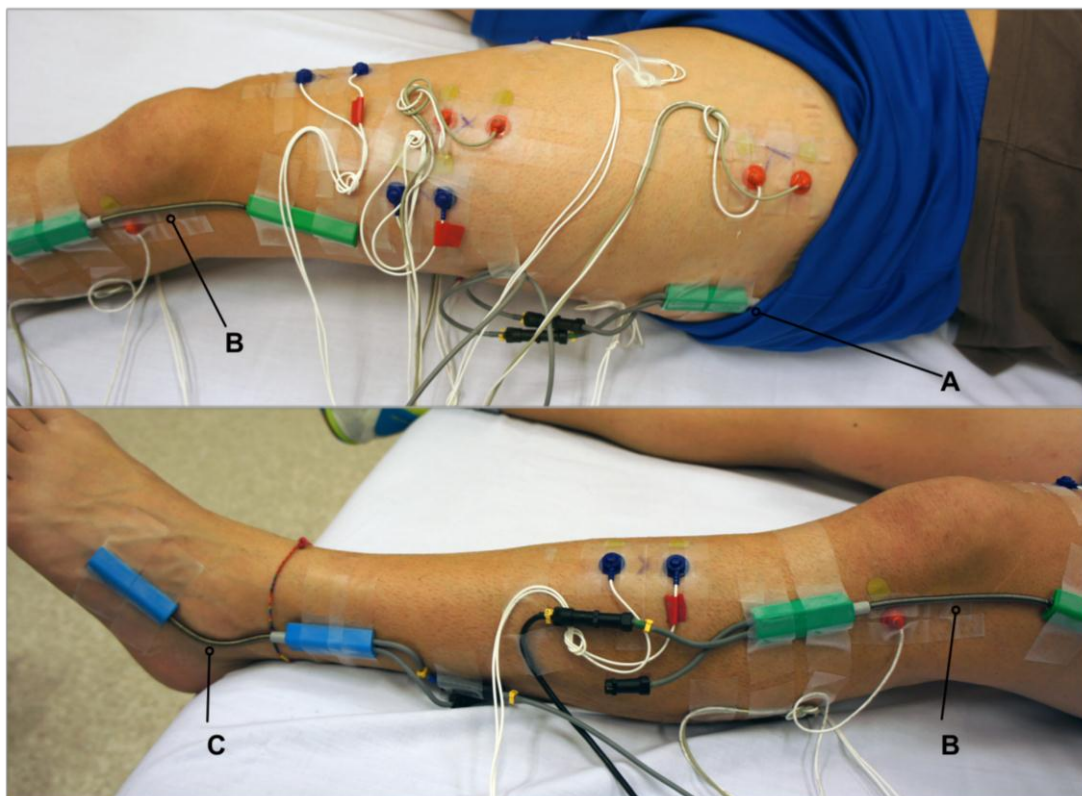


**Figure 3.13: Goniometer placement on the left leg (subject SG)**  
*A: hip joint, B: knee joint and C: ankle joint*

### 3.2.3 Data acquisition and analysis

Evoked myoelectric signals were recorded from quadriceps and hamstrings muscles using Ag/AgCl surface electrodes (FS-50 skintact, Leonhard Lang GmbH, Innsbruck,

Austria). The electrode pairs were placed equidistant on the muscle belly of the requested muscle with an inter-electrode distance of 2 cm. The signals were recorded with a custom-build analog amplifier having a bandwidth of 10 to 600 Hz and a gain of 600. The myoelectric signals were digitalized using an acquisition card (PCI-6221, National Instruments Inc., Austin, TX, USA) with a sampling rate of 10000 samples per second (SPS).

The physiological signals were acquired with DASyLab 12.0 (Measurement Computing Corporation, Norton, MA, USA) and processed in MATLAB R2014b (MathWorks Inc., Natick, MA, USA).

With MATLAB, myoelectric signals were notch-filtered before envelope curve was calculated via 3<sup>rd</sup> order butterworth lowpass filter (Table 3.8). Thereafter we separated each cycle of repetition into knee extension (KE) and knee flexion (KF) phase ( $KE_{1..n}$ ,  $KF_{1..n}$ ). Further we summed data of these motion segments and calculated mean and standard deviation over all cycles of motion ( $cycles = 3$ ).

$$KE_{mean} = \frac{\sum_1^{cycles} KE_n}{cycles}; KF_{mean} = \frac{\sum_1^{cycles} KF_n}{cycles} \quad (3.2)$$

---

#### notch filter

$$w_0 = \frac{f_{notch}}{0.5 * SR} \quad b_w = \frac{w_0}{10} \quad f_{notch} = 50Hz; SR = 5000$$

---

#### butterworth filter

$$n = 3 \quad W_n = \frac{f_{LP}}{0.5 * SR} \quad f_{LP} = 10Hz; SR = 5000$$

**Table 3.8: filter settings for data acquisition (notch and butterworth)**

$w_0$  location of notch,  $b_w$  bandwidth at -3dB point  
 $n$  order of filter,  $W_n$  cutoff frequency

Goniometer data was separated into knee extension and knee flexion phase too, sum and mean values were calculated like shown in equation (3.2).

### 3.2.4 Training protocol

For the current study we equipped one subject (male, 28y, 1.72m, 75kg) with EMG sensors and goniometers to collect muscle activation and joint angle data during the training. The subject had to perform both modes of training (isokinetic and vibration-proprioceptive), in all variations of voluntarily muscle activations (0%, 50% and 100%) we simulate in OpenSim. Training protocol was defined with 3 cycles of knee extension (KE) and knee flexion (KF), starting at max knee flexion  $\gamma = max$  (feet nearest to the body) illustrated in Figure 3.14.

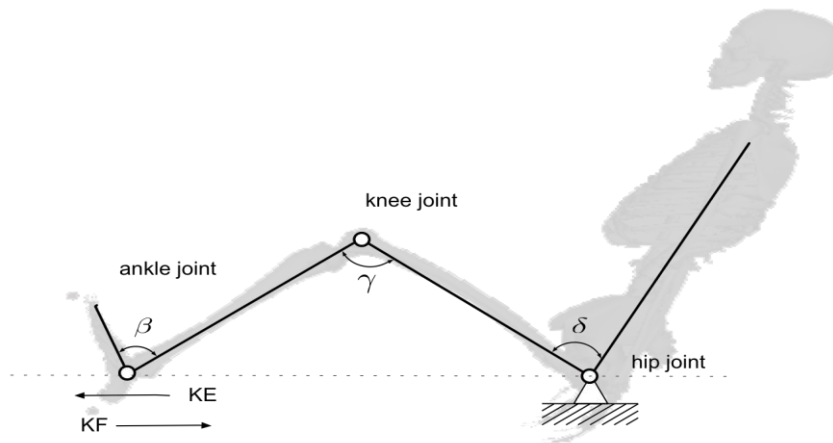


**Figure 3.14: Schema of position and movement of the subject the measurement**

*KE knee extension (foot sledge is moving away from the body)*

*KF knee flexion (foot sledge is moving to the body)*

Each trail was done 3 times, to allow the subject to get familiar with the training and the claimed voluntary activation. For regeneration reasons a 5 minutes rest was given and subject was allowed to remove its feet from the leg press pedals. Values of starting position are documented in Table 3.9 and definition of angles may be found in Figure 3.14. Due to measurement reasons during preparation, angles aren't defined in the same way like in OpenSim and therefore needed to be converted.

	start position [°]
hip angle (frontal)	$\varepsilon = 0^\circ$
hipt angle (sagittal)	$\delta = 96^\circ$
knee angle	$\gamma = 114^\circ$
ankle angle	$\beta = 93^\circ$

**Table 3.9: Angles of rest position of EMG and goniometer measurements**

Within the leg press software all parameters, like start and stop position, velocity and path of the pedals, amount of repetitions had been defined (see Table 3.10 and Figure 3.15).

defined parameters	
<b>isokinetic</b>	start: 8 cm, stop 26 cm velocity: $v_{KE} = 0.2 \text{ m/s}$ , $v_{KF} = 0.2 \text{ m/s}$ repetitions: 3 trails: 3
<b>vibration 50%</b>	start: 8 cm, stop 28 cm velocity: $v_{KE,1} = 0.3 \text{ m/s}$ , $v_{KE,2} = 0.2 \text{ m/s}$ $v_{KF,1} = 0.7 \text{ m/s}$ , $v_{KF,2} = 0.2 \text{ m/s}$ path: $x_{KE,1} = 20 \text{ cm}$ , $x_{KE,2} = -5 \text{ cm}$ $x_{KF,1} = -15 \text{ cm}$ , $x_{KF,2} = -5 \text{ cm}$ repetitions: 3 trails: 3

**Table 3.10: Parameters of isokinetic and vibration trainings protocol**

Record of data wasn't triggered with the movement of the leg press and had to be released and stopped manually. Further investigations (see chapter 4) were done with one trail of them. Selection was done via visual assessment of the goniometer and EMG data in MATLAB and the subjective response of the subject.

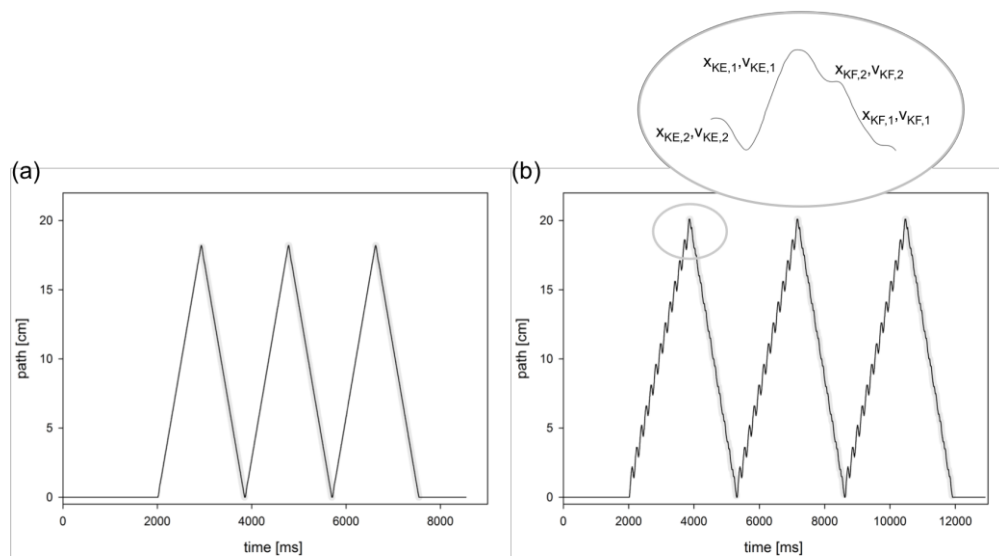


**Figure 3.15: Pathway of foot pedals for isokinetic (a) and vibration(b) mode and detail**  
*Shaped in gray: knee flexion phase (KF)*

## 4 Results: OpenSim – Simulation

The study in hand aimed to calculate forces and activation of the lower limb muscles during different leg press training. Therefore motions and loads were reproduced in simulation software and exercises had been computer-simulated. Results from these simulations are discussed in the following chapter.

### 4.1 Results: Inverse Kinematics (IK)

As stated in chapter 2.6.3.1, results of the IK-Tool are the generalized coordinate trajectories (angles) of every joint during the defined exercise. Figure 4.1 illustrates hip, knee and ankle joint angles of our model during isokinetic and vibration training onto the leg press. Simulations were done for exercises with 3 cycles of motion, and started with the maximum flexion of the knee.

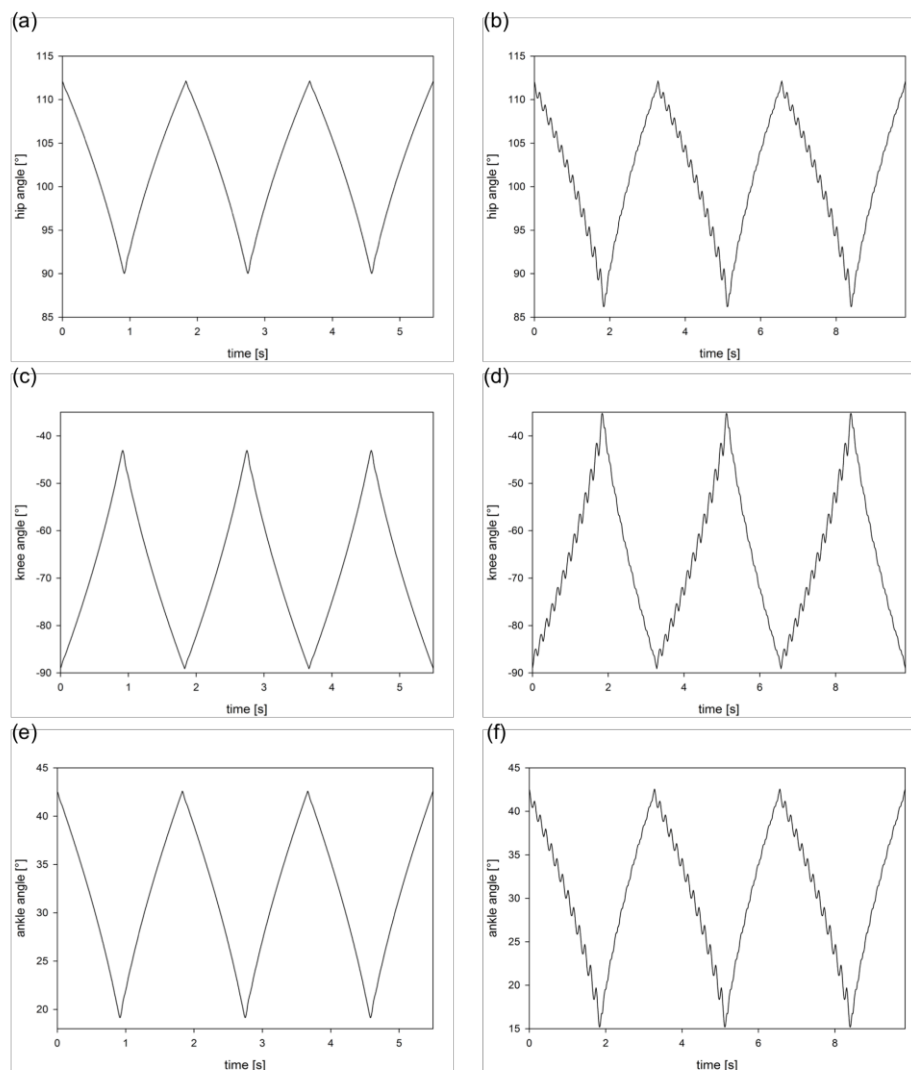


**Figure 4.1: Results of inverse kinematics simulation including hip-, knee- and ankle joint**  
*all shown angles are flexion angles of hip, knee and ankle*  
*isokinetic on the left, vibration on the right*

With the help of the IK-Analyses it was possible to transform the recorded data of the motion into OpenSim. Because we couldn't use motion capture systems to reproduce motion, we had to do it via path-data stored by the leg press software. Data, plots and simulations of the calculated motions and angles described the observed motion of the subject reasonable.

## 4.2 Results: Inverse Dynamics (ID)

Results of the Inverse Dynamics Tool imply all generalized force and torque data of each joint responsible for the defined movement of our model. In that case, resulting data provided torques for hip, knee and ankle flexion of the left leg of our simulation model described in chapter 3.1.1.

On basis of the input data (MOT-file, which results from IK-Tool), the Inverse Dynamic Analyses calculated all necessary torques for the defined 3 cycles of movement. Figure 4.2 depicts the computed values of the three effected joints and illustrates the difference between isokinetic and vibration training as well as the various voluntary activation levels of the subject, which resulted in different external forces (50% and 100%, see chapter 3.1.4.2).

Investigations of simulation data showed (Figure 4.2 and Table 4.1), knee torques were about 2 – 5 times higher than moments produced in the hip, and 5 – 7 times higher than computed ankle torques. As we suggested, results confirmed that the knee joint gets stressed most when doing leg press training. Therefore we concluded to focus on knee joint and the relevant muscles of it most in further analyses.

Taking a more detailed look onto Figure 4.2, it became apparent, that vibration training affects the hip joint more than the two other joints in use. We observed an increase of oscillation due to vibration motion from ankle (*f*), via knee (*d*) to the hip joint (*b*). Apart from that, there were only little differences in hip and ankle progress when we brought isokinetic and vibration motion face to face. Unlike hip and ankle, results of the knee joint showed peaks of calculated torque at different motion states. The maximal isokinetic knee flexion moment was located at the end of the motion (around  $-89^\circ$  of knee flexion), while peaks of the vibration data occur during the last third of the motion (around  $-76^\circ$  of knee flexion angle).

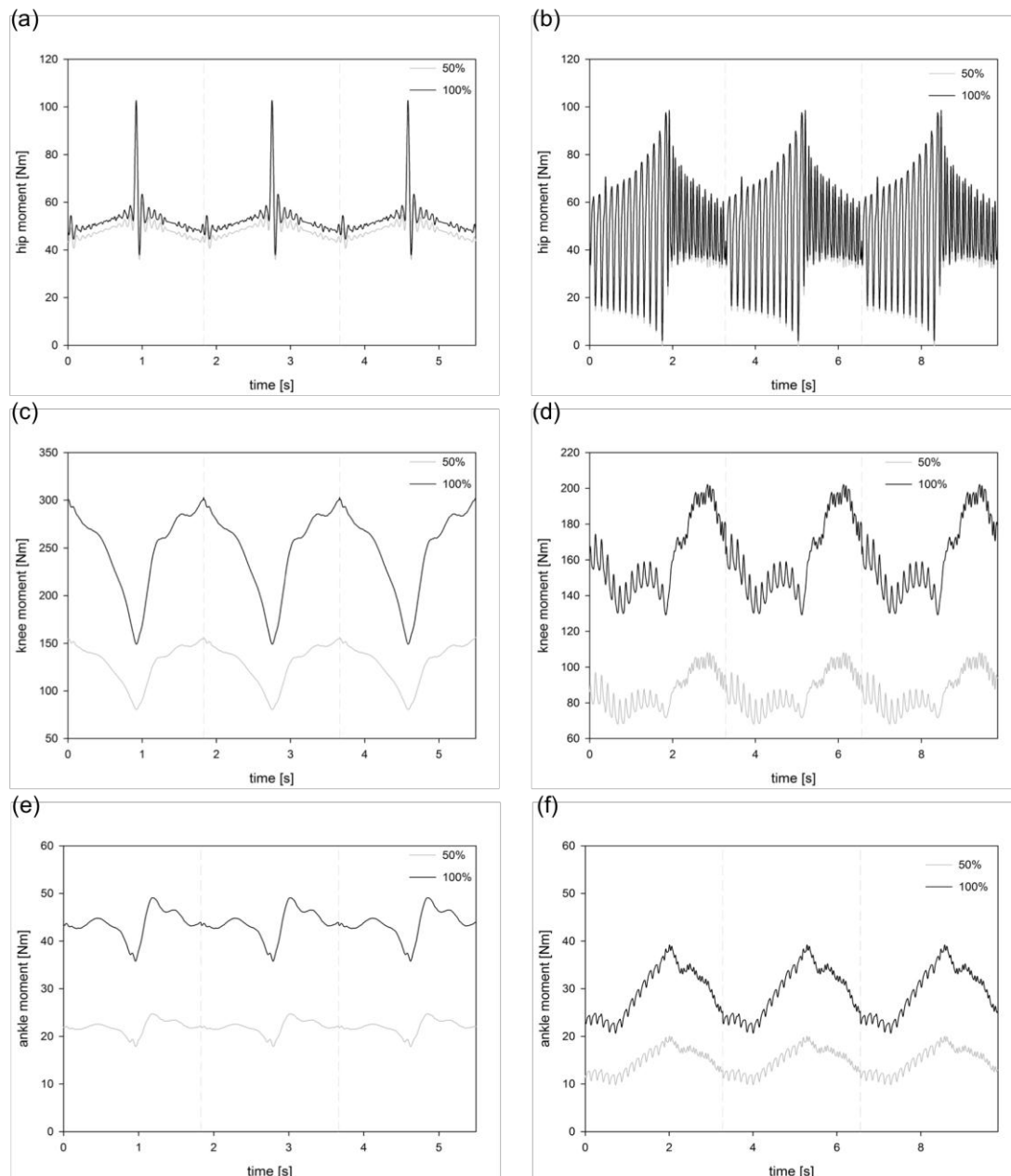


**Figure 4.2: Inverse dynamics results, including torques of hip, knee and ankle joints**  
*isokinetic on the left, vibration on the right*

Table 4.1 lists mentioned data of hip, knee and ankle torques at four specific knee angles, two during flexion and two during extension phase of motion. As point of interest (POI) we defined for both,  $\gamma = -75^\circ$  and  $\gamma = -60^\circ$  of knee flexion and extension, respectively. It is also shown that maximum hip, knee and ankle torques of isokinetic and vibration motion can be observed during flexion phase. In detail it is obvious, that maxima of knee moments arise at a higher angle of knee flexion than maximum values for hip and ankle did. Furthermore it is noticeable, that occurred torque values are higher while isokinetic motion. There was only small difference when calculated hip moments of isokinetic and vibration movements were compared.

But when knee and ankle torques were focused on, values of isokinetic were between 1.4 and 2 times higher than simulated torques for vibration training.

		hip moment [Nm]	knee moment [Nm]	ankle moment [Nm]
<b>isokinetic 50%</b>	-75° ext	46.88	139.35	22.08
	-60° ext	49.73	118.05	21.72
	-60° flex	<b>50.24</b>	132.73	<b>24.70</b>
	-75° flex	47.49	<b>146.88</b>	23.40
<b>vibration 50%</b>	-75° ext	41.91	75.67	11.11
	-60° ext	46.86	80.87	14.23
	-60° flex	<b>48.13</b>	94.81	<b>17.02</b>
	-75° flex	43.40	<b>104.27</b>	15.97
<b>isokinetic 100%</b>	-75° ext	50.83	268.18	43.86
	-60° ext	53.24	224.62	43.14
	-60° flex	<b>53.78</b>	254.04	<b>49.08</b>
	-75° flex	51.75	<b>283.31</b>	46.47
<b>vibration 100%</b>	-75° ext	45.94	139.66	22.11
	-60° ext	50.39	150.07	28.12
	-60° flex	<b>52.64</b>	177.85	<b>33.82</b>
	-75° flex	44.72	<b>197.87</b>	31.66

**Table 4.1: ID results, hip, knee and ankle moments at point of interest (POI)**  
bold values are maximum values of both phase (extension and flexion)

Table 4.2 lists maximal knee moments and responding knee angle of extension and flexion of isokinetic and vibration movement. We determined that for isokinetic and vibration training, maximal extension torques appeared at about the same knee angle (around -89° and -86°). Noticeable is, that when computing the flexion phase of both motions, maxima of isokinetic and vibration mode occur no longer at similar angles. Maximum flexion moments of isokinetic training appeared around -89°, while vibration training peaks at knee flexion angles around -76.5°.

	max. knee moment [Nm]	knee angle, $\gamma$ [°]	phase of motion	mean [Nm]
<b>isokinetic 50%</b>	154.95	-88.81	extension	127.37
<b>isokinetic 100%</b>	300.65	-88.83		243.90
<b>vibration 50%</b>	97.03	-86.33		79.49
<b>vibration 100%</b>	174.34	-86.33		147.85
<b>isokinetic 50%</b>	156.12	-89.11	flexion	132.63
<b>isokinetic 100%</b>	302.93	-89.10		254.41
<b>vibration 50%</b>	108.09	-76.47		95.36
<b>vibration 100%</b>	202.11	-76.50		179.66

**Table 4.2: ID results, knee moments and angles during extension and flexion**  
50% voluntary activation, 100% voluntary activation

Comparison of calculated ratio between mean values of isokinetic and vibration motion showed that for vibration movement lower knee torques (30 – 40%) are needed. Additionally we observed, that ration of both motion phases (flexion versus extension) showed a higher value for vibration training. Results of extension and

flexion phase for isokinetic were similar, unlike values of the vibration run. Thereby mean values of knee moments are about 1.2 times higher.

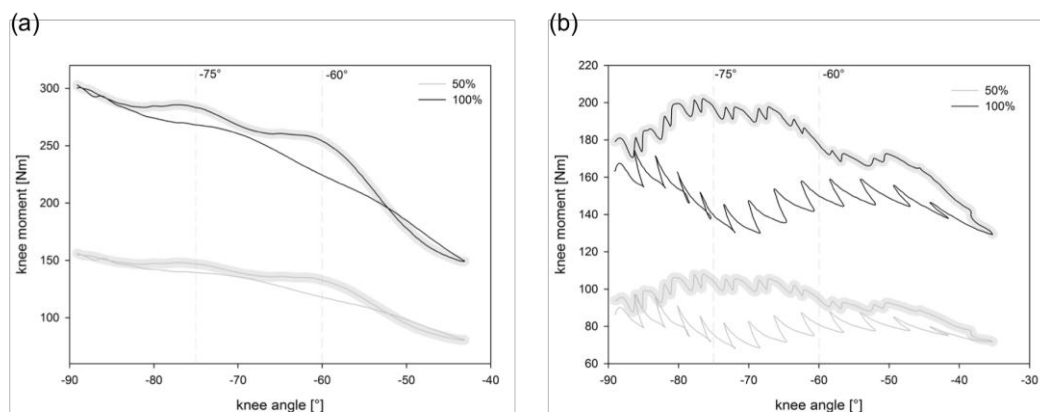


**Figure 4.3: ID results, knee moment vs. knee angle**

*isokinetic mode left, vibration mode right; shaded in grey: flexion phase*

Like other researchers (Lorenzetti et al. 2012; Gullett et al. 2009) did, we plotted knee moments versus knee angle data (Figure 4.3). Lines shaded in grey represent the flexion phase of the knee, others the extension phase. Vertical lines at  $-75^\circ$  and  $-60^\circ$  map the four points of interests (POI) listed in Table 4.1. It is obvious that torques of the knee joint decrease when knee extension was raised during isokinetic simulations (a). When knee extension was decreased – increase of knee flexion – knee moments increased and peaked at knee angles of  $-89^\circ$  and  $-88^\circ$  for 50% and 100% of voluntary activation. Vibration data did not look the same, knee moments did not decrease or increase steadily during both phases.

		knee moment [Nm]	external force [N]
<b>isokinetic 50%</b>	-75° ext	139.35	457.09
	-60° ext	118.05	449.93
	-60° flex	132.73	<b>512.49</b>
	-75° flex	<b>146.88</b>	484.37
<b>vibration 50%</b>	-75° ext	75.67	229.01
	-60° ext	80.87	293.16
	-60° flex	94.81	<b>351.74</b>
	-75° flex	<b>104.27</b>	330.76
<b>isokinetic 100%</b>	-75° ext	268.18	914.18
	-60° ext	224.62	899.86
	-60° flex	254.04	<b>1024.97</b>
	-75° flex	<b>283.31</b>	968.73
<b>vibration 100%</b>	-75° ext	139.66	458.19
	-60° ext	150.07	586.33
	-60° flex	177.85	<b>703.48</b>
	-75° flex	<b>197.87</b>	661.51

**Table 4.3: ID results, knee moments and external forces at POI**

*bold values are maximum values of each phase*

We noticed that maximum values of simulated knee moments and measured, external forces occurred simultaneous during the same phase of motion (flexion), but not at the same POI as it can be seen in Figure 4.4 and Table 4.3.

Highest and lowest ratio between knee moment and external force is for isokinetic motion about 0.3 and 0.26 with 50% and around 0.29 and 0.25 with 100% voluntary activation. Mean values are about 0.28 and 0.27 respectively.

Doing same calculations with data from vibration simulations maximum and minimum values of ratio are about 0.33 and 0.28 when activation is 50% and 0.3 and 0.26 for 100% of voluntary activation of the subject, respectively. Mean values are 0.3 and 0.28.

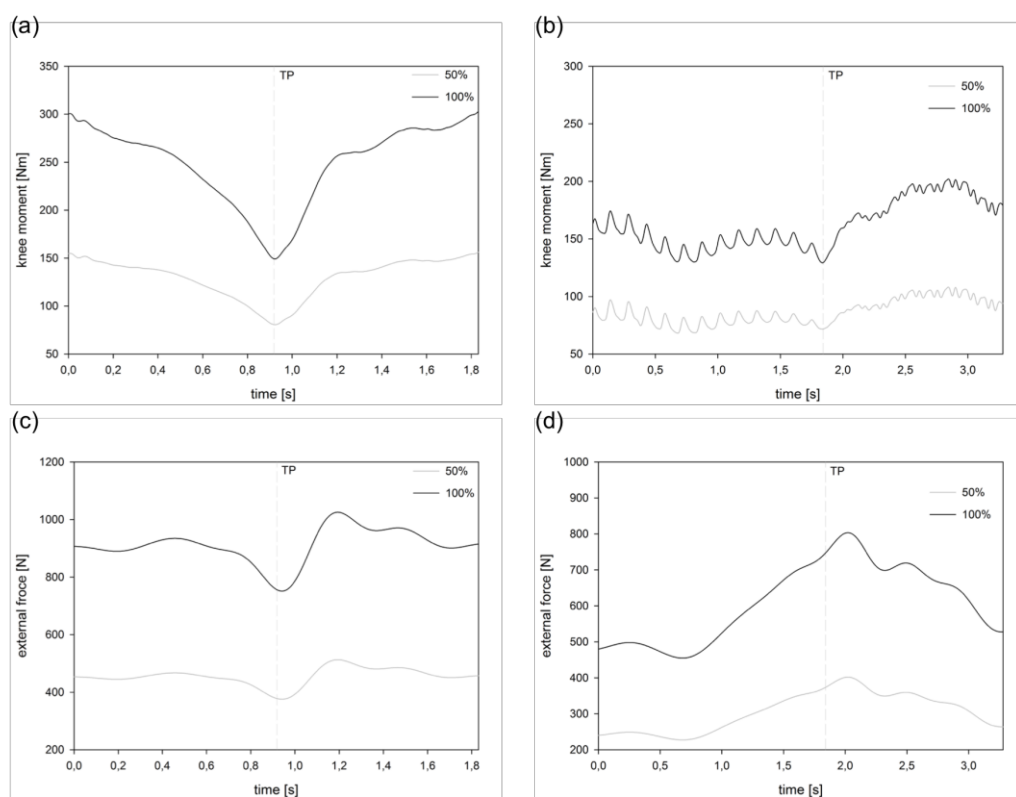


**Figure 4.4: ID results, knee moment (a, b) and external force (c, d)**  
*isokinetic mode left, vibration mode right, TP: turning point of motion*

### 4.3 Results: Computer Muscle Control (CMC)

Calculating muscle force and excitation of affected muscles was realized by the CMC-Analyses. Simulation included all muscles defined in chapter 3.1.3. Based on the work of Cho and Da Silva (Cho et al. 2008; Da Silva et al. 2008) we limited our investigations to a number of twelve muscles (see chapter 3.1.3). Furthermore we focused on musculus quadriceps femoris, and each of his four heads, rectus femoris (RF), vastus medialis (VM), vastus intermedius (VI) and vastus lateralis (VL), most As illustrated in Figure 4.5 only quadriceps muscles and m. tibialis anterior featured notable muscle activity. Results of all other muscles showed no activation. As mentioned in chapter 2.6.3.3 constant values of 0.02 (representing no excitation) result due to defined lower bound parameter in the muscle model (Hicks 2011). To enable comparison of isokinetic and vibration results, data was low pass filtered like we did with recorded force data in chapter 3.1.4.2.

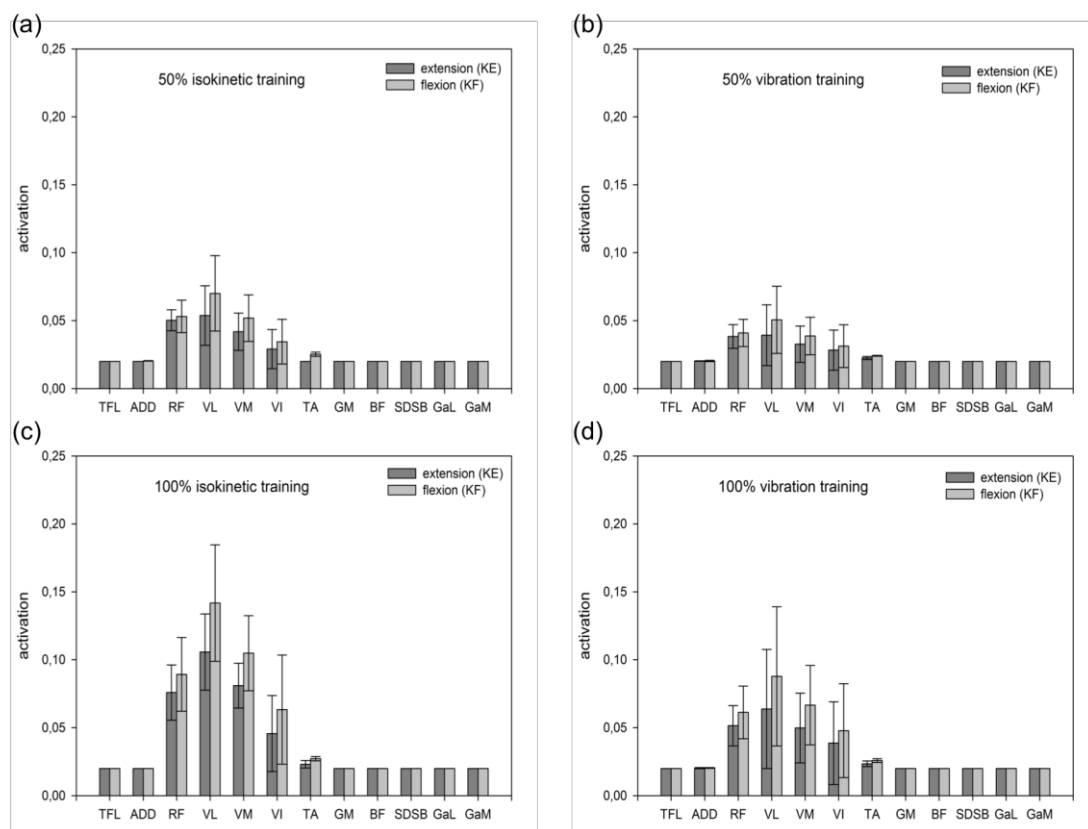


**Figure 4.5: Mean and standard deviation of twelve muscles of interest**

*Left: isokinetic; right: vibration mode, activation level from 0 (no activity) to 1 (maximal activity), dark grey: data of extension phase (KE), light grey: data of flexion phase (KF) left: isokinetic, right: vibration, with 50% and 100% external load*

CMC-Analyses computed time dependent values of muscle force and excitation while performing defined leg press training motion. Figure 4.6 depicts excitation data of all four quadriceps heads in the course of each simulation variation while one single cycle of movement. Grey lines represent raw simulation data without any

manipulation done. Black drawn through and dotted lines reflect low pass filtered activation data for 50% and 100% of voluntary activation. Vertical grey-dotted lines represent the change of movement from extension to flexion of the knee joint (TP).

		<b>muscle activation</b>			
		rect_fem	vas_med	vas_int	vas_lat
<b>extension</b>					
<b>iso50</b>	max	0.0593	0.0535	0.0531	<b>0.0724</b>
	$\gamma$	-111.47°	-97.19	-91.83°	-97.69°
	mean	0.0506	0.0414	0.0289	<b>0.0525</b>
<b>iso100</b>	max	0.0935	0.0977	0.0810	<b>0.1244</b>
	$\gamma$	-79.75°	-100.21°	-92.90°	-101.38°
	mean	0.0775	0.0829	0.0441	<b>0.1075</b>
<b>vib50</b>	max	0.0542	0.0453	0.0506	<b>0.0621</b>
	$\gamma$	-87.45°	-46.33°	-42.49°	-47.32°
	mean	0.0390	0.0326	0.0283	<b>0.0392</b>
<b>vib100</b>	max	0.0746	0.0699	0.0781	<b>0.0989</b>
	$\gamma$	-87.45°	-47.55°	-87.45°	-47.70°
	mean	0.0522	0.0492	0.0381	<b>0.0629</b>
<b>flexion</b>					
<b>iso50</b>	max	0.0599	0.0733	0.0583	<b>0.1039</b>
	$\gamma$	-107.88°	-97.78°	-96.13°	-97.47°
	mean	0.0533	0.0524	0.0345	<b>0.0719</b>
<b>iso100</b>	max	0.1074	0.1383	0.1211	<b>0.1950</b>
	$\gamma$	-105.45°	-98.73°	-97.61°	-98.35°
	mean	0.0862	0.1047	0.0624	<b>0.1407</b>
<b>vib50</b>	max	0.0479	0.0530	0.0565	<b>0.0773</b>
	$\gamma$	-62.38°	-48.66°	-43.46°	-46.68°
	mean	0.0414	0.0387	0.0387	<b>0.0504</b>
<b>vib100</b>	max	0.0742	0.0889	0.0940	<b>0.1234</b>
	$\gamma$	-76.42°	-48.48°	-45.02°	-46.76°
	mean	0.0612	0.0679	0.0487	<b>0.0895</b>

**Table 4.4: CMC results, mean and max values of muscle activation**

*bold values are maxima of all four heads*

*$\gamma$  represents knee angle where max value is located*

As other researchers (Alkner, Tesch, & Berg, 2000; Escamilla et al., 1998, 2001; Wretenberg, Feng, Lindberg, & Arborelius, 1993) suggested in their work, we observed most activity and force production in both motions in musculus vastus lateralis (g, h), followed by musculus vastus medialis (c, d), musculus vastus intermedius (e, f) and musculus rectus femoris (a, b). Further we observed, that mean values of activation levels are between 1.1 and 1.4 (50% and 100% of voluntary contraction) times higher performing flexion of the knee than extending it. Maximum values are around 1.1 to 1.4 (50%) and 1.4 to 1.6 (100%) times higher. Except rectus femoris, were a growth of less than one percent could be observed.

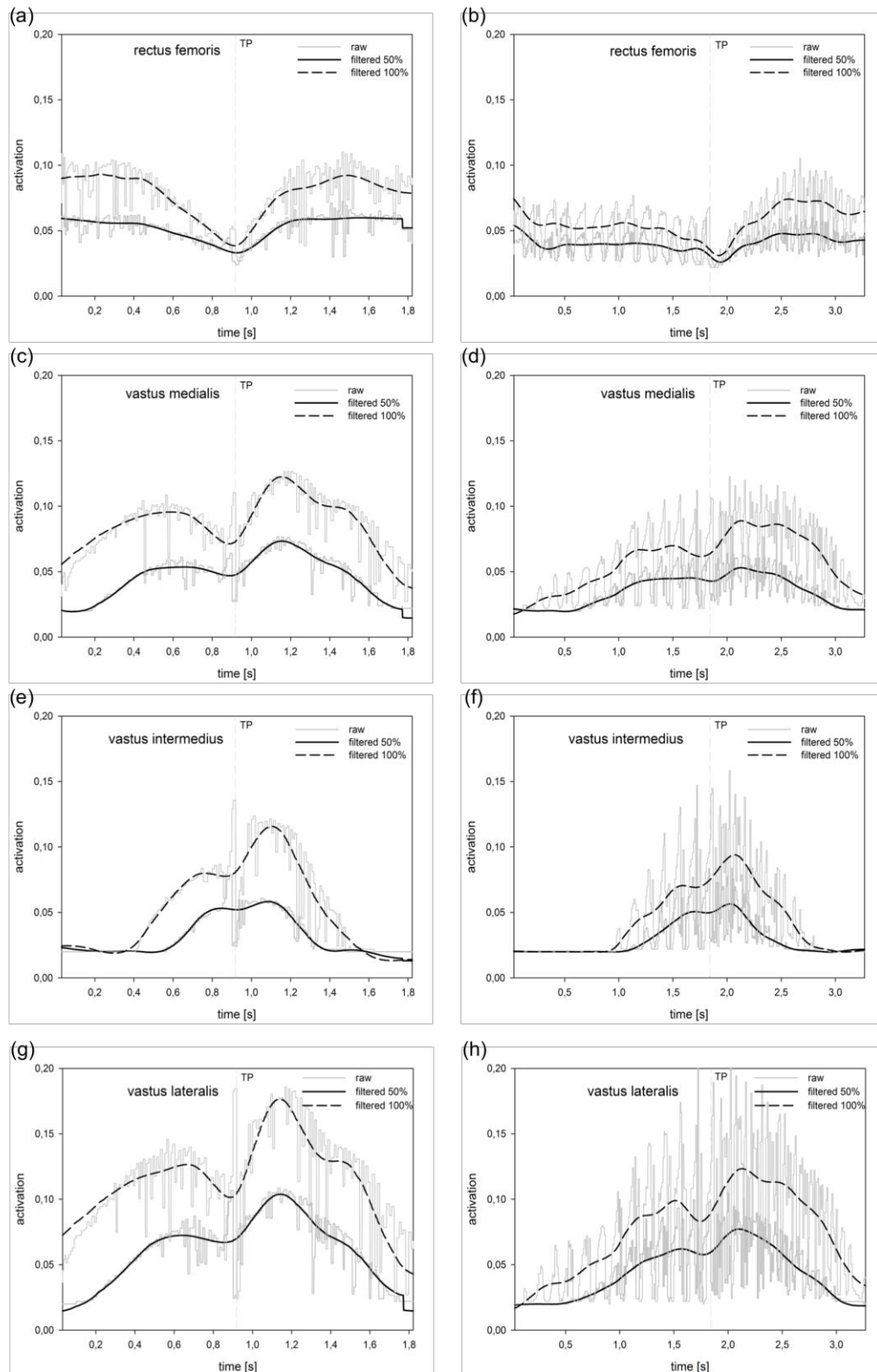


**Figure 4.6: CMC results, activation of all four quadriceps muscles (RF, VM, VI, VL)**  
*left: isokinetic, right: vibration, activation level from 0 (no activity) to 1 (maximal activity);  
 TP: turning point of motion (extension - flexion); grey lines represent raw data, black lines  
 are low-pass filtered data at 50% and 100% force level*

In general it could be hypothesized that excitation levels of both, isokinetic and vibration simulations were higher during the flexing phase of motion. Ratio between

mean values of extension and flexion phase range from 0.56 to 0.95, respectively. Supplementary to those numbers, Figure 4.8 illustrates the relationship between muscle activation and the actual knee angle and supports that assertion. It is evident that simulations with vibration motion result in lower excitation than calculating muscle activation for isokinetic training. Moreover pictures of Figure 4.8 show that during isokinetic flexion, three of the four quadriceps heads (VM, VI, VL) peaked near  $\gamma = -60^\circ$ , looking onto vibration data this could not be observed.

Higher activity during flexion phase could be observed in Figure 4.7. picturing the mean values (bars) of each single head of the quadriceps muscle while extension and flexion phase and the maximum values (error bars). Isokinetic motion left (a) and vibration training right (b), black bars represent data from simulation runs with 50% voluntary contraction, grey ones for 100% stress.

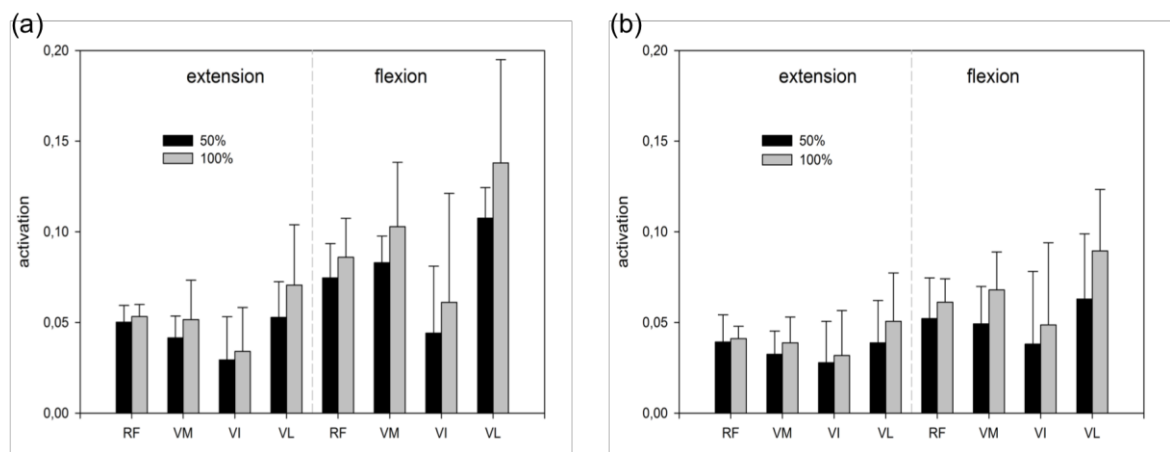


**Figure 4.7: CMC results, mean and max values (error bar) of quadriceps muscle activation**  
(a) isokinetic, (b) vibration

Comparing isokinetic and vibration values of each phase it has been postulated that muscle activation of all investigated muscles are at a lower level during vibration training. Differences between vibration and isokinetic data is higher when simulations were done with 50% of voluntary activation (0.83) than using force data of 100% activation (0.71).

Looking on the following illustration (Figure 4.8) isokinetic simulation data featured explicit deviation of all three vasti muscles (VM, VL and VI) between knee extension (KE) and knee flexion (KF, shaded grey) values. Deviation of rectus femoris muscle was much smaller or even missing. This could not be observed in vibration data, where differences between KE and KF phase of all four quadriceps muscles was in similar scale.

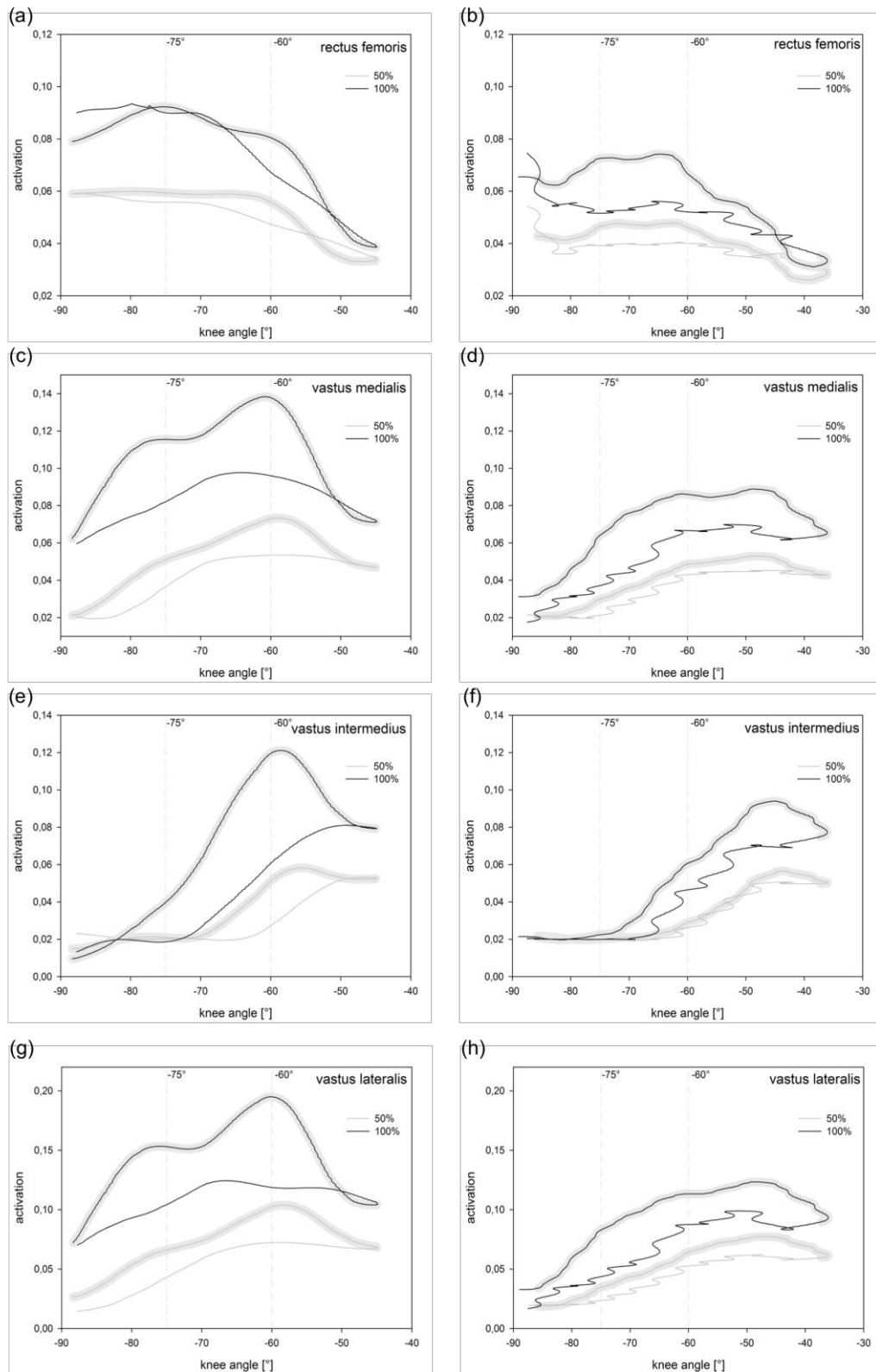


**Figure 4.8: CMC results, activation vs. knee angle of all four quadriceps muscles**  
 Left: isokinetic, right: vibration; activation level from 0 (no activity) to 1 (maximal activity);  
 grey shaded: flexion phase; averaged data of three cycles of movement, with both POI  
 (-75° and -60°)

Furthermore OpenSim calculated not only excitation data of all affected muscles for the whole simulated training, the simulation tool computed for each instance of time the specific and needed muscle forces, too.

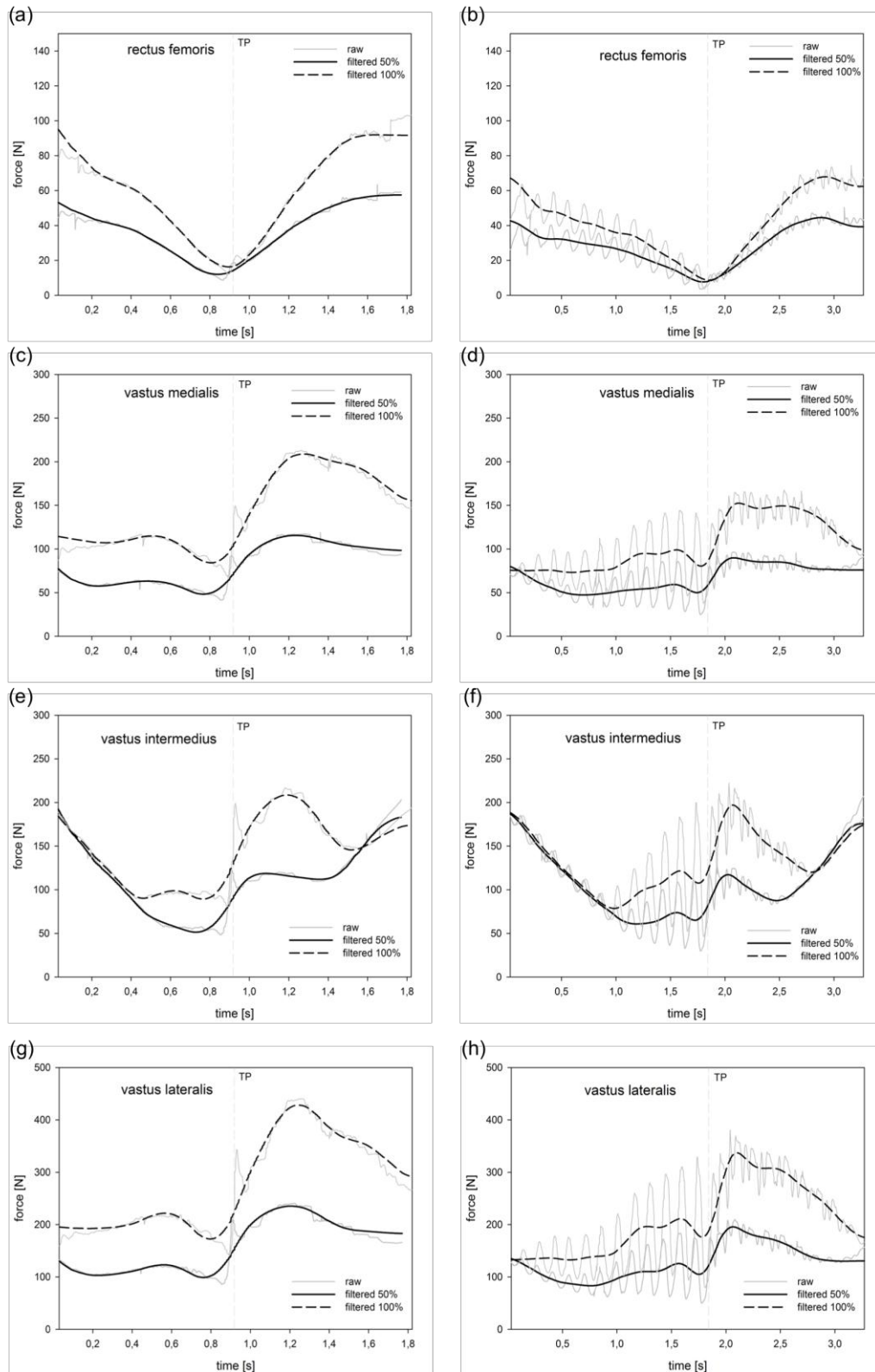


**Figure 4.9: CMC results, forces of all four quadriceps muscles (RF, VM, VI, VL)**  
*left: isokinetic, right: vibration, TP: turning point of motion (extension - flexion)*  
*grey lines represent raw data, black lines are low-pass filtered data*

As we did with muscle activation, we filtered raw force data with same parameters used in chapter 3.1.4.2 and proceed like with excitation data previously. Equal to the findings before higher muscle forces of all four quadriceps heads during both variations of motion could be observed when flexing the knee. Figure 4.9 confirms that fact and illustrates data of all quadriceps muscles during isokinetic (a, c, e, g) and vibration (b, d, f, h) simulations. Like excitation it occurred, that most force was produced by musculus vastus lateralis whether doing isokinetic or vibration simulation runs. While vastus medialis and vastus lateralis increased hardly during extension of the knee joint, others decreased rapidly when knee extension was raised. However all of them peaked when flexion was executed. That could also be observed when looking onto Figure 4.10, where we compared the calculated muscle force with relevant knee angles in the course of the complete range of motion.

		<b>muscle activationFORCE</b>			
		rect_fem	vas_med	vas_int	vas_lat
<b>extension</b>					
<b>iso50</b>	max	53.23	77.52	<b>192.53</b>	140.00
	$\gamma$	$-111.47^\circ$	$-111.47^\circ$	$-111.47^\circ$	$-90.84$
	mean	31.78	59.48	94.44	<b>112.47</b>
<b>iso100</b>	max	95.14	114.99	184.47	<b>225.27</b>
	$\gamma$	$-111.47^\circ$	$-100.92^\circ$	$-111.47^\circ$	$-99.47^\circ$
	mean	51.81	104.87	114.22	<b>198.77</b>
<b>vib50</b>	max	42.71	80.00	<b>187.11</b>	134.99
	$\gamma$	$-87.45^\circ$	$-87.45$	$-87.45$	$-87.45$
	mean	25.27	55.57	97.22	<b>104.82</b>
<b>vib100</b>	max	67.20	99.00	188.51	<b>211.22</b>
	$\gamma$	$-87.45^\circ$	$-47.55^\circ$	$-87.45^\circ$	$-47.70^\circ$
	mean	35.91	82.79	117.01	<b>162.21</b>
<b>flexion</b>					
<b>iso50</b>	max	57.53	115.58	183.06	<b>235.32</b>
	$\gamma$	$-111.81^\circ$	$-99.66^\circ$	$-111.81^\circ$	$-98.91^\circ$
	mean	41.63	102.92	127.22	<b>202.53</b>
<b>iso100</b>	max	91.96	208.90	208.59	<b>428.11</b>
	$\gamma$	$-109.57^\circ$	$-100.77^\circ$	$-98.60^\circ$	$-99.88^\circ$
	mean	88.71	179.74	173.12	<b>354.46</b>
<b>vib50</b>	max	44.55	89.89	175.75	<b>195.65</b>
	$\gamma$	$-75.54$	$-45.49$	$-85.68$	$-44.98$
	mean	31.69	80.76	117.30	<b>156.32</b>
<b>vib100</b>	max	67.95	152.54	197.06	<b>337.00</b>
	$\gamma$	$-76.42^\circ$	$-48.48^\circ$	$-45.02^\circ$	$-46.76^\circ$
	mean	47.80	132.25	154.87	<b>263.54</b>

**Table 4.5 CMC results, mean and max values of muscle force**

*bold values are maxima of all four heads*

*$\gamma$  represents knee angle where max value is located*

When using 50% external force in isokinetic mode, vastus medialis and vastus lateralis reached their maximum at  $\gamma = -62.81^\circ$  and  $\gamma = -61.27^\circ$ , respectively. Rectus femoris and vastus intermedius had their peak value at maximum knee flexion ( $\gamma = -88.33^\circ$ ). Results of vibration simulation showed maximum force values

at knee flexion of  $\gamma = -45.49^\circ$  for vastus medialis and  $\gamma = -44.98^\circ$  for vastus lateralis as well as  $\gamma = -75.54^\circ$  and  $\gamma = -85.68^\circ$  for rectus femoris and vastus intermedius in each case.

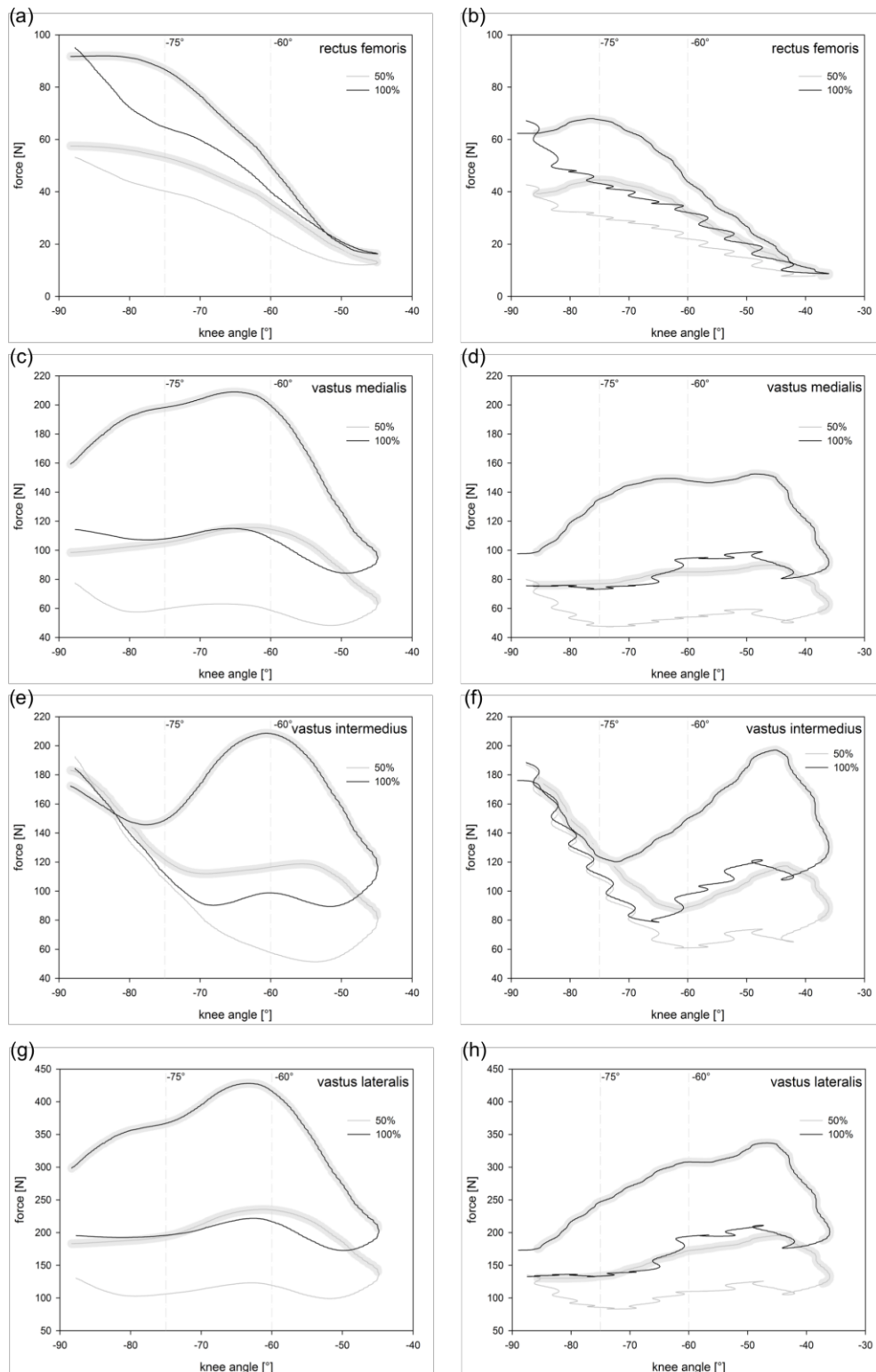


**Figure 4.10: CMC results, forces Vs. knee angle of all four quadriceps muscles**  
 left: isokinetic, right: vibration, grey shaded: flexion phase  
 averaged data of three cycles of movement, with both POI (-75° and -60°)

The same approach done with 100% external force data lead to different results, regarding positioning of peaks in calculated muscle force (see Table 4.5). During isokinetic simulation, force of musculus vastus medialis, vastus intermedius and vastus lateralis peaked within the same range of knee flexion,  $\gamma = -65.13^\circ$  (VM),  $\gamma = -60.62^\circ$  (VI) and  $\gamma = -63.28^\circ$  (VL), while musculus rectus femoris maximum value appeared at an angle of  $\gamma = -83.62^\circ$ . Vibration motion led to maximum values of ,  $\gamma = -48.48^\circ$ ,  $\gamma = -45.02^\circ$  and  $\gamma = -46.76$  for vastus medialis, vastus intermedius and vastus lateralis. Maximum force of musculus rectus femoris could be observed at flexion angle of  $\gamma = -76.42^\circ$ .

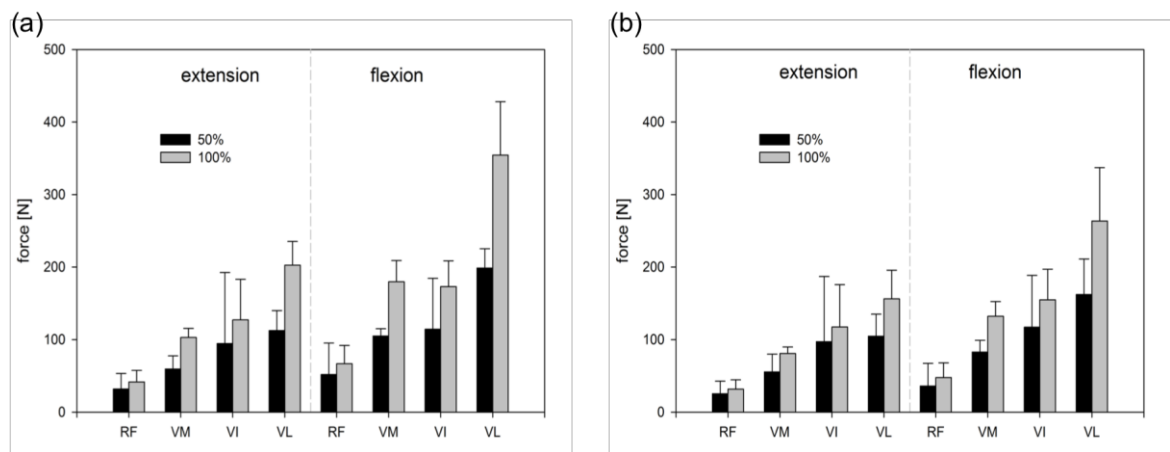


**Figure 4.11: CMC results, mean and max values (error bars) of quadriceps muscle forces**  
 (a) isokinetic, (b) vibration

Equivalent to activation data, calculated mean values of muscle forces behave nearly simultaneous when comparing extension and flexion phases as well as isokinetic and vibration movement. Illustrated in Figure 4.11, it could be suggested that more force need to be produced by quadriceps muscles to flex the knee joint. It also can be observed, that isokinetic motion lead to causes higher muscle forces than vibration movement did.

## 4.4 Discussion

Simulation data illustrated most stress at the knee joint during both isokinetic and vibration movement, although vibration training evoked less knee torques than isokinetic did. It could be observed that musculus vastus lateralis became most prominent muscle of lower limb muscles across all variations of leg press training followed by the other heads of the quadriceps muscle. Further simulations showed that, according to Inverse Dynamic results, higher muscle activations and muscle forces occurred when knee flexion (KF) was executed and during isokinetic training.

*Inverse Dynamics Analysis:* Simulation results pointed out, that the knee joint is highly stressed during leg press training. Compared with the two other observed joints of the lower limb (ankle and hip) torques were between two and seven times higher. Maximal computed values of knee moments were about 156 Nm (50% voluntary activation) and 303 Nm (with 100% voluntary activation) while isokinetic motion. Vibration training results in lower maximum values of 108 Nm and 202 Nm for 50% and 100% of voluntary activation. It is noticeable that all maximal values occur during knee flexion (KF).

Investigations of all three joints showed that oscillation due to vibration training caused lower vibrations inside the knee than inside the hip joint. Hip data showed plenty of noise referable to the movement type. On the contrary, ankle moments featured lower amplitudes in consequence of vibration training.

It is evident, that results of isokinetic simulations were higher in all three joints, compared with vibration data. Knee torque was around 1.5 times higher and peaked in isokinetic mode at the beginning and/or the ending of the cycle. Unlike in vibration mode where peaks occurred in the last third of the motion during the knee flexion phase (KF). Progression of hip and ankle torques featured maximum values at the turning point of motion (KE to KF, at  $\gamma = -43^\circ$  for isometric and  $\gamma = -35^\circ$  for vibration mode) whereas torques calculated for the knee joint had their maximum not located at these characteristic points. Isometric knee moment peaked at  $\gamma = -89^\circ$  and vibration data showed highest values at knee angle of  $\gamma = -76^\circ$ .

Maximum values of simulated knee moments and measured, external force data appeared simultaneous during the flexion phase. But there is a mismatch concerning the knee flexion angle (POI) those values occurred. External force data peaked at knee angles of  $\gamma = -60^\circ$  while knee moment progression showed higher values at knee angles of  $\gamma = -75^\circ$ . Ratio between moment and force data is below 0.3 for isometric and slightly above 0.3 for vibration simulations.

*Computer Muscle Control Analysis – muscle activation:* Results of simulated data are consistent with those documented by Alkner, Escamilla and others (Alkner et al.,

2000; Escamilla et al., 1998, 2001; Wretenberg et al., 1993), were most activity and force production during leg press training was observed in musculus vastus lateralis (VL). Simulation data of all variations (isokinetic, vibration, 50% and 100% of external force) showed same results. Beside of musculus rectus femoris, all other quadriceps heads illustrate same behavior with smaller values. Rectus femoris progression was unique looking at activation data.

In reviewing the literature, we found reports that quadriceps activity in the KE phase of leg press training was 25-50% higher than in KF phase. This could not be confirmed by our simulation data. Excitation values of all four quadriceps muscles showed higher values during flexion of the knee. We hypothesized that this results because of the special leg press machine, the automatic driven foot pedals and the higher external forces during KF. The three vasti (VL, VM, VI) peaked in the same range of flexion angle, no matter of isokinetic or vibration motion. They increased when flexion of the knee joint decreased and vice versa. Ratio between mean values of KE and KF results range from 56% to 96% and disprove the assertion of Escamilla and colleagues. Behavior of RF during isokinetic training was different to that. Data showed a decrease of muscle activity when knee angle was increased and deviation of KE and KF data was very small or even missing. In contrary, this could not be observed in vibration data. All quadriceps muscles featured notable and similar deviation between KE and KF.

Further results showed that vibration training evokes lower muscle excitation than isokinetic training did. It could be observed that differences between vibration and isokinetic data is higher when external force data of 50% was used as an input than using force data of 100% voluntary activation. Muscle activations were 20% lower with small external forces and 30% lower when using maximal external force.

Computer Muscle Control Analysis – muscle force: Looking on force data it is obvious that findings of excitation results can be observed herein too. Like muscle excitation, computed muscle forces reached their maximum during knee flexion. These results differ from the findings of other researchers. Furthermore they are consistent with our hypotheses from above when thinking of higher external forces and the special parameters of our leg press during the flexion phase of the knee.

Like muscle excitation results, simulation computed highest muscle forces for musculus vastus lateralis which supports the findings of Alkner, Escamilla and other researchers (Alkner et al., 2000; Escamilla et al., 1998, 2001; Wretenberg et al., 1993). Characteristics of the four quadriceps heads showed similarities of vastus medialis and vastus lateralis. Both hardly increased during knee extension. On the other side a rapidly decrease of rectus femoris and vastus intermedius could be observed when the movement started.

Comparing mean and maximum data of isokinetic and vibration simulation trails, prior findings of higher activation and forces could be met. Simulations of vibration training featured lower muscle activation values than for isokinetic training did.

Computer Muscle Control Analysis – validation: As OpenSim–developers proposed, we compared CMC results with the thresholds they provided in their work (Hicks 2011). These given standards are special values for full-body simulations of walking and running exercises. Data of models only moving lower limb segments in order to train on a leg press couldn't be found up to now.

Thresholds:	good	okay	bad
MAX pErr [trans, cm]	0 - 1cm	1 – 2cm	>2 cm
MAX pErr [rot, deg]	0 – 2 deg	2 - 5 deg	>5 deg
MAX Reserve [Nm]	0 – 25 Nm	25 – 50 Nm	>50 Nm

**Table 4.6: Thresholds for CMC results**

*pErr: Position errors of the generalized coordinates during the trail*

*Reserve: turn on when actuators cannot produce the needed force to enable the simulation to run, source: (Hicks 2011)*

Mean values of error and reserve data are shown in Table 4.7. Looking onto pErr-values, which represent the positioning errors of the generalized coordinates for every time step of the trail, results are far below the published thresholds. Unlike reserve actuators, especially of the knee and the hip joint which are above those standards. In order to enable the situation to run, additional torques, called reserve actuators are added about each joint to augment the actuator's force. They turn on when an actuator can't produce the needed force at a given time point.

		hip joint	knee joint	ankle joint
isokinetic 50%	pErr [°]	-0.016	0.049	0.647
	Reserve [Nm]	74.59	126.01	51.69
vibration 50%	pErr [°]	0.041	-0.115	0.246
	Reserve [Nm]	77.39	87.85	44.26
isokinetic 100%	pErr [°]	-0.052	0.189	0.716
	Reserve [Nm]	72.06	233.80	73.28
vibration 100%	pErr [°]	0.074	-0.218	0.046
	Reserve [Nm]	81.55	157.85	59.13

**Table 4.7: Error and Reserve values of all CMC simulation trails**

Hicks and colleagues remark that high reserves are related to the production of passive muscle forces (e.g., quadriceps from large knee flexion angles) which may induce active forces in the antagonistic muscles (e.g., hamstrings, gastrocnemius).

As OpenSim-developers advised in the User's Guide (Hicks 2011), there is a workflow how to minimize these values by changing specific parameters inside the body and muscle models (e.g., reduce the passive muscle stiffness property). Moreover, if muscles are acting at suboptimal fiber lengths as the time where the reserves are being generated, modifying either the tendon slack length or the optimal fiber length of the muscle may reduce the reserves. In case of the present study no

adaptions of the muscle parameters had been done, so there is still potential for further improvements.

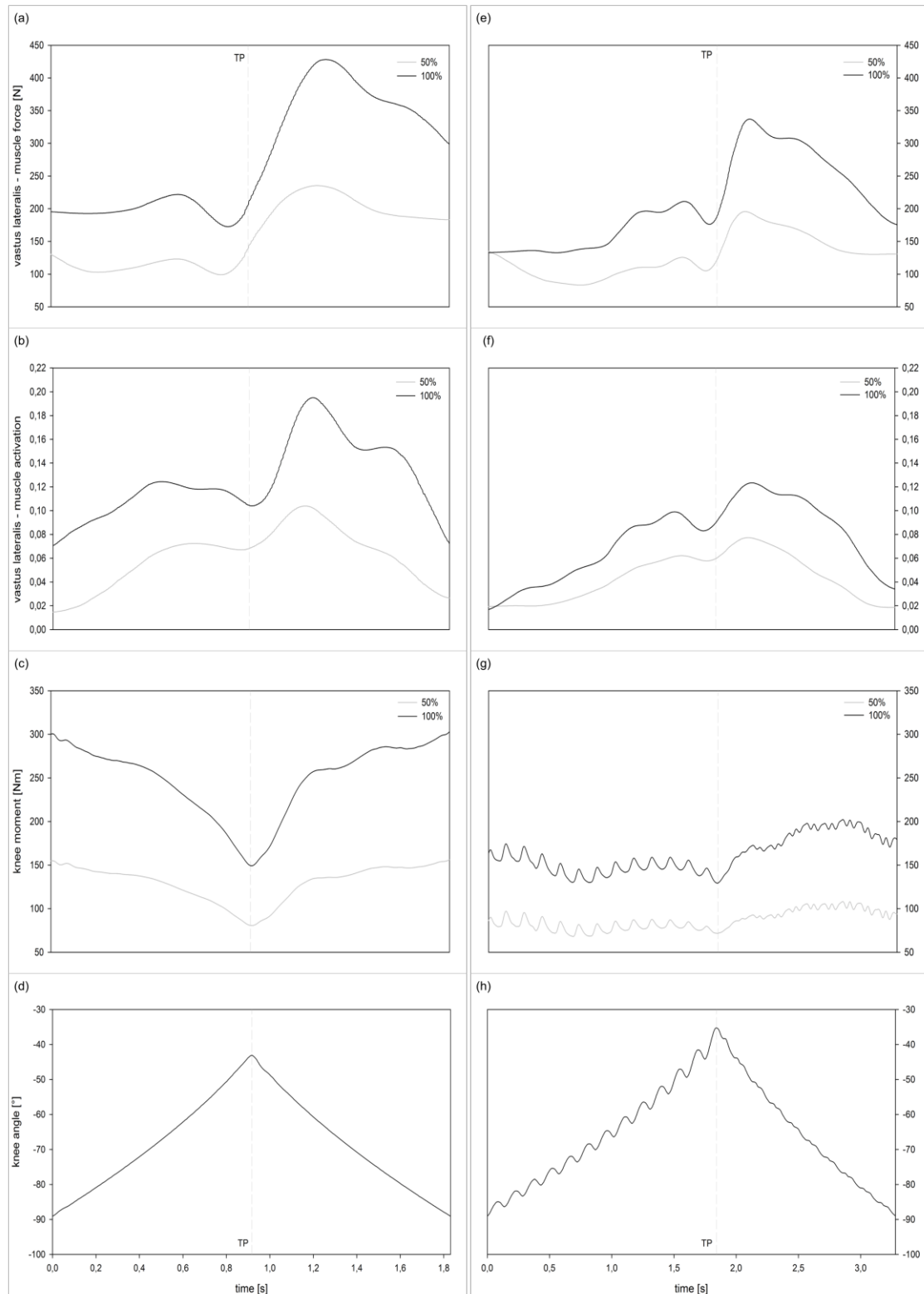


**Figure 4.12: All OpenSim results of musculus vastus lateralis**

*knee angle (d, h), knee moment(c, g), muscle activation (b, f) and muscle force (a, e) of VL of both types of motion (left: isokinetic, right: vibration) and both variations of input data (external force 50% and 100%); vertical, dotted lines represent the turning points, where motion changed from KE to KF*

## 5 Results: EMG/goniometer measurement

As mentioned in chapter 3.2 we did previous studies and measurements to get detailed information about the specific training on the leg press machine and their physiological effects. Therefore we equipped one subject (male, 28y, 1.72m, 75kg) with eleven EMG sensors (chapter 3.2.1) to record muscle activation and three goniometers (chapter 3.2.2) to visualize joint angles of the lower limb. The subject had to work through a defined training protocol (chapter 3.2.4) where all modes of training were prescribed.

### 5.1 Results EMG

Comparing mean and standard deviation data of isokinetic and vibration training with no voluntary activation during both phases (Figure 5.1) it is remarkable that knee agonist muscles (quadriceps femoris) show no considerable activities in contrast to the antagonistic muscles of the knee joint (e.g. hamstrings and m. gluteus maximus). In general it is obvious that EMG responses are little higher during vibration exercises. During knee flexion of vibration motion data of m. semitendinosus/m. semimembranosus (SDSB) features highest values of all muscles and measurements.

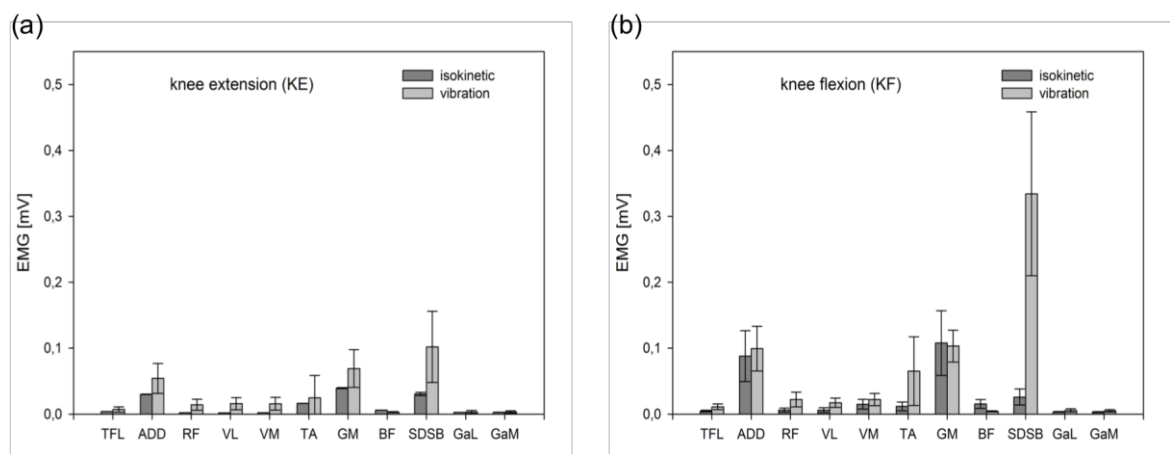


**Figure 5.1: Mean and SD values of EMG responses during isokinetic and vibration training with 0% voluntary activation, (a) knee extension (b) knee flexion**

Trials with higher levels of voluntary activation (50% and 100%) provided more activation of all muscles, especially of m. quadriceps femoris. Values increased continuously and when looking onto 100% records, rectus femoris and both vasti became dominant in comparison to all other observed muscles (see Figure 5.2 and Figure 5.3). Activation level of SBSB during vibration training could not be reached.

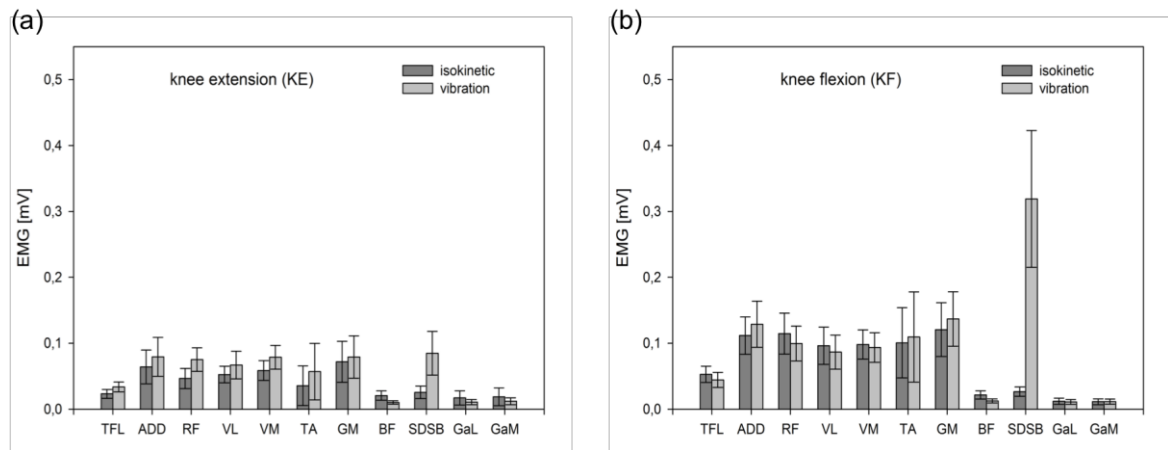


**Figure 5.2: Mean and SD values of EMG responses during isokinetic and vibration training with 50% voluntary activation, (a) knee extension (b) knee flexion**

Behavior of m. semitendinosus/semimembranosus (SBSD) needs to be mentioned separately. Within each group of motion (KE and KF) EMG signals of these muscles presented almost same mean values above all three levels of voluntary activation (0%, 50% and 100%). Further it is apparent that vibration training has high influence to SDSB, especially when flexing the knee joint. But when isokinetic and vibration results were brought face to face, especially during training with no voluntary activation, it is evident that not only SBSD is effected by the vibration training.

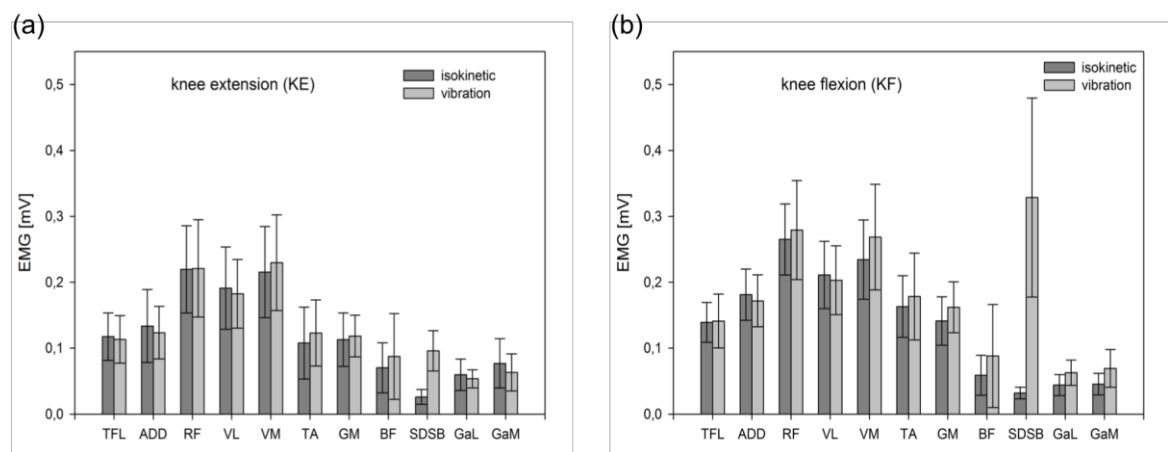


**Figure 5.3: Mean and SD values of EMG responses during isokinetic and vibration training with 100% voluntary activation, (a) knee extension (b) knee flexion**

Quadriceps muscles featured highest ratio between vibration and isokinetic results when data of 0% activation was used. It ranged from 6.2 to 8 (mean 7.1,  $\pm 0.73$ ) for KE and from 6.8 to 7.6 (mean 7.2,  $\pm 0.32$ ) for KF. During all other trainings (50% and 100%) ratio values were in the range of 0.1 to 3 (mean 1.7,  $\pm 0.91$  for KE and mean 0.9,  $\pm 0.16$  for KF, see Table 5.1). It could be hypothesized that there is coherence

between the level of voluntary activation and the ratio of vibration and isokinetic EMG signals.

	EMG [mV]			
	RF	VL	VM	SDSB
<b>extension (KE)</b>				
<b>iso0</b>	0.0023	0.0020	0.0022	0.0305
<b>iso50</b>	0.0255	0.0433	0.0390	0.0250
<b>iso100</b>	0.0934	0.19990	0.1954	0.0388
<b>vib0</b>	0.0142	0.0159	0.0157	0.1021
<b>vib50</b>	0.0753	0.0760	0.0788	0.0849
<b>vib100</b>	0.2156	0.0178	0.2245	0.0967
<b>flexion (KF)</b>				
<b>iso0</b>	0.0026	0.0021	0.0029	0.041
<b>iso50</b>	0.0750	0.0547	0.0785	0.0289
<b>iso100</b>	0.3056	0.1706	0.2667	0.0415
<b>vib0</b>	0.0198	0.0153	0.0198	0.2721
<b>vib50</b>	0.0738	0.0636	0.0696	0.2624
<b>vib100</b>	0.2060	0.1500	0.1984	0.2746
	ratio (vib/iso)			
	RF	VL	VM	SDSB
<b>extension (KE)</b>				
<b>vib0/iso0</b>	6.2	8.0	7.11	3.3
<b>vib50/iso50</b>	3.0	1.8	2.0	3.4
<b>vib100/iso100</b>	2.3	0.1	1.1	2.5
<b>flexion (KF)</b>				
<b>vib0/iso0</b>	7.6	7.3	6.8	6.6
<b>vib50/iso50</b>	1.0	1.2	0.9	9.1
<b>vib100/iso100</b>	0.7	0.9	0.7	6.6

**Table 5.1: Mean and ratio values of EMG, m. quadriceps femoris heads and one hamstring**

EMG signals indicate higher muscle activation in course of knee flexion phase. Mean of ratio between KF and KE was around 1.6 ( $\pm 0.74$ ) for isokinetic and about 2.1 ( $\pm 2.07$ ) for vibration trials.

Evoked myoelectric signals of dominant muscles and the flexion angle of the knee joint are illustrated in the figures below (Figure 5.4 with isokinetic and Figure 5.5 with vibration data). Black lines represent EMG signals recorded while training with 0% of voluntary muscle activation, data of 100% voluntary activation is colored in red. The figures depict data of all three cycles with both phases of movement (knee extension and knee flexion) and rest position before and after the training session.

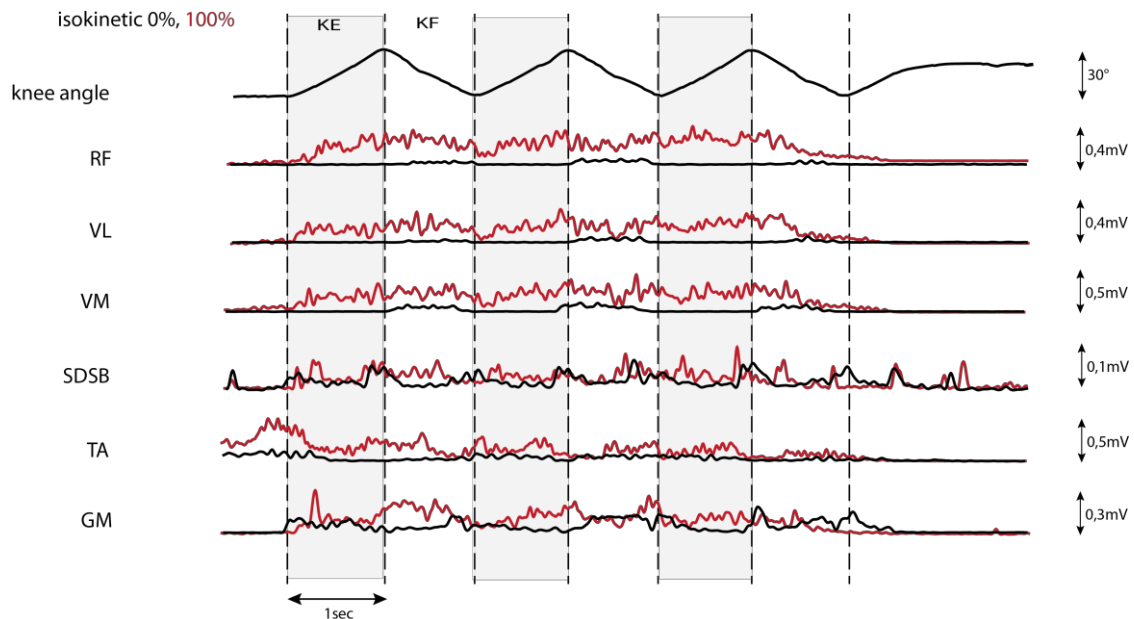


**Figure 5.4: EMG and goniometer data of isokinetic training**  
*0% of voluntary activation (black), 100% of voluntary activation (red)*

Predefined by the leg press software data differs between isokinetic and vibration mode. Data of the knee goniometer monitored a variation of 5° of knee flexion angle, and looking onto the time line vibration session last about one and a half time longer. Further, more myoelectric response and higher values of EMG signals could be observed during vibration mode. It is evident, that quadriceps muscles illustrate higher EMG response when the subject was training with 100% of voluntary muscle activation (red lines).

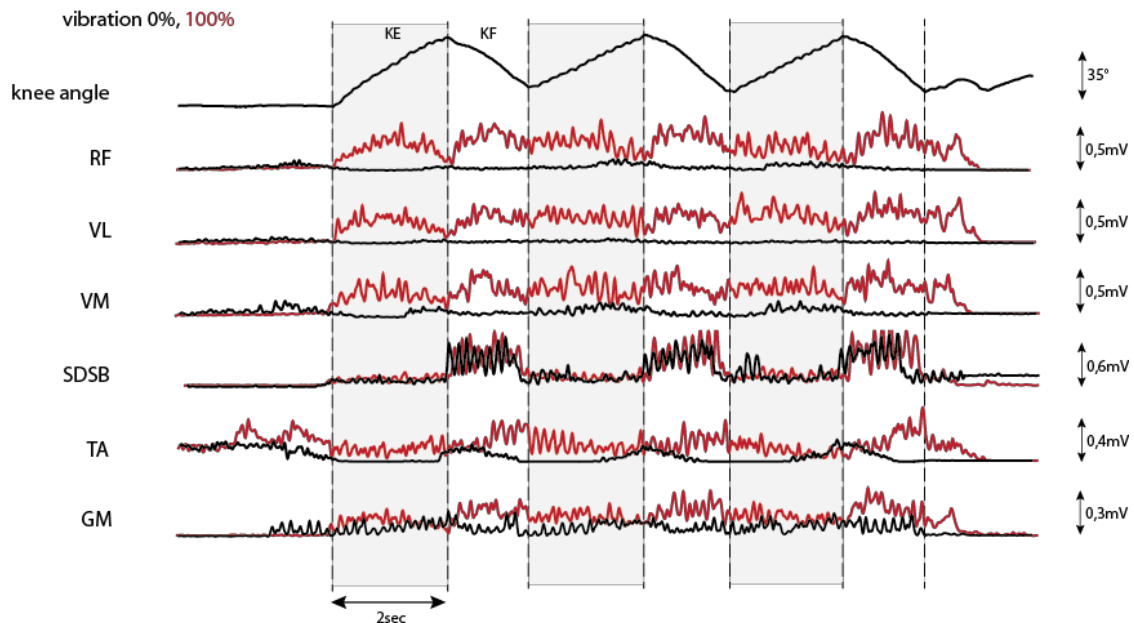


**Figure 5.5: EMG and goniometer data of vibration training**  
*Black: 0% of voluntary activation, Red: 100% of voluntary activation*

## 5.2 Results: GONIOMETER

In addition to EMG measurements progression of hip, knee and ankle joint angles were recorded during all trainings. Therefore we equipped our subject with three goniometer devices (see chapter 3.2.2.). Stored data was afterwards imported to MATLAB where further calculations were done.

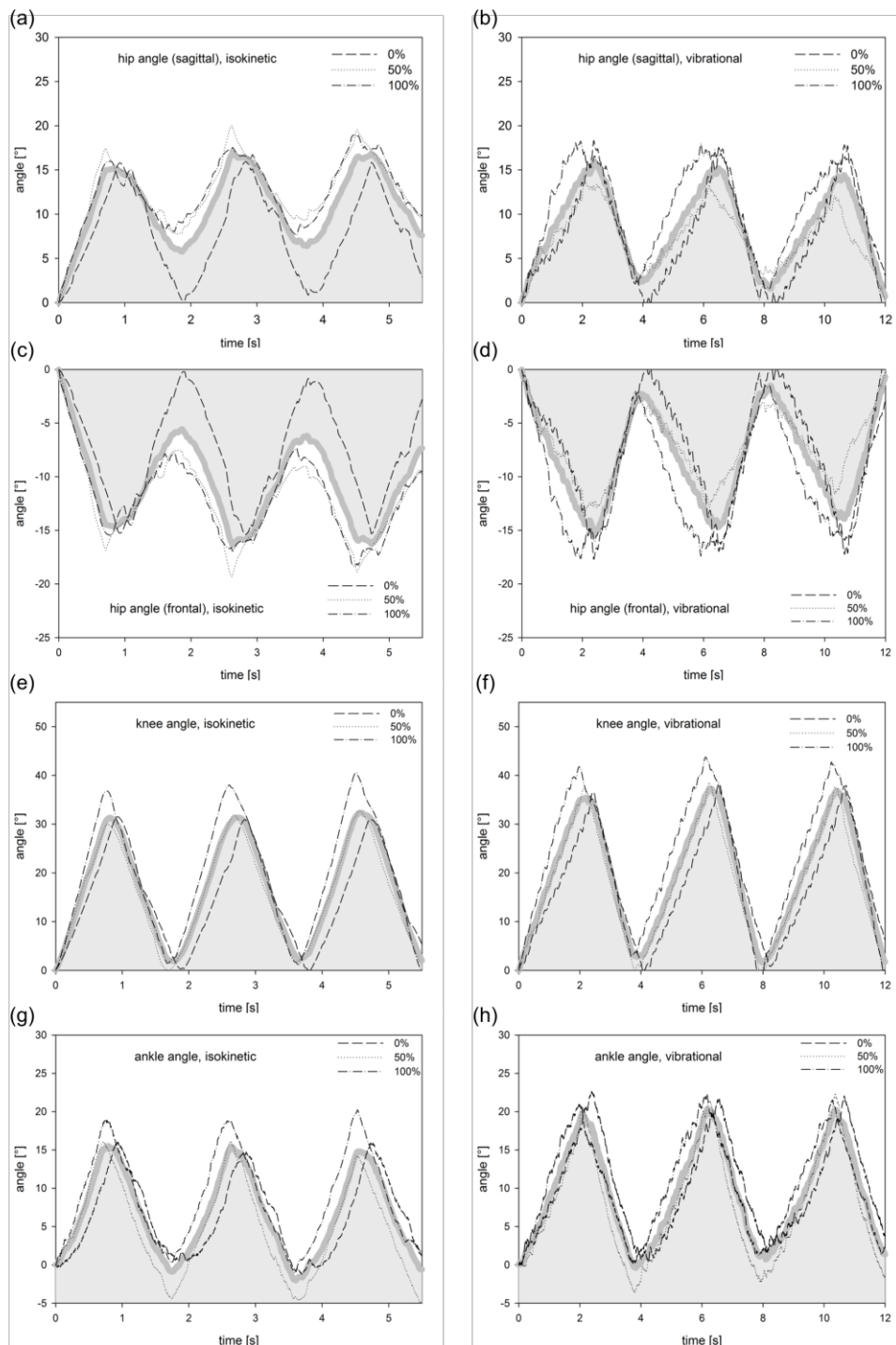


**Figure 5.6: Goniometer-data of sagittal hip flexion**

*0%, 50% and 100% voluntary activation (black lines), mean values of 0%, 50% and 100% in grey; left: isokinetic, right: vibration*

Goniometers were calibrated at defined start position (chapter 3.2.4). Data of isokinetic and vibration trials were summed up and mean values were calculated for each type of motion. Resulting and raw data is illustrated in Figure 5.6, where grey lines represent mean values and black curves are raw data of trials with 0%, 50% or 100% of voluntary activation.

The goniometer placed at the hip joint recorded two angles of motion, first sagittal flexion and second frontal flexion (abduction or adduction of the hip). The two others only recorded flexion of the respective joint (knee and ankle).

Goniometer data shown in Figure 5.6 represents net data of the three cycles of movement. Because there was no automatic trigger in use, data before training started and when motion was finished had to be erased via MATLAB script. Further goniometer data was used to define turning points of knee flexion to determine phase of motion (KE or KF).

### 5.3 Discussion

Myoelectric signals illustrated almost no activity of quadriceps muscles during trials with no voluntary activation and little activation of hamstring muscles. In the course of measurement EMG signals of quadriceps muscles became more dominant. Enhancement of hamstrings could be observed too but in a smaller scale. Goniometer data showed a dependence of joint angle values and the level of voluntary activation.

EMG – Data of myoelectric signals during isokinetic leg press training illustrated that there was almost no activity recorded in knee extension agonists (all heads of quadriceps muscle) during exercise without voluntary activation (0%). In reference to antagonistic muscles two of them, SDSB and GM were participating little. When the level of voluntary activation was raised (100%), evoked EMG responses of both, agonistic and antagonistic muscles increased. Measurements monitored that prime movers of knee extension (four heads of m. quadriceps) became more dominant than others. It is hypothesized, that signals of antagonists (hamstrings) were increased too because of muscle co-activation due to full voluntary activation. Purpose of these co-activation may be seen in maintaining knee stabilization of agonist and antagonist muscles which is described elsewhere (Escamilla et al. 1998; Stensdotter et al. 2003; Pincivero et al. 2000).

Looking onto knee extension (KE) and knee flexion (KF) in particular it is evident that higher EMG signals of quadriceps muscles were recorded during KF. It may be thought that muscles get more activated when they assume antagonistic tasks (eccentric movement) and that KF movement is easier to perform. Subjective subjects feedback is in accordance with these reflections.

Shank muscles didn't report significant EMG data, beside of TA where high activation was recorded at rest position, before the motion started. Decreasing the work angle of the pedals would probably lower that effect because activation decreases when motion started and ankle angle decreased.

Recorded muscle responses of vibration training differ only little compared to isokinetic signals. Agonists and antagonists behave almost the same, except m. semitendinosus/semimembranosus (SDSB) which showed high receptivity of vibration movement. For most other muscles it could be suggested that vibration training evoked little higher EMG signals. E.g. sensors placed at quadriceps heads monitored higher signals for RF and VM in both KE and LF phase, but lower once where detected for VL. Like in isokinetic exercises, in vibration trails co-activation of antagonists could be observed and values of quadriceps heads were higher during KF. It need to be mentioned that SDSB's EMG recordings were non-varying when vibration trails with 0% and 100% of voluntary muscle activation were compared, neither in KE than in KF phase. Values monitored during KF were about 3 times higher than recorded while KE.

Likewise calculation of mean values for both phases of isokinetic and vibration motion reported higher muscle activity during KF phase. Variety of values was higher for vibration trials. Ratio between vibration and isokinetic mean values of SDSB were 3.3 for KE and 6.6 for KF. For KE phase quadriceps group featured mean values of  $7.1 \pm 0.73$  and  $7.2 \pm 0.33$  for KF.

Goniometer - In reference to recorded goniometer data especially of the hip joint, it is obvious that subject could not perform leg press training without frontal flexion of the hip. Mean values of hip abduction angle featured a maximum range of  $15^\circ$  (isokinetic and vibration) and a reduction of frontal hip flexion when voluntary muscle activation levels were enhanced (see Figure 5.7). Further studies reported no significant differences in EMG signals concerning additional hip abduction during knee extension or flexion exercises (Bevilaqua-Grossi et al. 2006; Hertel et al. 2004).

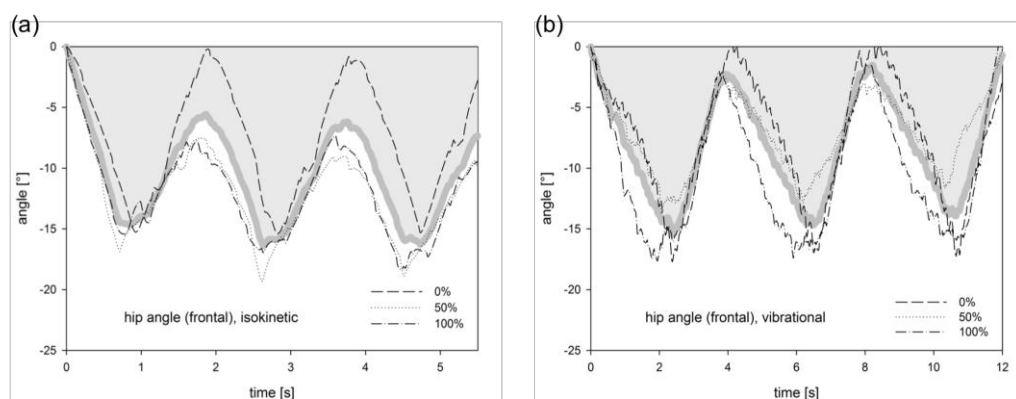


**Figure 5.7: Goniometer data of frontal hip flexion**  
(a) isokinetic, (b) vibration

As mentioned earlier, high ankle flexion ( $93^\circ$ ) at the beginning of the motion results in high TA activation. During the exercise ankle angle get reduced and TA activity followed. Because measurements were done only with one subject it could not be suggested if this is unique or a general finding of our tests. Variation of ankle angle was around  $0^\circ$  to  $15^\circ$  for isokinetic and  $0^\circ$  to  $20^\circ$  for vibration training mode, when mean values over all variations of voluntary activation were observed.

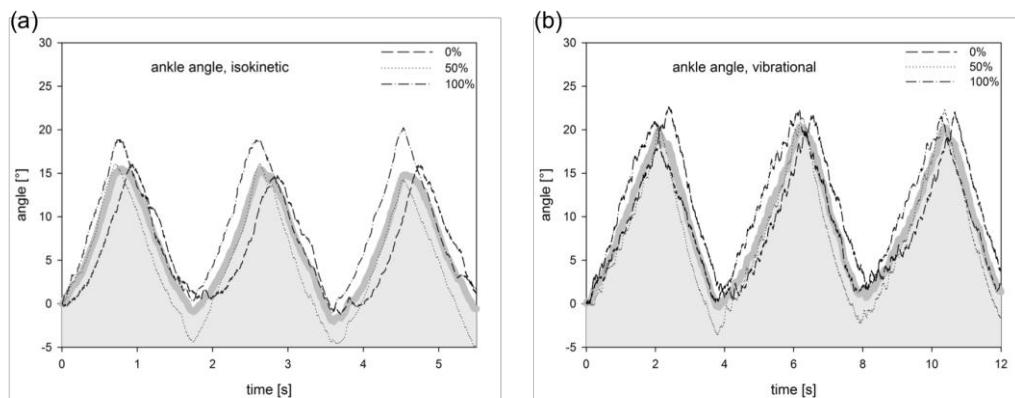


**Figure 5.8: Goniometer data of ankle flexion**  
(a) isokinetic, (b) vibration

Recorded data of knee joint angles behave similar to other joints discussed above. It is obvious that motion range was smaller when exercises were done with lower voluntary activation. Furthermore goniometer data pointed out, that vibration training led to bigger joint angles than isokinetic did. During KE data featured more varieties. Figure 5.9 depicts that trails with 100% of voluntary activation evoked higher knee joint angles and a faster increase too. Unlike KF-data, where all three trails are close and values differ only little. Observations could be found in isokinetic and vibration data and at all three joints monitored with goniometers.

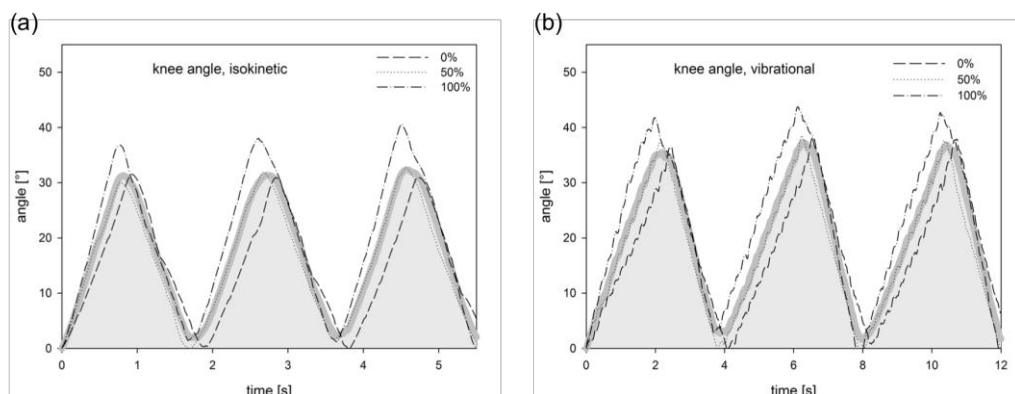


**Figure 5.9: Goniometer data of knee flexion**  
(a) isokinetic, (b) vibration

## 6 Comparison of simulation and EMG results

Contribution of leg press training in lower limb rehabilitation therapy is widely accepted. The possibility of practicing in a joint-friendly way in combination with new developed leg press machines allow more customized trainings with real-time monitoring.

In the course of the present study, training on a computer-controlled, linear motor-powered leg press was investigated. Procedures, recorded motion and force data of leg press exercises were transferred to OpenSim for simulation reasons and muscle forces and excitation of lower limb muscles were computed. Moreover, subject was equipped with EMG sensors and goniometers, to detect evoked muscle activities and joint angles, respectively.

Simulation results and recorded EMG signals stated higher muscle activity during the knee flexion phase where quadriceps muscles are claimed eccentric. According to these findings we postulate that in case of the investigated, special leg press training muscles get more activated when they assume antagonistic tasks like quadriceps heads did when flexion of the knee is increased. Further, subjects feedback claimed that subjective feeling during KF was more comfortable.

Moreover, activation of knee extension antagonists (hamstrings) had been observed in evoked myoelectric recordings, but not in simulation results. It is hypothesized that these observations are referable to co-activation of antagonistic muscles due to stabilization reasons of the knee joint when subject was practicing with full voluntary activation of the lower limb muscles. On the other side, Knee flexion agonists (quadriceps muscles) became more dominant when the level of voluntary muscle activation was raised and most activity and force production was simulated for musculus vastus lateralis (VL). EMG signals differ to those findings. Measured data displayed rectus femoris and vastus medialis muscle as main actuators of leg press training over both phases (KE and KF) of movement. Signals of shank muscles didn't report significant values, only m. tibialis anterior featured myoelectric signals. We suggest that these signals were evoked mainly because of huge ankle flexion during rest position. Because investigations were done only with one subject this argumentation would need further measurements with a higher amount of subjects.

Comparing simulation data only, isokinetic trails featured higher muscle activity and forces than vibration exercises. Unlike EMG data where vibration training evoked higher muscle activity than isokinetic trails did. Additional investigations on muscle modeling for simulations need to be done to compute muscle activity more close to their behavior in human.

## 7 Bibliography

- Alkner, B.A., Tesch, P.A. & Berg, H.E., 2000. Quadriceps EMG/force relationship in knee extension and leg press. *Medicine & Science in Sports & Exercise*, 32(2), pp.459–463. Available at: <http://www.ncbi.nlm.nih.gov/pubmed/10694132>.
- Anderson, F. et al., 2010. OpenSim - User's Guide Release 2.4. Available at: <https://simtk.org/home/opensim>.
- Anderson, F.C. & Pandy, M.G., 1999. A Dynamic Optimization Solution for Vertical Jumping in Three Dimensions. *Computer methods in biomechanics and biomedical engineering*, 2(3), pp.201–231. Available at: <http://www.ncbi.nlm.nih.gov/pubmed/11264828> [Accessed June 2, 2014].
- Benn, C. et al., 1998. The effects of serial stretch loading on stretch work and stretch-shorten cycle performance in the knee musculature. *The Journal of orthopaedic and sports physical therapy*, 27(6), pp.412–422.
- Bevilaqua-Grossi, D. et al., 2006. The effect of hip abduction on the EMG activity of vastus medialis obliquus, vastus lateralis longus and vastus lateralis obliquus in healthy subjects. *Journal of NeuroEngineering and Rehabilitation*, 3, p.13. Available at: <http://www.ncbi.nlm.nih.gov/pubmed/16817971>.
- Bird, S.P., Tarpenning, K.M. & Marino, F.E., 2005. Designing resistance training programmes to enhance muscular fitness: A review of the acute programme variables. *Sports Medicine*, 35(10), pp.841–851.
- Bosco, C. et al., 1998. The influence of whole body vibration on jumping performance. *Biology of sport*, 15(3), pp.157–164.
- Burke, J.R. et al., 1996. Age-dependent effects of muscle vibration and the Jendrassik maneuver on the patellar tendon reflex response. *Archives of physical medicine and rehabilitation*, 77(6), pp.600–604.
- Carter, S. et al., 2001. Short-term 17beta-estradiol decreases glucose R(a) but not whole body metabolism during endurance exercise. *J Appl Physiol*, 90(1), pp.139–146. Available at: <http://www.ncbi.nlm.nih.gov/pubmed/11133904>.
- Cho, Y. et al., 2008. Effect of Vibration Intervention on Leg-press Exercise. , pp.113–116.
- Cvecka, J. et al., 2009. Einfluss von serial stretch loading auf die Effektivität des isokinetischen Krafttrainings. *Basic Applied Myology*, 19(4), pp.175–180.
- Delp, S.L. et al., 1990. An interactive graphics-based model of the lower extremity to study orthopaedic surgical procedures. *IEEE Trans Biomed Eng*, 37(8), pp.757–767. Available at: <http://www.ncbi.nlm.nih.gov/pubmed/2210784>.
- Delp, S.L. et al., 2007. OpenSim: open-source software to create and analyze dynamic simulations of movement. *IEEE Trans Biomed Eng*, 54(11), pp.1940–1950. Available at: <http://www.ncbi.nlm.nih.gov/pubmed/18018689>.

- Denoth, J., 2005. Biomechanik II: Biologische und mechanische Grundlagen des Bewegungsapparates, Unterlagen zur Vorlesung - Teil 2. Der Muskel als Motor. , pp.44–91.
- Elaine, N. & Marieb, R.N., 2001. *Essentials of Human Anatomy & Physiology* -, Benjamin-Cummings Pub Co 7th edition.
- Epstein, M. & Herzog, W., 1998. *Theoretical models of skeletal muscle*, Chichester ; New York: Wiley.
- Escamilla, R.F. et al., 1998. Biomechanics of the knee during closed kinetic chain and open kinetic chain exercises. *Medicine and science in sports and exercise*, 30(4), pp.556–569.
- Escamilla, R.F. et al., 2001. Effects of technique variations on knee biomechanics during the squat and leg press. *Medicine & Science in Sports & Exercise*, 33(9), pp.1552–1566. Available at: <http://www.ncbi.nlm.nih.gov/pubmed/11528346>.
- Faulkner, J.A. et al., 1980. Dynamics of energetic processes in human muscle. *Proc. Int. Symp. Exer. Bioenergetics Gas Exchange*, pp.81–90.
- Faulkner, J.A., Claffin, D.R. & McCully, K., 1986. Power output of fast and slow fibers from human skeletal muscles. *Human Muscle Power*.
- Fleck, J. & Kreamer, J., 1997. Designing esstance training Programs. *USA: Human Kinetics*.
- Gordon, A.M., Huxley, A.F. & Julian, F.J., 1966. The variation in isometric tension with sarcomere length in vertebrate muscle fibres. *J Physiol*, 184(1), pp.170–192. Available at: <http://www.ncbi.nlm.nih.gov/pubmed/5921536>.
- Gullett, J.C. et al., 2009. A biomechanical comparison of back and front squats in healthy trained individuals. *J Strength Cond Res*, 23(1), pp.284–292. Available at: <http://www.ncbi.nlm.nih.gov/pubmed/19002072>.
- Hamner, S.R., Seth, A. & Delp, S.L., 2010. Muscle contributions to propulsion and support during running. *Journal of Biomechanics*, 43(14), pp.2709–2716. Available at: <http://www.pubmedcentral.nih.gov/articlerender.fcgi?artid=2973845&tool=pmcentrez&ndertype=abstract>.
- Henneman, E. & Olson, C.B., 1965. Relations between Structure and Function in the Design of Skeletal Muscles. *J Neurophysiol*, 28, pp.581–598. Available at: <http://www.ncbi.nlm.nih.gov/pubmed/14328455>.
- Henneman, E., Somjen, G. & Carpenter, D.O., 1965. Functional Significance of Cell Size in Spinal Motoneurons. *J Neurophysiol*, 28, pp.560–580. Available at: <http://www.ncbi.nlm.nih.gov/pubmed/14328454>.
- Hertel, J. et al., 2004. Combining isometric knee extension exercises with hip adduction or abduction does not increase quadriceps EMG activity. *British journal of sports medicine*, 38, pp.210–213.
- Hicks, J.B., 2011. User´s Guide - OpenSim 3.0 (online). Available at: <http://simtk-confluence.stanford.edu:8080/x/AoQz>.

- Hill, A. V, 1970. First and last Experiments in Muscle Mechanics. *Cambridge University Press*.
- Hill, A. V, 1938. The Heat of Shortening and the Dynamic Constants of Muscle. *Proceedings of the Royal Society of London. Series B, Biological Sciences*, 126(843), pp.136–195.
- Horowitz, R., Maruyama, K. & Podolsky, R.J., 1989. Elastic behavior of connectin filaments during thick filament movement in activated skeletal muscle. *J Cell Biol*, 109(5), pp.2169–2176. Available at: <http://www.ncbi.nlm.nih.gov/pubmed/2808523>.
- Horowitz, R. & Podolsky, R.J., 1987. The positional stability of thick filaments in activated skeletal muscle depends on sarcomere length: evidence for the role of titin filaments. *J Cell Biol*, 105(5), pp.2217–2223. Available at: <http://www.ncbi.nlm.nih.gov/pubmed/3680378>.
- Horowitz, R. & Podolsky, R.J., 1988. Thick filament movement and isometric tension in activated skeletal muscle. *Biophys J*, 54(1), pp.165–171. Available at: <http://www.ncbi.nlm.nih.gov/pubmed/3416026>.
- Hunt, K.H. & Crossley, F.R.E., 1975. Coefficient of restitution interpreted as damping in vibroimpact. *Journal of Applied Mechanics*, 42(2), pp.440–445. Available at: <http://link.aip.org/link/?JAMCAV/42/440/1>.
- Huxley, A.F., 1957. Muscle structure and theories of contraction. *Prog Biophys Biophys Chem*, 7, pp.255–318. Available at: <http://www.ncbi.nlm.nih.gov/pubmed/13485191>.
- Huxley, A.F. & Niedergerke, R., 1954. Structural Changes in Muscle During Contraction: Interference Microscopy of Living Muscle Fibres. *Nature*, 173(4412), pp.971–973.
- Huxley, H. & Hanson, J., 1954. Changes in the cross-striations of muscle during contraction and stretch and their structural interpretation. *Nature*, 173(4412), pp.973–976. Available at: <http://www.ncbi.nlm.nih.gov/pubmed/13165698>.
- Kern, H. et al., 2011. Atrophy/hypertrophy cell signaling in muscles of young athletes trained with vibrational-proprioceptive stimulation. *Neurol Res*, 33(10), pp.998–1009. Available at: <http://www.ncbi.nlm.nih.gov/pubmed/22196751>.
- Kern, H. et al., 2009. Beinschub-Trainingsmaschine A. P. Office, ed. , AT 5005 72, p.19.
- Kern, H., 2012. Vibrational-proprioceptive Resistance Exercise Training Versus Neuromuscular Electrical Stimulation Training in Elderly People With Muscle Weakness (MOBIL). Available at: <http://clinicaltrials.gov/ct2/show/NCT01679977>.
- Komi, P. V, 1984. Physiological and biomechanical correlates of muscle function: effects of muscle structure and stretch-shortening cycle on force and speed. *Exercise and sport sciences reviews*, 12, pp.81–121.
- Komi, P. V, 2000. Stretch-shortening cycle: a powerful model to study normal and fatigued muscle. *Journal of biomechanics*, 33(10), pp.1197–1206.
- Komi, P. V & Nicol, C., 2000. Stretch-shortening cycle fatigue. In *Biomechanics and Biology of Movement. Human Kinetics Publ, Champaign*.

- Krenn, M. et al., 2011. Safe neuromuscular electrical stimulator designed for the elderly. *Artif Organs*, 35(3), pp.253–256. Available at: <http://www.ncbi.nlm.nih.gov/pubmed/21401669>.
- Lorenzetti, S. et al., 2012. Comparison of the Angles and Corresponding Moments in the Knee and Hip During Restricted and Unrestricted Squats. *The Journal of Strength & Conditioning Research*, 26(10), pp.2829–2836  
10.1519/JSC.0b013e318267918b. Available at: [http://journals.lww.com/nsca-jscr/Fulltext/2012/10000/Comparison\\_of\\_the\\_Angles\\_and\\_Corresponding\\_Moments.29.aspx](http://journals.lww.com/nsca-jscr/Fulltext/2012/10000/Comparison_of_the_Angles_and_Corresponding_Moments.29.aspx).
- Luca, C.J. De, 1997. The use of surface electromyography in biomechanics S. Bouisset, ed. *Journal of Applied Biomechanics*, 13(July 1993), pp.1–38. Available at: [http://els.ui.ac.ir/file.php/59/EMG\\_Biomechanics.pdf](http://els.ui.ac.ir/file.php/59/EMG_Biomechanics.pdf).
- McGraw-Hill, 2009. *Anatomy & Physiology - The Unity of Form and Function*,
- McMahon, T.A., 1984. *Muscles, Reflexes, and Locomotion*, Princeton University Press, Princeton, New Jersey.
- Merletti, R. et al., 2005. Surface ElectroMyoGraphy for the Non-Invasive Assessment of Muscles. Available at: <http://www.seniam.org/>.
- Millard, M. et al., 2013. Flexing computational muscle: modeling and simulation of musculotendon dynamics. *Journal of biomechanical engineering*, 135(2), p.21005. Available at: <http://eutils.ncbi.nlm.nih.gov/entrez/eutils/elink.fcgi?dbfrom=pubmed&id=23445050&retmode=ref&cmd=prlinks>.
- Norman, R.W. & Komi, P. V., 1979. Electromechanical delay in skeletal muscle under normal movement conditions. *Acta physiologica Scandinavica*, 106(3), pp.241–248.
- Perez-Gonzalez, A. et al., 2008. A modified elastic foundation contact model for application in 3D models of the prosthetic knee. *Med Eng Phys*, 30(3), pp.387–398. Available at: <http://www.ncbi.nlm.nih.gov/pubmed/17513163>.
- Pincivero, D.M. et al., 2000. Quadriceps-hamstring EMG activity during functional, closed kinetic chain exercise to fatigue. *European journal of applied physiology*, 81(6), pp.504–509.
- Proske, U. & Morgan, D.L., 1987. Tendon stiffness: methods of measurement and significance for the control of movement. A review. *Journal of biomechanics*, 20(1), pp.75–82.
- Reeves, N.D. et al., 2009. Differential adaptations to eccentric versus conventional resistance training in older humans. *Experimental physiology*, 94(7), pp.825–33. Available at: <http://www.ncbi.nlm.nih.gov/pubmed/19395657> [Accessed January 21, 2014].
- Romaiguère, P., Vedel, J.P. & Pagni, S., 1993. Effects of tonic vibration reflex on motor unit recruitment in human wrist extensor muscles. *Brain research*, 602(1), pp.32–40.
- Rønnestad, B.R., 2004. *Comparing the performance-enhancing effects of squats on a vibration platform with conventional squats in recreationally resistance-trained men.*,

- Rosen, J., Fuchs, M.B. & Arcan, M., 1999. Performances of Hill-Type and Neural Network Muscle Models - Toward a Myosignal-Based Exoskeleton. *Computers and Biomedical Research*, 32, pp.415–439.
- Rothmuller, C. & Cafarelli, E., 1995. Effect of vibration on antagonist muscle coactivation during progressive fatigue in humans. *The Journal of physiology*, 485 ( Pt 3, pp.857–864.
- Rowe, P. et al., 2001. Validation of Flexible Electrogoniometry as a Measure of Joint Kinematics. *Physiotherapy*, 87(9), pp.479–488.
- Schmiedmayer, H.B., 2011. *Script to lecture "Modeling of the Human Locomotor System,"* Vienna University of Technology (TU Wien).
- Seth, A. et al., 2011. OpenSim: a musculoskeletal modeling and simulation framework for in silico investigations and exchange. *Procedia IUTAM*, 2(0), pp.212–232. Available at: <http://www.sciencedirect.com/science/article/pii/S2210983811000228>.
- Seth, A. & Pandy, M.G., 2007. A neuromusculoskeletal tracking method for estimating individual muscle forces in human movement. *Journal of Biomechanics*, 40(2), pp.356–366. Available at: <http://www.ncbi.nlm.nih.gov/pubmed/16513124>.
- Sherman, M.A., Seth, A. & Delp, S.L., 2011. Simbody: Multibody dynamics for biomedical research. In pp. 241–261. Available at: <http://www.scopus.com/inward/record.url?eid=2-s2.0-79959327891&partnerID=40&md5=9dc6d3b807e11cb094c1514cb7fd3cfa>.
- Shier, D., Butler, J.L. & Lewis, A., 2003. *Hole's Human Anatomy & Physiology*, McGraw-Hill Science/Engineering/Math.
- Da Silva, E.M. et al., 2008. Analysis of muscle activation during different leg press exercises at submaximum effort levels. *J Strength Cond Res*, 22(4), pp.1059–1065. Available at: <http://www.ncbi.nlm.nih.gov/pubmed/18545207>.
- Steindler, A., 1955. *Kinesiology of the Human Body Under Normal and Pathological Conditions*, Springfield: Charles C. Thomas.
- Stensdotter, A.K. et al., 2003. Quadriceps Activation in Closed and in Open Kinetic Chain Exercise. *Medicine and Science in Sports and Exercise*, 35(12), pp.2043–2047.
- Thelen, D.G., 2003. Adjustment of muscle mechanics model parameters to simulate dynamic contractions in older adults. *J Biomech Eng*, 125(1), pp.70–77. Available at: <http://www.ncbi.nlm.nih.gov/pubmed/12661198>.
- Thelen, D.G., 2003. *Adjustment of muscle mechanics model parameters to simulate dynamic contractions in older adults.*,
- Thelen, D.G. & Anderson, F.C., 2006. Using computed muscle control to generate forward dynamic simulations of human walking from experimental data. *J Biomech*, 39(6), pp.1107–1115. Available at: <http://www.ncbi.nlm.nih.gov/pubmed/16023125>.
- Thelen, D.G., Anderson, F.C. & Delp, S.L., 2003. Generating dynamic simulations of movement using computed muscle control. *J Biomech*, 36(3), pp.321–328. Available at: <http://www.ncbi.nlm.nih.gov/pubmed/12594980>.

- Verschueren, S., 2004. Effect of whole body vibration training on muscle strength and sprint performance in sprint - trained athletes. In *4th International Conference on Strength Training*. Budapest.
- Wilkie, D.R., 1968. *The Institute Of Biology's Studies In Biology NO. 11*, Edward Arnold.
- Winters, J., 1995. An improved muscle-reflex actuator for use in large-scale neuromusculoskeletal models. *Annals of Biomedical Engineering*, 23(4), pp.359–374. Available at: <http://dx.doi.org/10.1007/BF02584437>.
- Winters, J.M. & Woo, S.L., 1990. *Multiple Muscle Systems: Biomechanics and Movement Organization*, Springer.
- Wretenberg, P. et al., 1993. Joint moments of force and quadriceps muscle activity during squatting exercise. *Scandinavian journal of medicine & science in sports*, 3(Oxford), pp.244–250.
- Yamaguchi, G.T. & Zajac, F.E., 1989. A planar model of the knee joint to characterize the knee extensor mechanism. *Journal of biomechanics*, 22(1), pp.1–10. Available at: <http://www.ncbi.nlm.nih.gov/pubmed/2914967>.
- Zahalak, G.I., 1992. An overview of muscle modeling. *Neural Prosthesis, Replacing* , pp.17–57.
- Zajac, F.E., 1989. Muscle and tendon: properties, models, scaling, and application to biomechanics and motor control. *Crit Rev Biomed Eng*, 17(4), pp.359–411. Available at: <http://www.ncbi.nlm.nih.gov/pubmed/2676342>.

## 8 List of abbreviations

AD converter	Analog-to-Digital-Converter
CKCE	closed kinetic chain exercise
CMC	Computer Muscle Control
CNS	central nervous system
DOF	degrees-of-freedom
EMG	Electromyography
GUI	Graphical User Interface
ID	Inverse Dynamics
IK	Inverse Kinematics
JR	Joint Reaction
KE	knee extension phase (angle of knee joint decreases)
KF	knee flexion phase (angle of knee joint increases)
LBI	Ludwig Boltzmann Institute of Electrostimulation and Physical Rehabilitation
LP	leg press
OKCE	open kinetic chain exercise
PD	proportional-derivative
SO	Static Optimization
SSC	Stretch-Shortening Cycle